

Progress Toward a Practical GNSS-R Water Level Sensor

David Purnell

Department of Earth and Planetary Sciences

McGill University, Montreal

August, 2022

A thesis submitted to McGill University in partial fulfillment of the requirements
of the degree of Doctor of Philosophy in Earth and Planetary Sciences

©David Purnell, 2022

Abstract

Water levels are a fundamental measurement of the water bodies on Earth. Coastal water levels are used to study ocean tides, storm surges and changes in mean sea level, while river levels are a crucial tool for hydrologists to infer discharge and monitor the potential for inland flooding. As the climate continues to respond to human-induced changes, sea levels are predicted to rise at an increasing rate, flooding events are expected to happen more frequently and hence water level sensors are critical to inform climate adaptation efforts. Large stretches of global coastline are not being monitored, particularly in the arctic regions and in developing countries. This lack of water level sensors is partly because the instruments are costly to install and maintain outside of populated regions where the infrastructure that is commonly used to house instruments, such as piers, does not exist. Satellite altimetry is an increasingly precise technique for monitoring global water levels, but the measurements are less reliable near the coast and the spatial and temporal resolution is generally not fine enough for monitoring rivers or lakes.

In this thesis, a novel technique for coastal water level monitoring is developed by repurposing low-cost Global Navigation Satellite System (GNSS) technology that is often embedded in mobile devices for navigation purposes. This technique relies on the fact that coastal GNSS antennas simultaneously receive signals directly from a satellite and signals that reflect off the water surface prior to reaching the antenna. Water levels are obtained by analyzing the interference between the direct and reflected signals. The main advantage of this technique, called GNSS-Reflectometry (GNSS-R), is that the antennas can be positioned up to 10s of meters away from the coastline, thus making it easier to install and maintain sensors in remote regions. This thesis builds on a large body of GNSS-R literature, which is reviewed in Chapter 1. The key innovation of the technique

developed in this thesis is to use multiple low-cost antennas in the same location to obtain more accurate water levels.

There are three manuscripts that form the basis of this thesis. The first manuscript (Chapter 2) is a theoretical study of the sources of uncertainty in GNSS-R water levels. In this study, a modelling technique is presented to estimate the uncertainty in GNSS-R water levels and the technique is validated against observations from five sites. A comparison of the relative importance of different sources of uncertainty in GNSS-R water levels led to the discovery that random noise is a key source of uncertainty in GNSS-R water levels and hence the hypothesis that multiple antennas could be used to reduce the effect of this noise. The purpose of Chapter 3 is to test this hypothesis using an experimental array of low-cost antennas. By comparing with measurements from co-located pressure gauges at three sites, it is found that using four antennas instead of one improves the precision of GNSS-R water levels by 30–50%. In Chapter 4, the low-cost antenna array technique is developed further, with a focus on developing an algorithm for efficient in-situ data processing for flood monitoring. To validate the technique, data from a site with a large daily tidal range (up to 6 m) is used, which serves as a proxy for extreme flooding conditions. It is hoped that this thesis will act as a guide towards the development of a practical GNSS-R instrument that could be used to improve the global distribution of water level sensors.

Abrégé

Les niveaux d'eau sont une mesure fondamentale des étendues d'eau sur Terre. Les niveaux d'eau côtiers sont utilisés pour étudier les marées océaniques, les ondes de tempête et les changements du niveau moyen de la mer, tandis que les mesures du niveau des rivières sont un outil crucial pour les hydrologues qui en déduisent le débit et suivi le potentiel d'inondation des terres. Comme le climat continue d'être influencé par l'activité humaine, une accélération de l'élévation du niveau de la mer est attendu, ainsi que des inondations plus fréquentes, rendant les capteurs de niveau d'eau une nécessité pour des efforts d'adaptation aux changements climatiques plus éclairés. De grandes parties du littoral mondial ne sont pas suivi, notamment dans les régions arctiques et les pays en développement. Ce manque de capteurs de niveau d'eau s'explique en partie par le fait que les instruments actuels sont coûteux à installer et à entretenir en dehors des régions peuplées où les infrastructures généralement utilisées pour abriter les instruments, comme les jetées, n'existent pas. L'altimétrie satellitaire est une technique de plus en plus précise pour suivre les niveaux d'eau mondiaux, mais les mesures sont moins fiables près des côtes et la résolution spatiale et temporelle n'est généralement pas assez précise pour les rivières ou les lacs.

Dans cette thèse, une nouvelle technique de mesure des niveaux d'eau côtiers est développée en mettant à profit la technologie GNSS (Global Navigation Satellite System) à faible coût qui est souvent intégrée dans les appareils mobiles à des fins de navigation. Cette technique consiste à exploiter le fait que les antennes GNSS côtières reçoivent simultanément des signaux directement d'un satellite et des signaux qui se réfléchissent sur la surface de l'eau avant d'atteindre l'antenne. Les niveaux d'eau sont obtenus en analysant l'interférence entre les signaux directs et réfléchis. Le principal avantage de cette technique, appelée la réflectométrie GNSS (GNSS-R), est

que les antennes peuvent être positionnées jusqu'à des dizaines de mètres de la côte, ce qui facilite l'installation et la maintenance de capteurs dans des régions éloignées. Cette thèse s'appuie sur un grand nombre d'ouvrages sur la GNSS-R, qui sont résumés au chapitre 1. La principale innovation de la technique développée dans cette thèse est l'utilisation au même endroit de plusieurs antennes à faible coût pour améliorer la précision des niveaux d'eau obtenue.

Trois articles constituent la base de cette thèse. Le premier article (chapitre 2) est une étude théorique des sources d'incertitude des mesures de niveaux d'eau par GNSS-R, tandis que les deuxième et troisième articles (chapitres 3 et 4) concernent le développement de la technique GNSS-R utilisant plusieurs antennes à faible coût. L'étude théorique du chapitre 2 a permis de découvrir que le bruit aléatoire était une source clé d'incertitude dans les mesures de niveaux d'eau par GNSS-R, d'où l'hypothèse qu'augmenter la quantité d'antennes pourraient être utilisées pour réduire l'effet de ce bruit. Le chapitre 3 est une preuve de concept pour la technique GNSS-R utilisant un réseau d'antennes à faible coût, tandis que le chapitre 4 se concentre sur le développement d'un algorithme pour la mesure efficace du niveau d'eau. Cette thèse peut servir de guide au développement d'un instrument GNSS-R concret qui ainsi pourrait être utilisé pour améliorer la distribution globale des capteurs de niveau d'eau.

Acknowledgements

Firstly, I would like to thank and acknowledge my PhD supervisor, Dr. Natalya Gomez, for providing guidance and support throughout my thesis program. The commitment that Natalya has shown to her research, in addition to her impressive and numerous achievements to date, has been a constant source of inspiration. I cannot thank her enough giving me the opportunity to work with her and for leading me down the path of observational sea level research (the path that led to me becoming a GNSS-R devotee).

Dr. William Minarik and Gregory Langston have both been influential in the development of my PhD work. Without the enthusiasm that Bill exudes for testing out low-cost equipment for scientific research (and the numerous hours of his free time that he spent building instruments for field work), this thesis would look very different. Much of the field work that forms the basis of the results presented in Chapters 3 and 4 was only possible with assistance from Greg, who also helped me to become less useless in my capacity as a field scientist during this time.

It has been a pleasure to share an office with and get to know the Gomez Geodynamics Group (GGG) members during my PhD. Special thanks go to Holly Han, Anna Hayden, Jeannette Wan, Julia Morales-Aguirre, Erik Chan, Thomas Navarro and everybody else who has put up with my grumpy ramblings whilst working in the same office as me.

I have also been fortunate to work with and co-supervise several students at McGill: Asia Murphy, Isabelle McIntyre, Juan Morency-Trudel, Garrett Kinman and Natalie Hardin. I continue to learn a lot from these students and thank them for their time and patience while working with me.

I am indebted to the staff in the Department of Earth and Planetary Sciences at McGill, namely Kristy Thornton, Anne Kosowski and Angela Di Ninno (RIP), for their constant support and my committee members, Dr. Yajing Liu and Dr. Alfonso Mucci, who have both provided valuable input during my PhD.

Finally, I dedicate this thesis to my family, friends, pets and roommates who have all supported me and kept me sane during this period. Special mentions go to my parents, my brothers, Olly Osborne, George Copsey, Hala Fakhroo, Chris Barclay, Émilie Asselin, Andréane Nadeau, Claire Guimond, Ben Keenan, Pookie (RIP), Sally, Lilo and Scully.

Contribution to Original Knowledge

I confirm that this thesis presents original research and the results of my own work, unless otherwise referenced and acknowledged.

This thesis contributes to the original knowledge of the ground-based interferometric GNSS reflectometry (GNSS-R) technique for monitoring water levels using the Signal to Noise Ratio (SNR) recorded by GNSS receivers. It provides a technique for estimating the sources of uncertainty and total uncertainty in GNSS-R water levels. It details an original technique using multiple co-located low-cost GNSS antennas in the same location to obtain precise water levels. Finally, it also provides an efficient algorithm for in-situ and real-time processing of GNSS-R water levels when using multiple co-located antennas.

Contribution of Authors

This thesis is composed of three manuscripts that I have written as the first author and developed through collaboration with my advisor Natalya Gomez (NG) and colleagues Ngai Ham Chan (NHC), Joakim Strandberg (JS), David M. Holland (DH), Thomas Hobiger (TH), William Minarik (WM), Gregory Langston (GL) and David Porter (DP).

The first manuscript (Chapter 2) has been published as follows: D. Purnell, N. Gomez, N. H. Chan, J. Strandberg, D. M. Holland and T. Hobiger, "Quantifying the Uncertainty in Ground-Based GNSS-Reflectometry Sea Level Measurements," in *IEEE Journal of Selected Topics in Applied Earth Observations and Remote Sensing*, vol. 13, pp. 4419-4428, 2020, doi: 10.1109/JS-TARS.2020.3010413. For this manuscript, the approach to model SNR data to estimate uncertainty was conceptualised by myself, NG and NHC, and refined through discussions with JS, DH and TH. The code to run the model was written by myself, except some that was adapted from code provided by JS (for inverse modelling of SNR data). The writing was done by myself and NG, with comments from the other co-authors.

The introduction to Chapter 3 contains some results from field work in Greenland in June, 2018. The field work was led by NG and DH and the low-cost GPS unit was built by WM.

The second manuscript (Chapter 3) has been published as follows: D. J. Purnell, N. Gomez, W. Minarik, D. Porter, and G. Langston, "Precise water level measurements using low-cost gnss antenna arrays," *Earth Surface Dynamics*, vol. 9, no. 3, pp. 673–685, 2021. The idea of using multiple antennas in the same location was my own. The study was further conceptualized with help from NG and WM. WM designed and built the initial low-cost antenna array (including software). I performed analysis and wrote all codes to go along with the article. GL, DP and myself

built subsequent antenna arrays and performed field work. I wrote the initial article draft and NG, WM and DP helped to improve the article.

The third manuscript (Chapter 4) is currently being prepared for submission to a peer-reviewed journal. The idea of developing software for in-situ and real-time data processing was my own. The software was written and developed by myself. NG and WM helped to guide the analysis. The field work was performed by myself and GL. I wrote the initial article draft and NG, GL and WM helped to improve the article.

The thesis abstract was translated from English to French with help from Juan Morency-Trudel. Overall comments on the thesis provided by Kristine Larson and John Stix helped to improve the thesis.

Table of Contents

Abstract	i
Abrégé	iii
Contribution of Authors	v
Contribution of Authors	vii
Contribution of Authors	viii
List of Figures	xix
List of Tables	xx
1 Introduction	1
1.1 Water levels and their importance	1
1.2 Technology for recording water levels	4
1.2.1 Submersible sensors	6
1.2.2 Non-submersible sensors	7
1.2.3 Satellite measurements	8
1.2.4 Other in-situ water level sensors	8
1.3 Water level monitoring using GNSS-Reflectometry	9
1.4 GNSS and its applications	9
1.4.1 Development of the GNSS-Reflectometry technique	10
1.4.2 Interferometric GNSS-Reflectometry theory	12
1.5 Thesis overview	15

2	Quantifying the Uncertainty in Ground-Based GNSS-Reflectometry Sea Level Measurements	17
2.1	Abstract	18
2.2	Introduction	18
2.3	Error Analysis	21
2.3.1	Observed data	22
2.3.2	Sea level retrieval	23
2.3.3	Synthetic SNR data creation	26
2.3.4	RMSE calculations	30
2.4	Results	33
2.4.1	Observed RMSE	33
2.4.2	Comparison of observed and modeled RMSE	35
2.4.3	Sources of uncertainty	37
2.5	Conclusion and discussion	38
2.6	Supplementary Information	41
3	Precise water level measurements using low-cost GNSS antenna arrays	46
3.1	Abstract	47
3.2	Introduction	48
3.3	Inverse modelling of SNR data using multiple antennas	51
3.4	Instrumentation	55
3.5	Test sites	57
3.6	Results	61
3.6.1	Influence of multiple co-located antennas	62
3.7	Discussion of GNSS-R parameters	64
3.7.1	Elevation angle limits	65
3.7.2	Azimuth angle limits	66
3.7.3	B-spline knot spacing and time window	66
3.7.4	Satellite constellations	67

3.7.5	Temporal resolution of SNR data	67
3.8	Conclusions	68
3.9	Supplementary Information	70
3.9.1	Combined inversion of SNR data from multiple antennas	70
3.9.2	Data processing	71
4	Near real-time water levels for flood monitoring using GNSS-R with multiple low-cost antennas	73
4.1	abstract	74
4.2	Introduction	75
4.3	GNSS-R theory	78
4.4	Real-time data processing	79
4.4.1	Initial GNSS data processing and elevation angle interpolation	81
4.4.2	Analyzing satellite arcs	81
4.4.3	Quality control	83
4.4.4	Tropospheric delay correction	83
4.4.5	Spline fitting using a moving window	84
4.5	Instrumentation	86
4.6	Field work at Saint-Joseph-de-la-Rive	86
4.7	Additional data from Trois-Rivières	88
4.8	Results	89
4.8.1	Performance of moving window algorithm	89
4.8.2	Bias and tropospheric delay	93
4.9	Conclusion and Discussion	94
4.10	Supplementary Material	96
4.10.1	Sensitivity of tropospheric delay correction to atmospheric parameters	96
4.10.2	Elevation angles and satellite orbit data	96
5	Discussion	98

List of Figures

- 1.1 A schematic to show examples of submersible and non-submersible sensors for in-situ water level monitoring (pressure gauge and radar gauge, respectively), as well as a satellite altimeter as an example of instrumentation for remote sensing of water levels. The radar gauge must have a direct view of the water surface, whilst pressure gauges are often installed in stilling wells to limit the influence of short frequency waves on water levels. 5
- 1.2 A map showing stations that contribute data to the Global Runoff Data Center. These stations are used to monitor river discharge, however, the vast majority are water level sensors. Discharge measurements are obtained from water levels using a stage-discharge relationship. This is not a complete map of all the global inland water level sensors, but it is the largest organised global data set. Image retrieved from <https://www.bafg.de/GRDC>. 6
- 1.3 A map showing coastal water level sensors with 40 years or more of data from the Permenant Service for Mean Sea Level (PSMSL). It should be noted that this is not an exhaustive list of all coastal water level sensors because it does not include sensors with less than 40 years worth of data and it also does not include sensors that do not meet the data standards of the PSMSL network. Image retrieved from <https://www.psmsl.org/>. 7

1.4	A schematic to show the ground-based GNSS-Reflectometry technique for monitoring water levels. The two panels show the difference between the technique when using: a) a single upright-pointing geodetic-standard antenna (Larson et al., 2013a) and b) multiple co-located low-cost antennas. The latter is developed through Chapters 3 and 4.	13
1.5	The geometry of ground-based GNSS-Reflectometry. It is shown that the difference in path lengths between the direct and reflected GNSS signal is $2h \sin \theta$, where h is the height of the antenna above the reflecting surface and θ is the elevation angle of the satellite (the angle with the horizon).	14
2.1	Flowchart showing the error analysis process. The two bottom panels show examples of detrended SNR data (Watt/Watt) plotted as a function of $\sin \theta$, where θ is the elevation angle of a satellite relative to an antenna. The observed SNR data is collected at station SC02. The bottom right frame shows three stages of the synthetic SNR data creation process; the black line is the initial output from Nievinski and Larson (2014), the red dotted line has been modulated to account for the dynamic sea surface and the blue line has random noise added to it.	22
2.2	Three days of tide gauge and GNSS-R sea level data at site SC02 when using the high elevation angle interval given in Table 2.1.	26
2.3	Mean values of the LSP for all observed and synthetic SNR arcs at site SC02 high θ	31
2.4	Comparison of observed and modeled RMSE of a. individual measurements, b. daily means and c. monthly means at the sites given in 2.1. The difference between the modeled results is the input sea level data that is used to generate the synthetic SNR data.	34
2.5	The contribution of each source of uncertainty to the total modeled RMSE when using the spectral analysis method to retrieve sea level (top) and when using the inverse method to retrieve sea level (bottom). The total length of each bar corresponds to the values given in the ‘Modeled: tide gauge’ values in Figure 2.4a).	36

2.6	Comparison of tide gauge and GNSS-R sea level measurements at site BUR2 in May 2019.	42
2.7	A comparison of observed tide gauge and GNSS-R sea level measurements at site SPBY.	43
2.8	As in Figure 2.7 a but for modeled SNR data.	43
2.9	Mean values of the LSP for all observed and synthetic SNR arcs at site BUR2. . . .	44
2.10	As in Figure 2.9 a but for site SPBY.	44
2.11	As in Figure 2.9 a but for site SCOA.	45
3.1	An 8-hour comparison of GNSS-R water levels using low-cost and geodetic-standard GPS antennas in Greenland in June, 2018. The water levels are plotted alongside a tidal prediction for reference (Padman and Erofeeva, 2004).	47
3.2	Examples of the interference pattern observed in detrended SNR data as a function of satellite elevation angle for a) one of the GNSS100L antennas used in this study placed approximately 3 m above a water surface and b) a Leica AR25 antenna at site GTGU in Onsala, Sweden situated approximately 4 m above a water surface. The data for site GTGU is available online as part of the study Geremia-Nievinski et al. (2020). The oscillations in b) are dampened with increasing elevation angle whereas in a) the dominant oscillations have an approximately constant amplitude. It should be noted that the low-cost antenna is tilted towards the horizon to maximize its sensitivity to reflected GNSS signals whereas the geodetic-standard antenna is pointed vertically.	57
3.3	Pictures of antenna arrays a) at Trois-Rivières, b) and c) show different angles at Sainte-Anne-de-Bellevue and d) at Piermont. The antenna array showed in b) and c) was also temporarily installed at Trois-Rivières. The antennas are closer together in a) in comparison to the other two setups.	58
3.4	The area surrounding the antenna array and tide gauge at Sainte-Anne-de-Bellevue.	60

3.5	A comparison of GNSS-R and tide gauge measurements at a) Trois-Rivières, b) Sainte-Anne-de-Bellevue and c) Piermont. The mean of each time series is removed before plotting.	61
3.6	Reflector height measurements from four antennas at Sainte-Anne-de-Bellevue. The solid lines represent the b-spline solutions from inverse modelling and the dots are estimates from spectral analysis. The b-spline parameters that are used to plot the solid lines in this figure are averaged to form the single solution in Figure 3.5b. The curves are inverted because reflector height increases as water level decreases.	62
3.7	Comparison of GNSS-R and tide gauge measurements with residuals at a) Trois-Rivières, b) Sainte-Anne-de-Bellevue and c) Piermont, as in Figure 3.5 in the main text but for reduced periods. In each of these figures, the GNSS-R and tide gauge measurements are offset by an arbitrary amount from the residuals. In c), the GNSS-R and tide gauge measurements have been scaled by 0.2 for an easier comparison with the residuals.	72
4.1	Flow chart showing the stages of data processing to obtain water level measurements from the low-cost GNSS antennas using a moving window algorithm. 'QC' stands for quality control and 'TD' stands for tropospheric delay. The details of each step are discussed in Sections 4.4.1 – 4.4.5 and the step 'fit spline to arcs' is visualized in Figure 4.2. For each iteration, water levels (spline nodes) are computed for the previous 8 hours and a water level time series can be constructed from any of these nodes. The most recent node is considered to be a real-time measurement, whilst the other nodes are considered to be post-processing, with up to 8 hours delay from real-time.	80

4.2	An example to show the parameters and outputs for one time step of the moving window algorithm. A spline is used to represent 8 hours of water level changes and is fit to the data from satellite arcs (represented as grey dots by using equation 4.3). The spline is defined by 5 nodes and the water levels between these nodes are obtained using cubic spline interpolation. The dotted black lines mark the beginning and end of the moving window. The node on the leading edge of the moving window is considered to be a real-time measurement, whereas the other points along the spline are considered to be post-processing. A water level time series could be formed by taking a measurement from the same point along the spline at each time step. The moving window algorithm is explained in more detail in Section 4.4.5.	82
4.3	a) A Picture of the site at Saint-Joseph-de-la-Rive and b) a top-down view of the reflection zones from https://gnss-reflections.org/rzones (Roesler and Larson, 2018). In the left picture, the stilling well that contains the pressure gauge can be seen to the left of the tripod, with a padlock attached to it. The different coloured ellipses refer to reflection zones from satellites at an elevation of 5, 10 and 15 degrees (yellow, blue and red, respectively).	88
4.4	Water levels from GNSS-R and co-located pressure gauge at Saint-Joseph-de-la-Rive and Trois-Rivières. The GNSS-R water levels are constructed from the "optimal node" of the moving window algorithm labelled in Figure 4.2 (4 hours delay from real-time). At Saint-Joseph-de-la-Rive, the water levels are relative to chart datum and at Trois-Rivières, the datum is arbitrary as both pressure gauge and GNSS-R levels have had the mean removed for comparison.	91

4.5	The RMSE of GNSS-R water levels when compared to co-located pressure gauges at Saint-Joseph-de-la-Rive and Trois-Rivières as a function of the time delay after which the GNSS-R water levels are processed. The time delay of 0 minutes corresponds to the a time series being formed using the "real-time node" labelled in Figure 4.2. Whereas, a time delay of 240 minutes at Saint-Joseph-de-la-Rive corresponds to the "optimal node" labelled in Figure 4.2. The limits on the x-axis are different between the two sites because the node spacing is different between the two sites, as explained in Sections 4.6 and 4.7.	92
4.6	GNSS-R water level measurements at Saint-Joseph-de-la-Rive from the moving window algorithm. The real-time water levels are constructed from the "real-time node" labelled in Figure 4.2, while the near real-time water levels are post-processed with an hour delay from real-time.	93
4.7	Van de Casteele diagrams showing the effect of tropospheric delay (TD) on the GNSS-R water level measurements (pink dots) at Saint-Joseph-de-la-Rive. The error is the difference between surveyed levels from GNSS-R and pressure gauge measurements. Deviations from the solid vertical line at 0 cm error suggest a bias.	94
4.8	Tropospheric delay corrections produced for different geometrical and environmental parameters using the methodology of Nikolaidou et al. (2021). The pink dots refer to control values for each parameter that are fixed whilst the others are varied. The relative humidity is given for reference as it is a standard parameter recorded by weather stations, but it is not independent from temperature and partial pressure of water vapor, hence it is shown in black.	97

List of Tables

1.1	A comparison of commercial water level sensors. The estimated cost is a rough guide adapted from (IOC, 2006). The accuracy and precision may depend on the cost of the instrument. The cost of a pressure transducer is highly variable because they are prone to long term drift and the more costly instruments are designed to reduce this effect.	6
2.1	Key parameters for the two sites used.	24
2.2	Details of the instrumentation and other parameters used at additional sites.	42
2.3	Observed and modeled RMSE at sites BUR2, SPBY and SCOA for the month of May 2019.	42
3.1	Information about the three test sites. 'SAB' refers to Saint-Anne-de-Bellevue. Antenna heights refer to mean heights above the water surface.	58
3.2	Summary of results obtained using different combinations of antennas to retrieve water level measurements. For 1–3 antennas, the RMSE for every combination of antennas at each site was calculated but only the lowest and highest values are shown in the table.	63

Chapter 1

Introduction

1.1 Water levels and their importance

The sea surface is not stationary. An observer standing at the coast will likely notice waves caused by the interactions between the atmosphere and the sea surface. If they remained there long enough, they would likely notice changes in the mean water level that the waves are superimposed upon - tides, that reach a high and low point at most locations every 12 hours. If the observer was to return to the same location for decades, they may notice that the mean water level that the tides are superimposed upon has risen. In a different location, the observer may see tides that reach a high and low point once in 24 hours or they may observe a fall in mean sea level over decades. A lakeside or riverside observer will notice changes in water levels that are more controlled by weather events (e.g., precipitation and wind) that occur on timescales of up to several days. These water levels, and the many spatiotemporally variable processes that control them, are important to monitor not only out of scientific interest, but also because humans rely on understanding them for their livelihoods. For example, knowledge of local tides is often essential for fishing, whilst monitoring the supply of fresh water to reservoirs is critical for maintaining hydroelectric dams that provide power for approximately 20% of the global population (Lehner et al., 2011). In more extreme cases, storm surges, tsunamis and river floods have the potential to devastate local commu-

nities and mean sea level rise may contribute to a future global climate migration crisis (Nicholls et al., 2011; McLeman, 2018).

Tides, caused by the gravitational interaction between the ocean, the sun and the moon, have long been a subject of human interest due to their importance for navigating the sea, for example for fishing and trading (Cartwright, 2001). The earliest known example to demonstrate an understanding of tides dates back over 3500 years ago, to a tidal dock that was built in India to keep ships afloat during low tide (Panikkar and Srinivasan, 1971). Progress toward developing a more complete understanding of tides was relatively slow and the first record of a local tidal prediction chart dates back to over 4000 years later, in the 11th century in China (Zuosheng et al., 1989). Today, sophisticated models are used to predict tides at different locations that are based largely on observations of water levels (Egbert and Ray, 2017) and these models support navigation for global shipping routes, which form the backbone of the global supply chain.

A more contemporary interest in coastal water levels is to monitor the threat posed by changes in mean sea level. The rate of global mean sea level rise has been accelerating over the past 100 years (Pörtner et al., 2019; IPCC, 2021), from approximately 1.3 mm yr^{-1} during 1901 – 1971, to 1.9 mm yr^{-1} from 1971 – 2006, to 3.7 mm yr^{-1} from 2006 – 2018 (IPCC, 2021). Approximately 680 million people (10% of the global population) currently live in low-lying coastal zones that are vulnerable to the effects of sea level rise and this population is expected to almost double by 2050 (Pörtner et al., 2019). Flooding events are increasingly common with sea level rise (Taherkhani et al., 2020) and it is predicted that at least 300 million people will be living within the floodplain for 100-year storm surge events (i.e., storm surges that are likely to happen once in 100 years) by 2060 (Neumann et al., 2015). The combination of sea level rise with issues such as coastal erosion, land loss and increased frequency of extreme events has led to the prediction that annual coastal flood damages will increase by 2 – 3 orders of magnitude by 2100 compared to today (Pörtner et al., 2019).

The dominant contribution to current and future sea level change is expected to be from ice sheets losing mass to the ocean (Pörtner et al., 2019; IPCC, 2021) and yet the response of the ice sheets to the changing climate in Greenland and Antarctica remains uncertain and relies on un-

derstanding the complex interactions and feedbacks that arise between the ice and the surrounding atmosphere, ocean and solid Earth (Golledge et al., 2019; Pattyn and Morlighem, 2020; Goelzer et al., 2020; Seroussi et al., 2020; Gomez et al., 2015). Alarmingly, a mechanism has been proposed through which large tidewater glaciers could rapidly lose mass to the ocean and cause a far greater rise in sea level than what would be predicted otherwise (Pollard et al., 2015; DeConto et al., 2021). There is evidence of rapid sea level change in paleo sea level records that could be corroborated by this mechanism (Dutton et al., 2015). Further complications in predicting the impacts of future ice loss arise from the non-uniform spatial pattern of sea level change that occurs when ice sheets lose mass, due to solid earth deformation and a combination of gravitational and rotational effects (Mitrovica et al., 2009). As an ice sheet loses mass, sea level falls in close proximity to the ice sheet (within ~ 2000 km) and rises at a greater distance from the ice sheet. The magnitude of the sea level fall close to the ice sheet is much greater than the rise in sea level further away (Gomez et al., 2010), hence sea level measurements in close proximity to a melting ice sheet could theoretically be used to help constrain rates of ice mass loss.

Cryospheric and other climate-related changes are also expected to have an impact on inland hydrology. For example, winter runoff (the melting of snow that has accumulated over winter) is expected to increase in magnitude and peak earlier in spring (Pörtner et al., 2019). At the time of writing, the snowpack in parts of Canada is the largest it has ever been (Water Resources Branch, Department of Environment, Government of Yukon, 2022). Precipitation is expected to increase in high latitudes and extreme precipitation events are expected to become more frequent in most parts of the world as the climate warms (IPCC, 2021). On the other hand, increased evapotranspiration, associated with warmer weather and increased droughts in some parts of the world (IPCC, 2021), poses a risk to water security and it is already estimated that four billion people have severe issues with water availability for at least one month per year (Mekonnen and Hoekstra, 2016). The combination of these factors will place an unprecedented stress on rivers and lakes that is difficult to predict.

Research in the fields of tides, mean sea level change and hydrology has traditionally been carried out independently, but recent interdisciplinary research has highlighted their interconnec-

tions. For example, flooding events are likely to become more intense due to both sea level rise and increased tide and storm surge events (compound flooding events) (Kirezci et al., 2020). Other recent studies have highlighted the importance of interactions between mean sea level change and tides (Devlin et al., 2017; Talke and Jay, 2020; Hayden et al., 2020) and tides and the Antarctic ice sheet (Richter et al., 2022).

It is critical to monitor both coastal and inland water levels to study the processes discussed above and to guide climate adaptation efforts. Additionally, water levels are necessary on a more operational basis to alert people to the dangers of flooding and to guide safe marine navigation. Yet, as discussed in the following section, we have an incomplete picture of global water levels, owing to various issues with the water level sensor technology that is currently used. This thesis aims to introduce a new technique for monitoring water levels that could be used to build a more complete global picture of ongoing and future changes and the processes that drive them.

1.2 Technology for recording water levels

Continuous records of coastal water levels date back to 1700 (van Veen, 1945) and there are numerous examples of tide gauge records that last for over 100 years (Talke et al., 2018; Marcos et al., 2021). During this time, many different instruments for monitoring water levels have been developed. The most simple water level sensor is a staff gauge, a stick submerged in water with labelled markings (i.e., like a large ruler). This works very well for monitoring water levels except that it requires someone to be physically present to record the levels. The first automatically recording water level sensors were mechanical systems that consisted of a float in a stilling well attached to a marker to track changes as the float moves up and down.

Today, commercial water level sensors can be classed into two main categories: submersible and non-submersible. As shown in Figure 1.1, both types of sensors can be challenging to install outside of populated areas because they often require infrastructure such as a pier to be installed on or a stilling well to be housed in (Hersch, 2008). In addition to the difficulties and costs associated with installation, it can also be challenging and expensive to maintain the sensors depending on

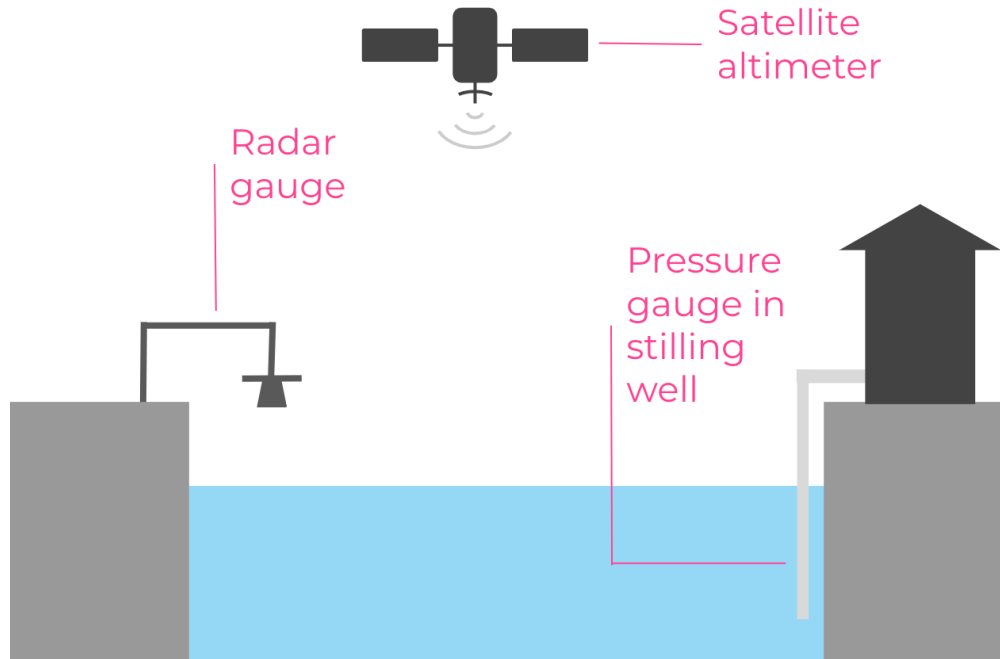


Figure 1.1: A schematic to show examples of submersible and non-submersible sensors for in-situ water level monitoring (pressure gauge and radar gauge, respectively), as well as a satellite altimeter as an example of instrumentation for remote sensing of water levels. The radar gauge must have a direct view of the water surface, whilst pressure gauges are often installed in stilling wells to limit the influence of short frequency waves on water levels.

the type (as summarized in Table 1.1 and as will be discussed in the following sections). As such, the global distribution of water level sensors around both inland waters and coasts is highly biased towards populated areas. This bias can be seen in Figure 1.2, where it is shown that many of the sensors in areas of Africa, Central Asia and South America are not currently active. There is also a bias of coastal water level sensors toward populated areas in the Northern Hemisphere, as shown in Figure 1.3. Another important feature of Figure 1.3 is the lack of water level sensors in the polar regions, especially in Greenland, Antarctica and large parts of Arctic Canada. As explained in the previous section, these regions are especially vulnerable to the effects of climate change. Hence, new technology is needed to improve the global coverage of water level sensors that is easier to install and maintain relative to the current state of the art technology.

Table 1.1: A comparison of commercial water level sensors. The estimated cost is a rough guide adapted from (IOC, 2006). The accuracy and precision may depend on the cost of the instrument. The cost of a pressure transducer is highly variable because they are prone to long term drift and the more costly instruments are designed to reduce this effect.

Sensor type	Estimated cost (USD)	Accuracy	Installation notes
Pressure transducer	1,000 – 30,0000	< 1 cm	In stilling well or on floor with cable to shore
Bubbler gauge	5,000 – 20,0000	< 1 cm	Requires gas supply
Radar	5,000 – 20,0000	< 1 cm	Requires direct view of water surface

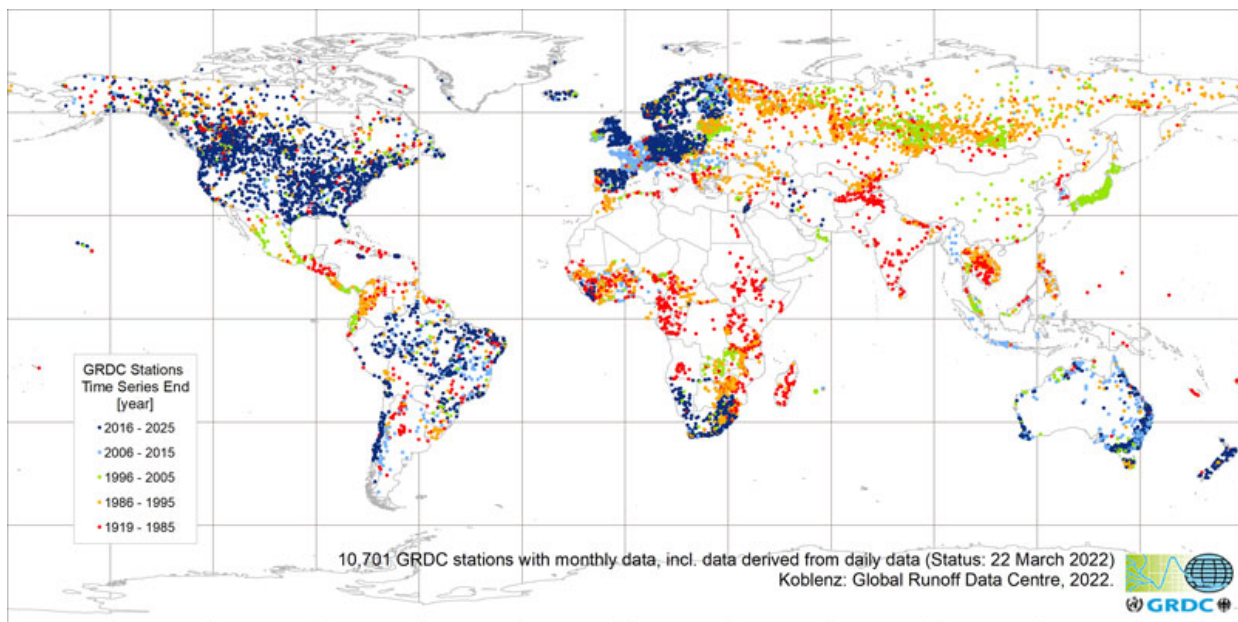


Figure 1.2: A map showing stations that contribute data to the Global Runoff Data Center. These stations are used to monitor river discharge, however, the vast majority are water level sensors. Discharge measurements are obtained from water levels using a stage-discharge relationship. This is not a complete map of all the global inland water level sensors, but it is the largest organised global data set. Image retrieved from <https://www.bafg.de/GRDC>.

1.2.1 Submersible sensors

The majority of global water level sensors are submersible sensors (Hersch, 2008). The accuracy of these instruments vary (along with the cost) but they are generally claimed to have mm-scale precision. Examples of submersible sensors are pressure transducers and bubbler gauges. Sub-



Figure 1.3: A map showing coastal water level sensors with 40 years or more of data from the Permanent Service for Mean Sea Level (PSMSL). It should be noted that this is not an exhaustive list of all coastal water level sensors because it does not include sensors with less than 40 years worth of data and it also does not include sensors that do not meet the data standards of the PSMSL network. Image retrieved from <https://www.psmsl.org/>.

mersible sensors suffer issues with instrument drift (Míguez et al., 2005; Pytharouli et al., 2018), they need to be cleaned often and they are vulnerable to be damaged or moved during flooding conditions or by ice (Asante et al., 2007; Pomeroy et al., 2016; Apel et al., 2022). Pressure gauges also need to be corrected for changes in atmospheric pressure, temperature and salinity effects (Hersch, 2008). Crucially, installing submersible gauges often requires for field engineers to physically get in water for the installation, which makes installation and maintenance challenging or potentially dangerous.

1.2.2 Non-submersible sensors

Examples of non-submersible sensors are radar and acoustic sensors. These instruments do not need to be submerged in water, but they need to be hanging directly over the water surface. Like pressure gauges, these instruments also boast mm-scale accuracy, but they tend to be considerably

more expensive than submersible gauges (GLOSS, 2012) and can only be installed where there exists infrastructure for them to hang from. This may sound trivial, but it is not practical to install a radar sensor on a rocky coastline, for example.

1.2.3 Satellite measurements

Satellite altimeters are used to form a global picture of water levels or topography from space. A traditional radar altimeter, such as TOPEX/POSEIDON or the subsequent Jason satellite series, consists of a radar pointing downward towards earth (i.e., at the nadir) to send and receive microwave pulses (just like a radar gauge). The altitude of the surface below the satellite is inferred from the orbit of the satellite and the time it takes for the microwave pulses to reflect back from Earth. Whilst satellite altimetry missions have provided the first global picture of mean sea level change (Leuliette et al., 2004) and some of the most compelling evidence that global mean sea level rise is accelerating (Nerem et al., 2018; Cazenave et al., 2018), the radar altimeter measurements are limited in that they only provide information about a small area on Earth at one time. Furthermore, it may take days or weeks for the altimeter to return to the same point on Earth for successive measurements and the measurements tend to be poor near the coast and for monitoring rivers and lakes. The Surface Water and Ocean Topography Satellite (SWOT), planned for launch in November 2022, boasts improved capability for coastal and inland water level monitoring (Durand et al., 2010). Regardless, satellite measurements do not currently provide a comprehensive solution to global water level monitoring, especially at the local level.

1.2.4 Other in-situ water level sensors

There are other types of in-situ water level sensors that are less widely used or available. One example that has been developed recently is a camera combined with a staff gauge to automatically monitor water levels (Kim et al., 2014; Zhang et al., 2019). This technique has the advantage of being built from commercially available parts and being relatively low-cost. The camera is installed

out of water, but the staff gauge must be submerged in water and hence this technique suffers from some of the same issues as for other submersible sensors.

Another alternative technique for in-situ water level monitoring that has gained popularity recently relies on Global Navigation Satellite System (GNSS) technology (Larson et al., 2013a). This non-intrusive technique for water level monitoring is called GNSS-Reflectometry and is the focus of this thesis.

1.3 Water level monitoring using GNSS-Reflectometry

To understand the concept of GNSS-Reflectometry (GNSS-R) first requires some understanding of the concept of GNSS. In this section we begin with an introduction to GNSS, before providing an overview of relevant GNSS-R literature and finally some fundamental theory on GNSS-R water level monitoring that is used throughout this thesis.

1.4 GNSS and its applications

The concept of GNSS is based on triangulation; to use the position of satellites orbiting earth to infer a position on the Earth. This concept was first brought into fruition by the US Global Positioning System (GPS), for which the first satellite was launched in 1978, followed by the Russian GLONASS system, for which the first satellite was launched in 1982. The use of GPS was primarily intended for the military, but the usefulness for the wider population quickly became apparent after it became operational. GNSS technology is now ubiquitous, with the most common application today being in cell phones. Given the success of the GNSS concept, other countries have recently launched their own systems, most notably the Galileo system of the European Union and the Chinese BeiDou system.

GNSS instruments have also been widely applied for scientific research. For example, geophysical phenomena such as plate tectonics or glacial isostatic adjustment can be monitored using precise positioning from GNSS instruments with mm-scale accuracy (Wang et al., 2001; Khan

et al., 2016). This level of accuracy is impressive given the relative scale of the GNSS satellite orbits (approximately 20,000 km above the Earth's surface). There have also been some less intuitive applications of GNSS in remote sensing, such as for meteorology and space weather (Jin et al., 2014). These applications take advantage of modifications to the path and propagation speed of GNSS signals as they pass through the atmosphere. These modifications cause a delay in the arrival of the GNSS signals compared to what would be expected if they were traveling through a vacuum. The amount of delay depends on the refractivity of the troposphere (pressure, temperature and moisture content) and the electron density in the ionosphere. The state of the atmosphere can therefore be inferred by the time that GNSS signals are received compared to when they were transmitted by the satellites.

1.4.1 Development of the GNSS-Reflectometry technique

The idea of GNSS-Reflectometry (GNSS-R) was first proposed as a solution for increasing the spatial coverage of satellite altimetry measurements (Martin-Neira et al., 1993). Instead of sending and receiving microwave pulses (as described in Section 1.2.3), an instrument was proposed to analyze signals emitted from GPS satellites. This instrument, named the Passive Reflectometry and Interferometry System (PARIS), receives signals that travel directly from a GPS satellite as well as signals that reflect off the surface of the Earth. The delay and doppler shift of the reflected signal relative to the direct signal is used to infer the altitude of the surface at the location of reflection. The spatial coverage of measurements is an improvement upon that of radar altimeters because signals from multiple GPS satellites can be analyzed at the same time. This PARIS concept is simple, but specialized instrumentation is required to separate the direct and reflected signals. Spaceborne GNSS-R altimetry has now been explored in great detail for nearly 30 years (Ruffini et al., 2004; Rius et al., 2010; Pascual et al., 2014) and there are several active satellites for GNSS-R remote sensing, including the Cyclone Global Navigation Satellite System (CYGNSS) (Ruf et al., 2012) and Spire constellation (Masters et al., 2020). Aside from altimetry, the spaceborne GNSS-R concept has proven to be useful for other remote sensing opportunities, including surface wind speed, soil moisture, sea ice detection and canopy cover (Jin et al., 2014).

An alternative GNSS-R approach using ground-based instrumentation was proposed in the year 2000 (Anderson, 2000). Rather than trying to directly analyse the reflected GNSS signals (i.e., the PARIS technique), the author made use of the pattern resulting from interfering direct and reflected signals to infer water levels, which could be seen in the Signal-to-Noise Ratio (SNR, a standard parameter recorded by GNSS receivers). The author compared their "interferometric GPS tide gauge" measurements with a collocated NOAA tide gauge in San Diego and found a standard deviation between the measurements of less than 12 cm. The major innovation of this approach, as noted by the author, was the ease-of-installation of the system and the fact that no special instrumentation was required (a commercial GNSS receiver and a laptop computer). However, It should be noted that the GNSS antenna was pointed towards the horizon by 20 degrees in order to maximise the sensitivity to reflected GNSS signals and this change in orientation degrades the performance of the antenna for positioning applications. This study was largely overlooked for over 10 years, during which there were other ground-based GNSS-R altimetric studies, but they were either variations of the PARIS approach or they required additional specialist instrumentation (Treuhaft et al., 2001; Caparrini et al., 2003; Rivas and Martin-Neira, 2006; Löfgren et al., 2011).

In 2007, Bilich and Larson showed that SNR data from a standard upright-pointing GNSS antenna could be used to infer information about the surrounding environment. Whilst the technique proposed by Anderson (2000) relied on ray tracing of direct and reflected signals, Bilich and Larson (2007) simplified the problem by showing that the height of the antenna above the reflecting surface is related to the frequency content in the SNR data. This SNR-based technique with an upright antenna was then applied for soil moisture monitoring (Larson et al., 2008), snow depth monitoring (Larson et al., 2009) and water level monitoring (Larson et al., 2013a). A schematic to help visualize the geometry of this technique for monitoring water levels is given in Figure 1.4 a. This technique, now commonly referred to as GNSS Interferometric Reflectometry (GNSS-IR), has since been studied in great detail (Löfgren et al., 2014; Santamaría-Gómez et al., 2015; Strandberg et al., 2016; Larson et al., 2017) and is the focus of this thesis. More recently, this technique has been applied using compact low-cost GNSS antennas (such as the ones that are embedded in mobile devices) with great success (Fagundes et al., 2021; Karegar et al., 2021; Williams et al.,

2020; Purnell et al., 2021). The authors of these recent studies all found a similar if not better precision of GNSS-R water levels when using low-cost antennas compared to what would be expected when using geodetic-standard antennas (i.e, the types of antennas used by Anderson (2000) or Larson et al. (2013a)). A novel technique for water level monitoring using multiple co-located low-cost antennas will be presented in Chapters 3 and 4, as shown in Figure 1.4b. It should be noted that the low-cost devices do not perform as well as the geodetic instruments for positioning applications.

1.4.2 Interferometric GNSS-Reflectometry theory

Microwaves emitted from GNSS satellites may reach a GNSS antenna either directly or indirectly after reflecting off a nearby surface. The difference in the direct and indirect path lengths changes as a satellite moves relative to the antenna and this causes the signals to interfere: when the signals arrive at the antenna in phase the signal is strong and when they are out of phase the signal is weak. This effect, known as multipath, can lead to undesirable positioning errors and various techniques have been developed to reduce these errors (Braasch, 1994). However, this interference can also contain useful information about the surrounding environment (Bilich and Larson, 2007).

For ground-based GNSS-R, it is a very good approximation that the direct and reflected paths of GNSS signals are parallel (prior to reflection). It can therefore be shown using trigonometry (see Figure 1.5) that the difference between the direct and reflected path lengths is given by $2h \sin \theta$ (Georgiadou and Kleusberg, 1988), where h is the difference in height between the antenna and the reflecting surface (henceforth, the reflector height) and θ is the angle between the horizon and the satellite from the point of view of the antenna. In the case of signals reflecting off a water surface, the reflector height increases as the water level decreases and vice versa. As the satellite moves relative to the antenna, θ changes, the path length difference changes and hence the signals move in and out of phase in a predictable way. The phase difference between the direct and reflected signals, or the interferometric phase, is given by

$$\phi_i = \frac{4\pi h}{\lambda} \sin \theta \quad (1.1)$$

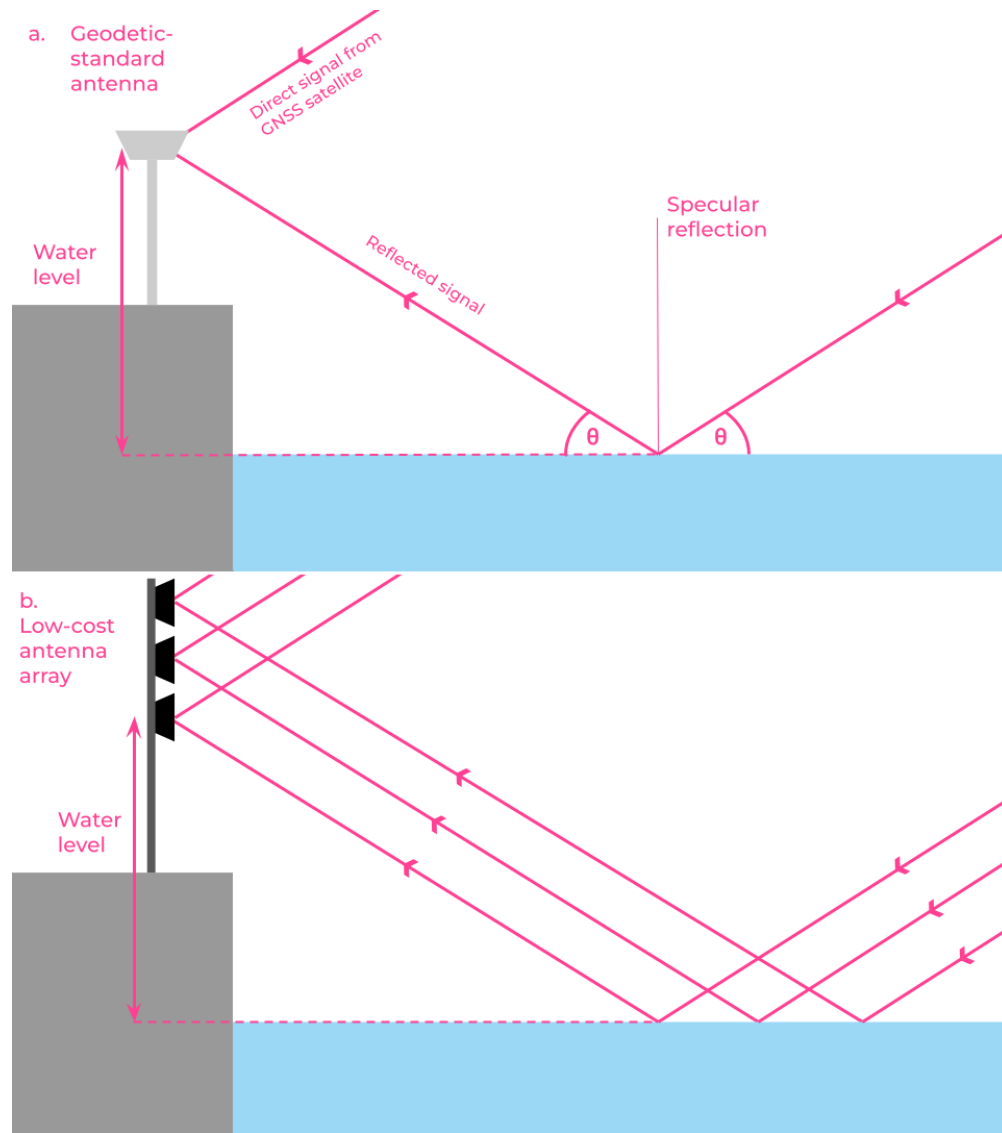


Figure 1.4: A schematic to show the ground-based GNSS-Reflectometry technique for monitoring water levels. The two panels show the difference between the technique when using: a) a single upright-pointing geodetic-standard antenna (Larson et al., 2013a) and b) multiple co-located low-cost antennas. The latter is developed through Chapters 3 and 4.

where λ is the carrier wavelength of the GNSS signal (approximately 19 cm for the legacy GPS L1 coarse/acquisition code). Given that a water surface is a good reflector of microwaves, the interference manifests itself as an oscillation in the strength of the received signal, which is recorded using the SNR. The oscillation is superimposed on a long period variation due to the changing distance between the antenna and the satellite and the antenna gain pattern. The long period variation can

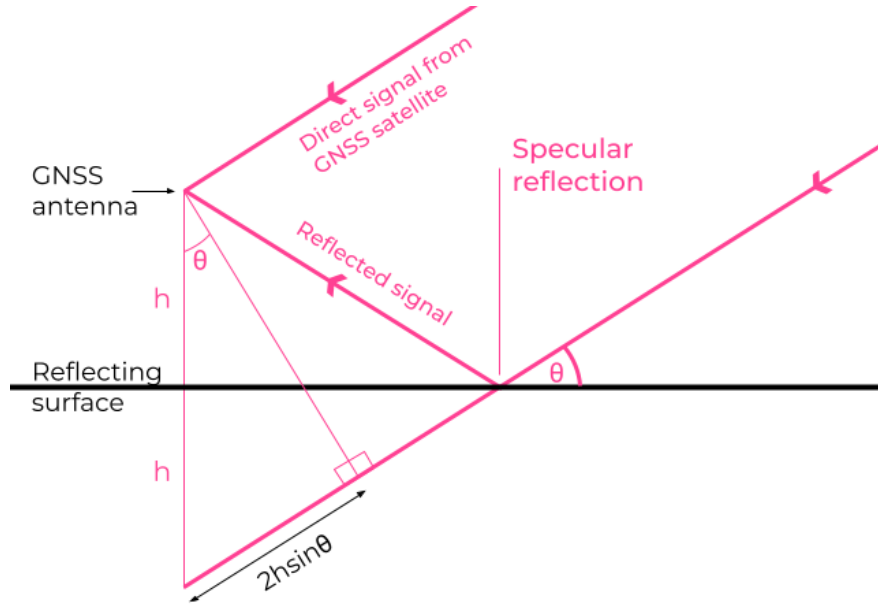


Figure 1.5: The geometry of ground-based GNSS-Reflectometry. It is shown that the difference in path lengths between the direct and reflected GNSS signal is $2h \sin \theta$, where h is the height of the antenna above the reflecting surface and θ is the elevation angle of the satellite (the angle with the horizon).

be removed by detrending the SNR data (removing a low order polynomial) (Larson et al., 2013a). The detrended SNR data can then be approximately represented by

$$\delta \text{SNR} = A \cos \left[\frac{4\pi h}{\lambda} \sin \theta + \phi_0 \right] \quad (1.2)$$

where A is the amplitude of the oscillations and ϕ_0 is a phase offset. Both A and ϕ_0 are not constants, they depend on environmental and instrument specific factors, such as the roughness or dielectric constant of the reflecting surface and the antenna gain pattern (Nievinski and Larson, 2013).

If δSNR is plotted as a function of $\sin \theta$ and h is assumed to be independent of $\sin \theta$ then

$$f = \frac{2}{\lambda} h \quad (1.3)$$

where f is the frequency of the oscillations. This useful approximation implies that the frequency of the oscillations scales linearly with h . However, both h and θ are changing in time and are therefore not independent. They are related using

$$2\pi f = \frac{\partial \phi_i}{\partial \sin \theta} = \frac{\partial \phi_i / \partial t}{\partial \sin \theta / \partial t} \quad (1.4)$$

and hence below (initially derived by Larson et al. (2013b)),

$$f = \frac{2}{\lambda} \left[h + \frac{\partial h}{\partial t} \frac{\tan \theta}{\partial \theta / \partial t} \right]. \quad (1.5)$$

The relationship between the h and f has recently been further developed to account for the acceleration of the reflecting surface (Tabibi et al., 2020). However, this correction is assumed small and is not applied in this thesis..

The reflector height, h , can be retrieved from the SNR by using two distinct techniques, both of which feature throughout this thesis. The first technique involves analysing the frequency content of δSNR using spectral analysis (Larson et al., 2013b). The dominant frequency obtained by spectral analysis is assumed to be f in Equation 1.5 and h can then be estimated. The second technique involves modelling δSNR using a modified version of equation 1.2 and then retrieving h by fitting the observed and modelled δSNR .

1.5 Thesis overview

The purpose of this thesis is to provide a new technique for monitoring water levels that could be used to improve the global distribution of water level sensors. The GNSS-R technique proposed by Larson et al. (2013a), who used a coastal GNSS antenna for monitoring sea level, is fit for this purpose. Commercially available pressure gauges or radar gauges are not practical to install in remote regions, for the reasons discussed in Section 1.2, whereas a coastal GNSS antenna can be easily installed on rocky coastline. However, the accuracy of GNSS-R measurements, such as those obtained by Larson et al. (2013a), is not as good as that obtained when using commercial water

level sensors (cm-scale as opposed to mm-scale) and the geodetic-standard GNSS instruments are more expensive than most submersible gauges, thus limiting their accessibility.

To adapt the GNSS-R technique for widespread operational use, this thesis aims to develop a new technique that is more accurate and more accessible (lower cost) in comparison to previously developed techniques. Chapter 2 contains an investigation into the sources and quantification of uncertainty in GNSS-R water levels, whilst Chapters 2 and 3 contain a description of a novel technique for obtaining water levels using multiple low-cost GNSS antennas, as shown in Figure 1.4.

Chapter 2

Quantifying the Uncertainty in Ground-Based GNSS-Reflectometry Sea Level Measurements

This Chapter is a general analysis of the sources of uncertainty in GNSS-R water levels, using techniques and instrumentation similar to that initially used by Larson et al. (2013a). The purpose of this study is twofold:

1. To provide a technique for estimating the uncertainty in water levels at a site where there is no co-located sensor for validation
2. To investigate the contribution of different sources of uncertainty to the total uncertainty in GNSS-R water levels.

The technique presented relies on modelling SNR data using a model developed by Nievinski and Larson (2013) and comparing the modelled data with observations at two different sites. The results from this chapter were crucial in guiding the direction of subsequent research detailed in Chapters 3 and 4.

2.1 Abstract

Global Navigation Satellite System Reflectometry (GNSS-R) tide gauges are a promising alternative to traditional tide gauges. However, the precision of GNSS-R sea level measurements when compared to measurements from a co-located tide gauge is highly variable, with no clear indication of what causes the variability. Here we present a modelling technique to estimate the precision of GNSS-R sea level measurements that relies on creating and analyzing synthetic Signal-to-Noise-Ratio (SNR) data. The modelled value obtained from the synthetic SNR data is compared to observed RMSE between GNSS-R measurements and a co-located tide gauge at five sites and using two retrieval methods: spectral analysis and inverse modelling. We find that the inverse method is more precise than the spectral analysis method by up to 60% for individual measurements but the two methods perform similarly for daily and monthly means. We quantify the contribution of dominant effects to the variations in precision and find that noise is the dominant source of uncertainty for spectral analysis whereas the effect of the dynamic sea surface is the dominant source of uncertainty for the inverse method. Additionally, we test the sensitivity of sea level measurements to the choice of elevation angle interval and find that the spectral analysis method is more sensitive to the choice of elevation angle interval than the inverse method due to the effect of noise, which is greater at larger elevation angle intervals. Conversely, the effect of tropospheric delay increases for lower elevation angle intervals but is generally a minor contribution.

2.2 Introduction

Tide gauges provide records of coastal sea level change that extend back in some cases to the 18th century (Woodworth, 1999). The longevity of these records highlights the abnormality in the recent acceleration of global mean sea level rise and thus these records provide key evidence for human-induced climate change (Church and White, 2011; Hay et al., 2015). Whilst the capability for monitoring global sea level has greatly improved with the development of satellite altimetry, tide gauges remain at the core of modern sea level observations, both for providing continuous coastal sea level records and for validating satellite altimetry missions (Watson et al., 2015). Despite

their advantages, tide gauge records suffer from limited global coverage in remote regions and are prone to misinterpretation due to the effect of vertical land motion (Church and White, 2011; Santamaría-Gómez et al., 2012). To monitor the effects of vertical land motion, the Global Sea level Observing System (GLOSS) implementation plan (GLOSS, 2012) requires new tide gauges to be installed with a co-located Global Navigation Satellite System (GNSS) station. However, recent work has shown that a coastal GNSS station may also be used as a tide gauge to directly monitor sea level, using a technique called GNSS-Reflectometry (GNSS-R) (Larson et al., 2017). Compared to acoustic or radar tide gauges, these instruments are similar in cost but more practical to install and maintain in remote regions because they can be installed several meters away from the coast and do not need to be hanging directly over the sea surface. If GNSS-R methods are improved, a stand-alone coastal GNSS station may be sufficient to meet the GLOSS requirements, thus greatly reducing installation and maintenance costs.

A GNSS-R sea level time series obtained in previous literature may consist of approximately 20-100 measurements per day at unevenly spaced time intervals with a precision of 2-50 cm (Larson et al., 2013b, 2017; Löfgren et al., 2014; Strandberg et al., 2016; Reinking, 2016) (it should be noted that some of these results could be improved using updated techniques from more recent literature). This temporal and spatial resolution is sufficient to monitor storm surges (Peng et al., 2019) and resolve tides (Larson et al., 2013b, 2017; Löfgren et al., 2014) but it is probably not sufficient for tsunami early-warning systems. With tides resolved, it is possible to remove them in order to form a time series of daily or monthly means that may then be used to study seasonal or multi-year trends. In Larson et al. (2017), the authors compared GNSS-R sea level measurements to those from a standard tide gauge over a 10 year period and found a Root Mean Square Error (RMSE) of 1-2 cm for daily and monthly mean measurements. This was sufficient to estimate a linear annual trend with sub-mm precision, which is the desired resolution for studies of sea level rise (GLOSS, 2012). However, GLOSS stations are required to provide hourly sea level measurements with 1 cm accuracy - a feat that is yet to be achieved at any GNSS station.

On the path towards the integration of GNSS-R tide gauges into the global sea level monitoring network, two key issues remain. Firstly, literature to date is focused on the precision as opposed

to the accuracy of sea level measurements because the vertical datum, assumed to be the antenna phase centre, is generally unknown. A procedure to determine the location of the antenna phase center must be developed such that sea surface height above the reference ellipsoid can be monitored and compared with satellite altimetry measurements. Secondly, it is challenging to evaluate the precision of sea level measurements at sites with no co-located tide gauge and the causes for the highly variable precision at different sites is unclear. In the present paper, we address the latter issue, by providing a technique to estimate the precision at any site and using any retrieval method.

One method to retrieve sea level measurements from a coastal GNSS antenna is via spectral analysis of the Signal-to-Noise-Ratio (SNR) data for periods when the antenna is receiving reflected signals from a satellite. A number of factors have been identified to influence the precision when using this approach. For example, Larson et al. (2013b) and Löfgren et al. (2014) showed that it is necessary to correct for the movement of the sea surface during the time that the SNR data is collected and found an improvement in the precision of sea level measurements in doing so. More recently, Williams and Nievinski (2017) and Santamaría-Gómez and Watson (2017) have shown that the effect of tropospheric delay may lead to bias in sea level retrievals.

Inverse modelling of SNR data is a fundamentally different approach to obtaining GNSS-R sea level measurements. As opposed to using an isolated period of SNR data from a particular satellite to obtain a single measurement, this approach uses SNR data from multiple satellites over a given time frame to obtain a sea level time series, thereby reducing the effect of noisy measurements. In Strandberg et al. (2016), the authors developed an inverse method that produced a sea level time series in the form of a continuous b-spline curve and found an improvement in the precision compared to spectral analysis. A similar approach was taken in Reinking (2016), who used global optimization based on interval analysis to fit the SNR data and found an improvement in both the precision and the computation time in their analysis compared to spectral analysis. A rigorous forward model to produce synthetic SNR data has been developed by Nievinski and Larson (2013) and used to retrieve snow depth measurements via inverse modelling (Nievinski and Larson, 2014b; Tabibi et al., 2017), but this approach has not yet been applied to sea level measurements.

The forward modelling approach has also been applied to error analysis of GNSS-R snow depth and soil moisture measurements in Nievinski and Larson (2014a) and Tabibi et al. (2015). However, they do not consider all sources of uncertainty that apply to sea level measurements, such as the effect of a non-stationary reflecting surface. Least squares adjustment techniques, such as used in Strandberg et al. (2016) and Reinking (2016) have built-in error estimation, but these values are unreliable without comprehensive knowledge of the local environment and instruments that would be needed to build error covariance matrices.

We build on previous work and provide a more versatile error analysis technique that relies on forward modelling of SNR data. Our technique is validated by using two different retrieval methods at four sites with co-located tide gauges and comparing our estimated precision with the observed precision of the GNSS-R measurements relative to the tide gauge. A year of data is analyzed for the two sites that are discussed in the main text and a month of data is analyzed at three sites in the supplementary information. For the main sites, precision is evaluated for individual measurements as well as for calculated daily and monthly means. We also use our technique to quantify the different sources of uncertainty and a discussion of how they lead to variations in the precision.

2.3 Error Analysis

Figure 2.1 describes the process of obtaining estimates of the precision of sea level measurements and quantifying the sources of uncertainty. This process relies on creating synthetic SNR data for a particular coastal GNSS site given the location, geometry relative to the sea surface, instrumentation and some characteristics of the observed SNR data over a chosen time period. The effects of the dynamic sea surface, tropospheric delay, random noise and surface roughness are then added to the synthetic SNR data as sources of uncertainty, via the methodologies described in Section C. The precision is estimated using the Root Mean Square Error (RMSE) of the sea level time series that is retrieved from the synthetic SNR data compared to the sea level time series that is used as an input to create the synthetic SNR data. We refer to this value as the ‘modeled RMSE’ henceforth.

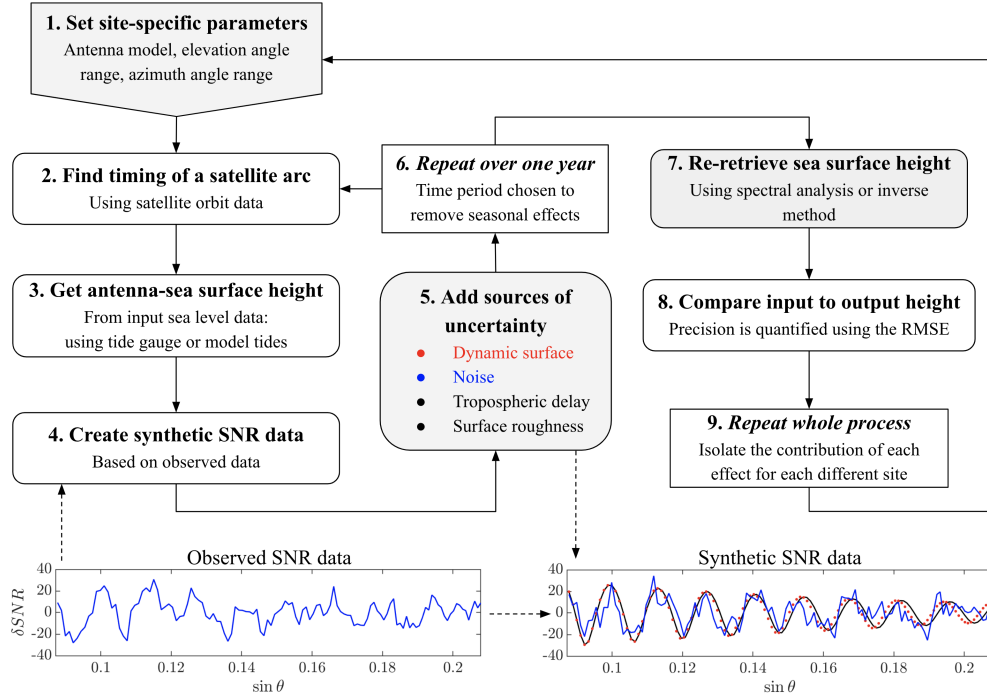


Figure 2.1: Flowchart showing the error analysis process. The two bottom panels show examples of detrended SNR data (Watt/Watt) plotted as a function of $\sin \theta$, where θ is the elevation angle of a satellite relative to an antenna. The observed SNR data is collected at station SC02. The bottom right frame shows three stages of the synthetic SNR data creation process; the black line is the initial output from Nievinski and Larson (2014), the red dotted line has been modulated to account for the dynamic sea surface and the blue line has random noise added to it.

In order to validate our results, the modeled RMSE is compared to the observed RMSE between GNSS-R sea level measurements and a co-located tide gauge for the same time period. Note that this observed RMSE is an approximation of the precision of the GNSS-R measurements because it also contains error from the tide gauge, as discussed in the following section.

2.3.1 Observed data

Two main sites are chosen for analysis that have been used in previous GNSS-R literature (Larson et al., 2017; Strandberg et al., 2016); they both have a co-located tide gauge and differ in their local tidal range (See Table 2.1). Site SC02 in Friday Harbor, Washington, USA is a Trimble TRM29659.00 choke ring antenna with a SCIT radome and a Trimble 4700 receiver situated ap-

proximately 5.5 m above mean sea level. Site GTGU in Onsala, Sweden consists of a Leica AR 25 antenna and a Leica GRX1200 receiver situated approximately 4 m above mean sea level. Both GNSS sites record data with a frequency of 1-Hz, however we decimate this data to intervals of 15 seconds because the more frequent data increases processing time and tests (not shown here) indicate that this does not significantly impact the precision of the resulting sea level measurements. In Friday Harbor there is an Aquatrak acoustic tide gauge and we retrieved data from this site with a temporal resolution of 6 minutes. According to the instrument specifications the accuracy should be sub-cm but studies have shown that it suffers from errors due to changes in temperature in the sounding tube that may require corrections up to 3 cm (Hunter, 2003). In Onsala, our results are compared to a sea level record from a nearby Campbell CS476 radar gauge that records data every minute. A comparison between the radar gauge and co-located laser gauge at this site reports a standard deviation of 4.3 mm over a one month period (Elgered et al., 2019). At both sites the tide gauges are positioned approximately 300 m away from the GNSS antennas, therefore the GNSS-R and tide gauge measurements are not expected to exactly match each other.

We perform our analysis using a year of data at each of the main sites in order to account for seasonal variations that may affect the GNSS-R measurements. For SC02 the period of study is the whole of 2015 and for GTGU it is the period from July 2015 to the end of June 2016.

Details of additional sites BUR2, SPBY and SCOA that are analyzed for a shorter period of one month are given in the supplementary information.

2.3.2 Sea level retrieval

For GNSS-R analysis, the key variable is the SNR (usually recorded in dB-Hz) for a given GNSS satellite and signal of interest. For simplicity, our analysis is limited to the use of the GPS L1 C/A signal but we note that the precision and frequency of sea level measurements would likely improve with more satellite constellations or when using different signals (Strandberg et al., 2016; Tabibi et al., 2017). In preparation for retrieving sea level measurements, the SNR data is arranged into time periods during which the elevation angle, θ , and azimuth angle, α , of the satellite relative to the antenna are within pre-defined limits. These time periods, known as satellite arcs, correspond

Table 2.1: Key parameters for the two sites used.

Identifier	Tidal range	Elevation interval	Azimuth interval
SC02	1.5 m	Low θ : 1.5-10.5 High θ : 5-13	50-240
GTGU	0.3 m	1-10.5	70-260

to when the antenna is receiving reflected signals from the sea surface. The range of elevation angles that are used for analysis is expected to be a dominant control on the precision of sea level measurements, hence we repeat the error analysis for two elevation angle intervals at site SC02. The elevation and azimuth intervals given in Table 2.1 are mostly taken from published literature (Larson et al., 2013b, 2017; Strandberg et al., 2016).

For each of the following retrieval methods, the SNR data for each satellite arc is first converted from units of dB-Hz to a linear scale using

$$\text{SNR}_{linear} = 10^{\text{SNR}_{dB-Hz}/20} \quad (2.1)$$

where SNR_{linear} is in units of Watt/Watt assuming a 1 Hz bandwidth. The SNR data is then detrended (henceforth denoted by δSNR) by removing a second order polynomial. The latter step removes the influence of the antenna gain pattern and changing antenna-satellite distance, both of which are not of interest for sea level measurements.

The spectral analysis method

The first retrieval method, discussed in detail in (Larson et al., 2017), relies on spectral analysis of SNR data. As θ changes during a satellite arc, the direct and reflected signals interfere periodically, which causes an oscillation in the SNR data. If plotted as a function of $\sin \theta$, the frequency of these oscillations is linearly related to the height of the antenna above a static reflecting surface,

$$f = \frac{2h_s}{\lambda} \quad (2.2)$$

where λ is the wavelength of the GNSS signal of interest, h_s is the static reflector height and f is the frequency of the detrended SNR oscillations, in units of $(\sin \theta)^{-1}$. An initial estimate of the time series of h is then formed by taking the frequency of the spectral peak from a Lomb-Scargle Periodogram (LSP) of the detrended SNR data for each satellite arc and converting it to h_s using (2.2).

For a sea surface that is non-stationary during a satellite arc, Larson et al. (2013b) showed that

$$f = \frac{2}{\lambda} \left[h_d + \frac{\partial h_d}{\partial t} \frac{\tan \theta}{\partial \theta / \partial t} \right] \quad (2.3)$$

where h_d is the dynamic reflecting surface height. This equation is solved iteratively, first by assuming that h_d takes the form of a summation of 145 tidal constituents with known frequencies and lunar nodal corrections but unknown phases and amplitudes. By substituting this tidal form of h into (2.3), then rearranging and substituting equation (2.2), it is found that

$$h_s = h_{tidal} + \frac{\partial h_{tidal}}{\partial t} \frac{\tan \theta}{\partial \theta / \partial t}. \quad (2.4)$$

The unknown tidal phases and amplitudes are subsequently estimated by minimizing the residual between the left and right hand side of (2.4), via a least squares approach. The final time series of h_d is then obtained by subtracting the second term on the right hand side of (2.4) from the initial h_s time series.

The inverse method

In Strandberg et al. (2016), the authors developed an inverse method whereby the detrended SNR data is modeled as a function of the dynamic reflector height, h_d , and several other unknown parameters. A continuous time series of h_d is imposed to take the form of a b-spline curve, the nodes of which are estimated simultaneously along with some unknown model parameters by minimizing the residual between the observed and modeled δ SNR, via a least squares approach. This analysis is very sensitive to the initial parameter choice and we found that it is necessary to estimate b-spline nodes using the initial time series of h_s from (2.2) prior to the least squares

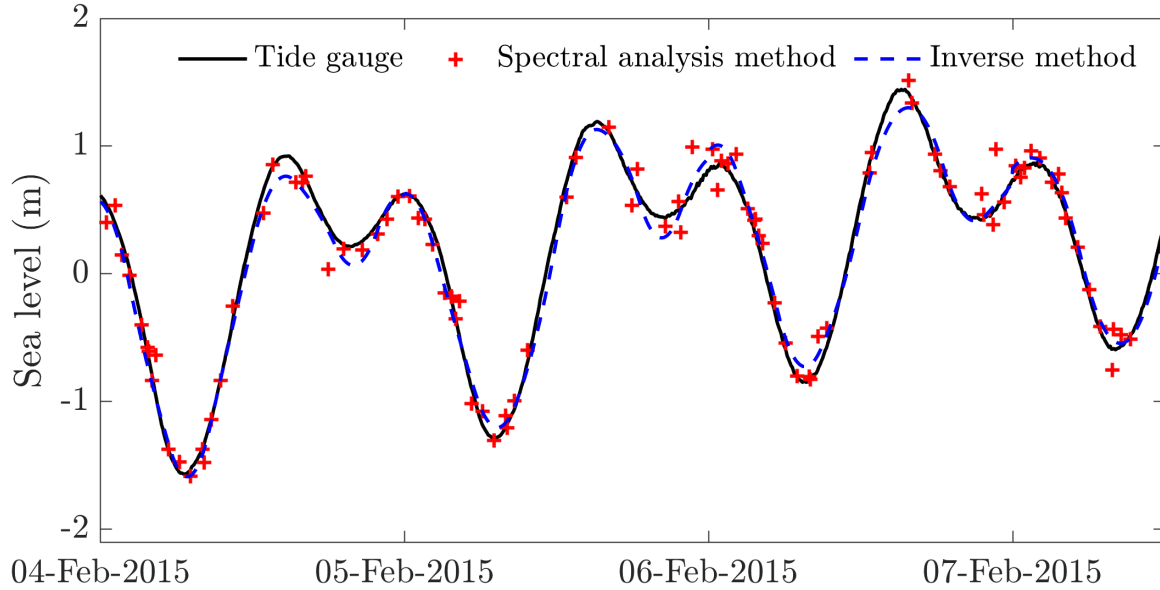


Figure 2.2: Three days of tide gauge and GNSS-R sea level data at site SC02 when using the high elevation angle interval given in Table 2.1.

analysis. In order to avoid instabilities, this process is performed over consecutive three day periods and only the data from the middle day is used.

A comparison of tide gauge and GNSS-R sea level time series at site SC02 when using both retrieval methods is given in Figure 2.2.

2.3.3 Synthetic SNR data creation

To create synthetic SNR data, the multipath simulator model (henceforth *mpsim*) provided by Nievinski and Larson (2014) is used. This forward model is based on the physics of electromagnetic wave propagation, reflection off rough surfaces and antenna response. The model requires site-specific inputs such as the GNSS signal used, antenna and radome model, elevation angle interval, reflector height and reflecting surface material to create synthetic SNR data for a single satellite arc. A year-long time series of synthetic SNR data is then created given the timings and statistics of observed satellite arcs. The frequency and resolution (in dB-Hz) of the model output is imposed to match those recorded at the site of interest. As is described in the following

sections, we then process the model output to account for the effects of the dynamic sea surface, tropospheric delay and random noise.

Surface roughness

Surface roughness is quantified as the standard deviation of the surface from its mean position and is an input for *mpsim*. This value is related to one of the unknown parameters that is retrieved along with the sea level time series when using the inverse method and therefore we set the modeled surface roughness by matching the mean value retrieved from the observed data.

Dynamic sea surface

The *mpsim* model does not have an option to account for movement of the sea surface during a satellite arc. However, by increasing the spacing between the elevation angle coordinates for some modeled SNR data, the frequency of oscillations and the corresponding antenna-sea surface height difference is decreased. Conversely, the height difference is increased by decreasing the spacing between the elevation angle coordinates. Modeled SNR data for a static sea surface is therefore modulated such that it corresponds to a dynamic sea surface by applying this theory. The elevation angle array corresponding to a dynamic sea surface, θ_d , is taken directly from satellite orbit data but the elevation angle array for a static sea surface, θ_s , is unknown and must be calculated in order to initially produce the modeled SNR data.

The relationship between the frequency of SNR oscillations and the height of a static or dynamic reflecting surface are given by (2.2) and (2.3) respectively. Given that f is in units of $(\sin \theta)^{-1}$, the ratio of the static and dynamic frequencies is equivalent to the inverse of the ratio of the change in $\sin \theta$ at each time step,

$$\frac{f_d}{f_s} = \frac{\Delta \sin \theta_s}{\Delta \sin \theta_d} = \frac{1}{h_s} \left[h_d + \frac{\partial h_d}{\partial t} \frac{\tan \theta_d}{\partial \theta_d / \partial t} \right] \quad (2.5)$$

for a fixed h_s and $h_d(t)$ at some time t . The θ_s array is obtained by solving (2.5) for $\Delta \sin \theta_s$ at each time step over a full satellite arc. We note that this is only a first order correction and a more

accurate solution may be obtained by editing the governing equations in the *mpsim* model to allow for a changing reflector height. Synthetic SNR data is produced for h_s over the full range of θ_s , such that the SNR data either corresponds to a static sea surface if plotted using θ_s or a dynamic sea surface if plotted using θ_d . An example of some modeled SNR data is given at the bottom right of Figure 2.1, where the black line corresponds to a static sea surface and the red dotted line corresponds to a dynamic sea surface.

Tropospheric Delay

The pressure, temperature and humidity of the lower atmosphere causes a delay in the arrival of GNSS signals at an antenna compared to what would be expected if they were travelling through a vacuum. The amount of delay increases for low elevation angles because the signals take a longer path through the lower atmosphere. This leads to an overestimation of the path difference between the direct and reflected signals that changes during a satellite arc and in turn leads to an underestimation of the reflector height. The offset between the true and estimated reflector height can be split into two components: a mean offset and a time varying offset that changes as a function of the true reflector height and the state of the atmosphere. The mean offset is important when considering the accuracy of GNSS-R sea level measurements and is not quantified herein.

In Williams and Nievinski (2017), the authors showed that the effect of tropospheric delay causes an offset of the frequency of oscillations retrieved via spectral analysis, giving rise to the following modification of (2.3),

$$f = \frac{2}{\lambda} \left[h + \frac{\partial h}{\partial t} \frac{\tan \theta}{\partial \theta / \partial t} + \frac{1}{2} \frac{\partial \tau_{td}}{\partial \sin \theta} \right] \quad (2.6)$$

where τ_{td} is the additional difference between the direct and reflected signals due to the effect of tropospheric delay (represented as a distance) and may be calculated at different values of h and θ using the GTP2w model (Böhm et al., 2015) and the Vienna Mapping Function VMF1 (Boehm et al., 2006). Rather than using a constant frequency offset, we convert τ_{td} to an equivalent elevation angle offset which varies during a satellite arc, analogously to the dynamic surface correction

in the previous section. The elevation angle offset, $\delta\theta_{td}$, is calculated using

$$2h \sin \theta + \tau_{td} = 2h \sin(\theta + \delta\theta_{td}) \quad (2.7)$$

where θ refers to the geometric elevation angle from satellite orbit data and $\theta = \theta_d$, following notation from the previous section. Then $\theta_{td} = \theta_d + \delta\theta_{td}$, is used instead of θ_d in (2.5). Synthetic data is generated using θ_{td} , but θ_d is used for retrieving sea level from the synthetic data, in order to simulate the effect of uncorrected tropospheric delay. We find that the improvement of the precision of retrievals when applying this correction to observed SNR data is approximately equal to the deterioration in the precision of retrievals when incorporating this effect in the synthetic SNR data, thus validating our approach.

Noise

We define noise here as any additional contributions to the SNR data other than the oscillating signal due to reflections from the sea surface. This noise is likely caused by reflections from other nearby surfaces, interference from other microwave sources or instrument noise and causes the observed SNR signal shown at the bottom of Figure 2.1 to diverge from a sinusoidal signal. For this study, rather than being concerned with the cause of this noise, which may be physical in origin, we aim to characterize and reproduce it such that the effect it has on the precision of sea level measurements can be quantified. Initially we tried using white noise but we found this method to be insufficient for matching observed characteristics of the SNR data. Instead our approach is to represent the noise as a summation of sine waves with random amplitudes, frequencies and phase offsets, which must be scaled simultaneously with the synthetic SNR data in such a way that, on average, it is equivalent to the noise in the observations.

In order to constrain the power of the noise compared to the clean oscillating signal, the metrics of interest are the power of the clean signal, P_{max} , as determined from an LSP, and the variance of the total signal, σ^2 . The noise and the clean signal are scaled via a least squares approach such that the residual between the observed and synthetic values of P_{max} and σ^2 are minimized. The two

scaling factors to be determined, A and B , are defined by

$$\delta\text{SNR}_{noisy} = A[\delta\text{SNR}_{clean}] + B[\sum_{i=1}^N S_i a_i \sin(2\pi f_i \sin \theta + \phi_i)] \quad (2.8)$$

where δSNR_{clean} and δSNR_{noisy} are the synthetic signals before and after noise has been added, and a_i , f_i and ϕ_i are the random amplitudes, frequencies, and phase offsets, respectively, for N sine waves. The random frequencies are chosen up to a maximum value of the mean Nyquist frequency, which is equal to $K/(2\Delta \sin \theta)$, where K is the number of measurements in the interval $\Delta \sin \theta$. The function $S_i = S(f_i)$ is applied to scale the random amplitudes such that the mean power of the noise in the frequency domain matches observations. The function $S(f_i)$ is unique for each site and is determined by fitting a curve to the mean LSP over the frequency ranges that are not affected by reflections from the sea surface. An example of the observed and modeled mean LSP is given in Figure 2.3 and further examples are given for three sites in the supplementary information. The value of N is somewhat arbitrary, but we found that setting $N = 15$ produces a mean LSP that most closely matches the observed data and also produces SNR data that looks qualitatively similar to the observed data (See Figure 2.1). This process is sensitive to the (random) values of a_i , f_i and ϕ_i , hence each set of synthetic SNR data that has noise added to it must be produced and then analyzed many times until the modeled RMSE converges.

2.3.4 RMSE calculations

In order to obtain the observed RMSE of individual measurements, the sea level time series obtained from the spectral analysis or inverse method is compared to observations from the co-located tide gauge. In the case of the inverse method this process is trivial because the output is a b-spline curve that may be evaluated at every time that there is a tide gauge observation. Conversely, as can be seen in Figure 2.2, the output of from the spectral analysis method is unevenly spaced in time, depending on the timing of satellite arcs. In this case the RMSE is obtained by linearly interpolating the tide gauge measurements to match the timing of the satellite arcs. In theory, the

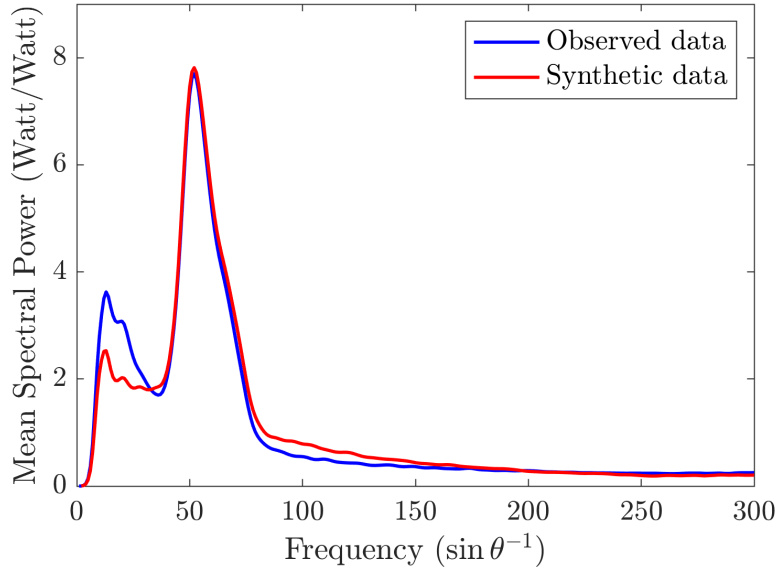


Figure 2.3: Mean values of the LSP for all observed and synthetic SNR arcs at site SC02 high θ .

sea level measurements obtained by GNSS-R analysis correspond to the vertical distance from the antenna phase center to the sea surface. Given that the exact position of the antenna phase center is unknown, the mean value of each time series is removed prior to calculating the RMSE. Removing the mean from the GNSS-R time series also removes the mean offset of the reflector height due to the effect of tropospheric delay and hence it is only the time-varying component of the tropospheric delay offset that affects the RMSE.

The modeled RMSE is obtained by the same process except that the sea level measurements are compared to the input sea level time series that is used to create the synthetic SNR data. One of the key objectives of this paper is to provide a method to evaluate the precision of sea level measurements at sites with no co-located tide gauge. Hence we compare the modeled RMSE obtained when using the co-located tide gauge as an input to that obtained when using modeled tides from Egbert and Erofeeva (2002). If the modeled RMSE is insensitive to the choice of input sea level data then model tides may be used to estimate the precision at sites with no co-located tide gauge. Tidal variations are not the only source of sea level change at these sites. In the case of site GTGU, where the tidal variations are very small, we scaled up the tide model output to match

the range of observed sea levels from the tide gauge during the same period. The observed sea level variations are largely driven by meteorological forcing at this site.

Daily and Monthly means

In addition to comparing individual measurements, we also consider daily and monthly means. These are obtained following the same process outlined in Larson et al. (2017). Firstly, tides with a period of diurnal or shorter are estimated and removed from each time series. An hourly sea level time series is then obtained by averaging in a 6 hour moving window and subsequently a low pass filter with a passband frequency of $1/60 \text{ hours}^{-1}$ is applied. Daily and monthly means are then formed from the filtered hourly data. This process is repeated for each sea level time series individually before calculating the RMSE.

Quantifying the sources of uncertainty

The different sources of uncertainty that are the focus of this paper are not independent, which makes it impossible to perfectly separate them. However, it is possible to estimate the contribution of each source of uncertainty to the total modeled RMSE by comparing the modeled RMSE obtained with different combinations of the four sources of uncertainty added to the synthetic SNR data. We have found that the total modeled RMSE can be formed by a linear addition of different sources of uncertainty when using the following approach, thus suggesting that their correlations tend to 1. The calculations used are,

$$\epsilon_{\text{noise}} = \text{RMSE}_{\text{noise,dyn,td,sfr}} - \text{RMSE}_{\text{dyn,td,sfr}} \quad (2.9)$$

$$\epsilon_{\text{dyn}} = \text{RMSE}_{\text{noise,dyn}} - \epsilon_{\text{noise}} \quad (2.10)$$

$$\epsilon_{td} = \text{RMSE}_{\text{noise,dyn,td}} - \text{RMSE}_{\text{noise,dyn}} \quad (2.11)$$

$$\epsilon_{\text{sfr}} = \text{RMSE}_{\text{noise,dyn,td,sfr}} - \text{RMSE}_{\text{noise,dyn,td}} \quad (2.12)$$

where ϵ refers to the value that is used to represent the contribution of each effect to the total RMSE in Figure 2.5. The RMSE values in the above equations refer to the modeled RMSE that is obtained when using tide gauge data as an input and including the effects listed in the subscript. The subscripts ‘noise’, ‘dyn’, ‘td’ and ‘sfr’ refer to the effects of random noise, the dynamic surface, tropospheric delay and surface roughness, respectively. We tried other approaches for quantifying the sources of uncertainty and found that the key results when comparing sites and retrieval methods are robust regardless of the way in which these values are calculated.

Additional sources of uncertainty, such as the resolution of SNR data, the azimuth angle range and the mean antenna-sea surface height difference are constrained by the observed data at each site, hence their contribution to the RMSE is consumed by one or more other sources.

2.4 Results

2.4.1 Observed RMSE

Figure 2.4 shows the first direct comparison of the performance of different GNSS-R techniques at different sites and elevation angle intervals, for individual measurements and for daily and monthly means. The spectral analysis results for SC02 high θ and the RMSE of individual measurements using the inverse method at GTGU are comparable to Larson et al. (2017) and Strandberg et al. (2016) but the majority of these results are new.

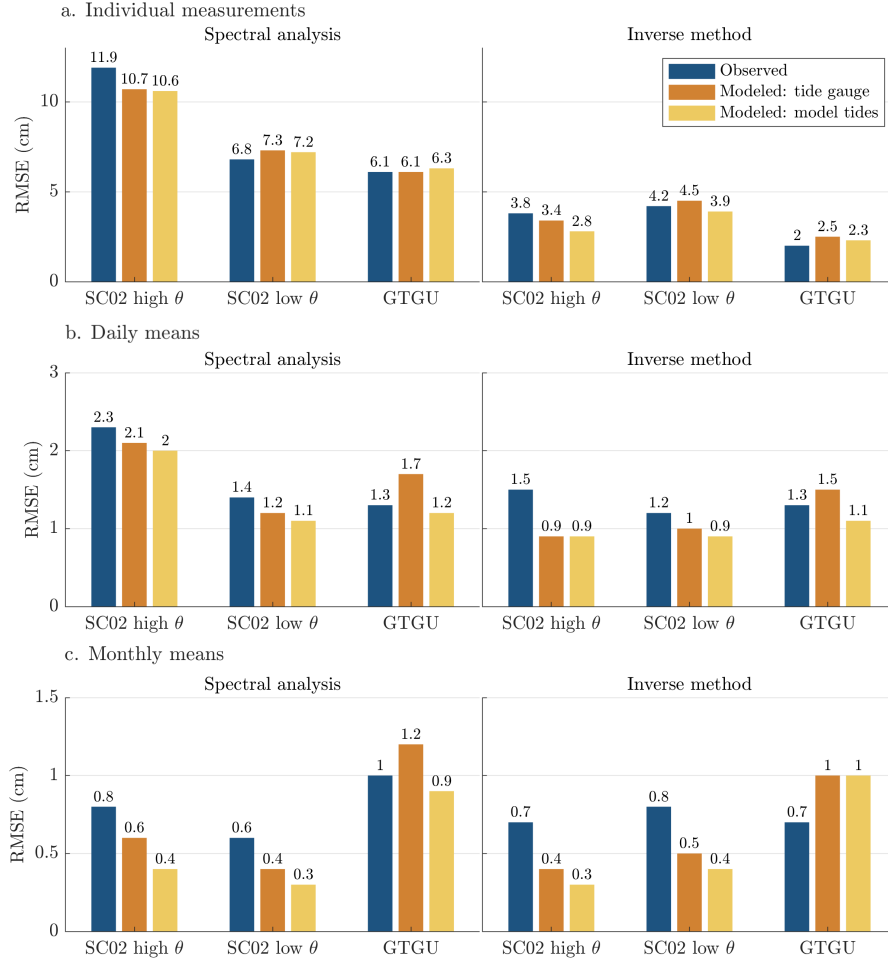


Figure 2.4: Comparison of observed and modeled RMSE of a. individual measurements, b. daily means and c. monthly means at the sites given in 2.1. The difference between the modeled results is the input sea level data that is used to generate the synthetic SNR data.

For individual measurements, the inverse method consistently performs better than spectral analysis, particularly for SC02 high θ and GTGU, where there is a $> 60\%$ reduction in the RMSE when using the inverse method. As discussed in Section IV, this does not necessarily mean that the inverse method should always be used over spectral analysis. Nevertheless, the spectral analysis method is also more sensitive to the choice of elevation angle interval, as evidenced by the 5 cm decrease in the RMSE when comparing the lower to the higher elevation angle interval at SC02. Conversely, there is a modest increase in the RMSE of 0.4 cm comparing the lower to higher elevation angle interval when using the inverse method.

Compared to the large differences between the observed RMSE of individual measurements, the observed RMSE of daily and monthly means shown in Figure 2.4b and c are more uniform between different techniques, stations and elevation angle intervals. Excluding the RMSE of daily means when using spectral analysis at SC02 high θ , all of the observed daily means range between 1.2 – 1.5 cm. All of the observed results for monthly means range between 0.6 – 1 cm. For context, a precision of 1 cm for a 20-year time series corresponds to a maximum error of 1 mm/yr for a linear trend, which agrees with the results for the linear trend calculated in Larson et al. (2017) (they found $\sigma = 0.5$ mm/yr). These results imply that the sources of uncertainty that cause variable errors for individual measurements become less important when taking daily or monthly means.

2.4.2 Comparison of observed and modeled RMSE

In Figure 2.4a, the values for the observed RMSE (in blue) and modeled RMSE (in orange and yellow) agree to within 1 cm with the exception of SC02 high θ when using the spectral analysis method. Similar results are obtained for the three additional sites discussed in the supplementary information. As mentioned in section II, some differences between the observed and modeled RMSE are to be expected. The observed RMSE contains instrument error from the tide gauges and possibly some bias due to the difference in the area that is being sampled to make a sea level measurement between the tide gauge and the GNSS-R measurement. On the other hand, the modeled RMSE contains uncertainty due to the models used to create the synthetic SNR data. In light of these differences and in particular given that the tide gauge at SC02 is prone to errors (Hunter, 2003), the results presented in Figure 2.4a validate our precision estimation technique for individual measurements. Furthermore, the modeled RMSE values are largely insensitive to the choice of using either a tide gauge (orange bars) or model tides (yellow bars) as input sea level data for the analysis, hence our technique may be applied to estimate the precision of individual sea level measurements at sites with no co-located tide gauge. The correspondence of the observed and modeled RMSE also implies that there are no major sources of uncertainty missing from our analysis.

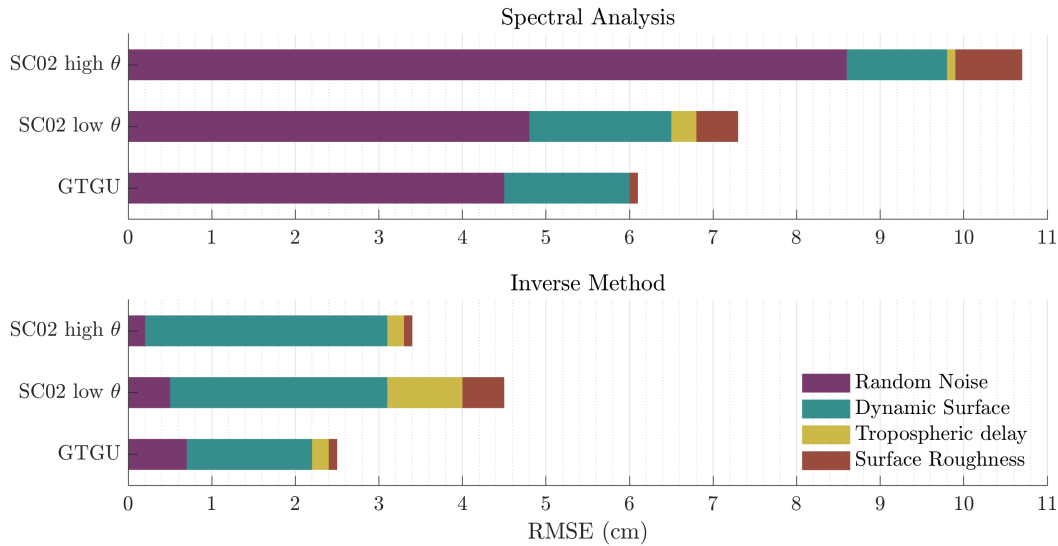


Figure 2.5: The contribution of each source of uncertainty to the total modeled RMSE when using the spectral analysis method to retrieve sea level (top) and when using the inverse method to retrieve sea level (bottom). The total length of each bar corresponds to the values given in the ‘Modeled: tide gauge’ values in Figure 2.4a).

For daily means (Figure 2.4b), the modeled RMSE values agree to within 1-6 mm of the observed values, with the largest difference at SC02 high θ when using the inverse method, where both modeled values are 40% less than observed. The modeling technique becomes significantly less reliable for monthly means (Figure 2.4c), where both modeled values underestimate the observed RMSE by at least 50% at SC02 using both elevation angle intervals and retrieval techniques. This underestimation for modeled values produced using model tides (yellow bars) is likely in part because the magnitude of the tidal signal is unrealistically small once tides of diurnal periods or shorter have been removed; observed sea level records contain signal due to meteorological forcing that may cause sea level variations of up to 10s of cm per day. More work is needed to improve modelling estimates of the precision of daily and monthly means.

2.4.3 Sources of uncertainty

As shown in Figure 2.5, the contributions of different sources of uncertainty to the total modeled RMSE vary greatly between retrieval methods and sites. The difference between the dominant contributions is most striking when comparing the different retrieval methods.

The effect of noise is the dominant contribution to the RMSE at all sites when using the spectral analysis method, making up 65 – 80% of the RMSE, compared to a lesser contribution of between 5 – 30% when using the inverse method. These results highlight the fundamental differences in the retrieval methods: the inverse method is less sensitive to the effect of noise because sea level measurements are restricted to fit a b-spline curve, hence the influence of outliers or noisy satellite arcs is reduced compared to the spectral analysis method. On the contrary, the effect of the dynamic surface is the dominant contribution of 60 – 85% of the RMSE at all sites when using the inverse method, compared to 10 – 25% when using the spectral analysis method. This is in part because an observed sea level time series cannot be perfectly represented by a smooth b-spline curve, thus leading to a large contribution to the RMSE due to the dynamic sea surface for the inverse method. The output from the spectral analysis method is not restricted to fit a curve hence it is theoretically possible to perfectly capture any time series. Instead, the contribution of the dynamic surface to the RMSE for the spectral analysis method is due to the assumptions made in order to solve equation (2.3).

The differences in the modeled RMSE obtained for the two elevation angle intervals at SC02 are due to a combination of factors. For the spectral analysis method, the effect of noise contributes 4 cm less to the RMSE for the lower elevation angle interval compared to the higher elevation angle interval. This is because the oscillations in the SNR data are dampened with increasing elevation angle whilst the magnitude of the noise remains constant. The effect of tropospheric delay is much smaller in magnitude overall but it is larger for the low elevation angle interval regardless of the retrieval method, as would be expected from Williams and Nievinski (2017). For lower elevation angles, the reflected GNSS signal takes a longer path through the lower atmosphere and the longer the path length the more that the signal is slowed and bent and hence delayed in reaching the antenna. For the same reason, the effect of tropospheric delay increases as the height of the

antenna above the sea surface increases. Therefore, the tidal range is also important; at low tide the GNSS signals will take a longer path through the atmosphere than during high tide. At GTGU the elevation angle interval is similar to SC02 low θ but the tidal range is much smaller (see Table 2.1) and hence the contribution of tropospheric delay to the RMSE is reduced in comparison to SC02 low θ .

The difference in the RMSE of individual measurements at different sites when using the same technique and similar elevation angle range (i.e., comparing GTGU and SC02 low θ), can mostly be accounted for by differences in the dynamic surface effect, which is larger at site SC02 due to larger tides (See Table 2.1). This result is in agreement with previous literature (Löfgren et al., 2014) and we expect the dynamic surface effect to increase at sites with a greater tidal range.

It is not clear why the contributions of surface roughness and tropospheric delay to the modeled RMSE vary between the spectral analysis and inverse method at the same sites. However, their contribution is generally small, especially in the case of surface roughness, which represents less than 15% of the modeled RMSE for both the spectral analysis and inverse method.

2.5 Conclusion and discussion

We have developed a modelling technique to estimate the precision of GNSS-R sea level measurements at any site and using any retrieval technique. The modeled RMSE for individual measurements closely agrees with the observed RMSE at all combinations of sites, elevation angle intervals and retrieval methods and to within 1 cm for 9 out of the 11 combinations (including the results in the supplementary information). The results are largely insensitive between using model tides or a tide gauge as an input for creating synthetic SNR data. Therefore, for sites with no co-located tide gauge, model tides could be used as an input to create synthetic SNR data and hence estimate the precision of individual sea level measurements. If the tidal range is small, such as at site GTGU, the model tides can be scaled to match observed sea level variations (i.e., from the observed GNSS-R sea level time series).

We also used our precision estimation technique to provide a quantitative analysis of the sources of uncertainty that lead to variations in the precision of sea level measurements and found that noise is the dominant source of uncertainty for the spectral analysis method and the dynamic surface is the dominant source of uncertainty for the inverse method. The agreement between observed and modeled results suggests that we have included the dominant sources of uncertainty in our analysis. However, the nature of our approach means that sources of uncertainty that are likely to be important (e.g., the azimuth angle range, the resolution of SNR measurements, the mean height of the antenna above the sea surface) are not explicitly quantified and further analysis would be required to understand their influence. Our approach to produce noise based on the mean LSP of the observed data may mean the effect of noise also represents other physical processes (such as reflections from other nearby surfaces, preferential reflections from wave troughs). Furthermore, the nonlinear combination of effects makes it difficult to quantify their contributions to the RMSE and our results should only be taken relative to each other as opposed to looking at absolute values of each source of uncertainty. A more rigorous quantification of the different sources of uncertainty could be achieved by investigating the correlations between different sources.

Our analysis suggests that the inverse method produces more precise GNSS-R sea level measurements than the spectral analysis method. However, it is important to note that the inverse method may not be suitable for all sites (for example, if there is a narrow azimuth angle range) and can be prone to instabilities due to the initial choice of parameters that go into the least squares estimation. When the parameters are not carefully chosen, the sea level output may differ greatly from the physical signal, with an observed RMSE of up to 1 m on a given day. Whilst the spectral analysis method is prone to the influence of outliers that are difficult to detect, it is more stable and unlikely to produce an extended period of data (i.e., an entire day) with such large errors.

Our observed results show that the differences in the performance of retrieval methods was much less pronounced for daily and monthly means compared to individual measurements; the observed RMSE for monthly means is 1 cm or less at all sites using both retrieval techniques. Our modelling technique was less reliable for daily and monthly means, particularly when using model tides as an input to create the synthetic data. This is in part because model tides are not sufficient

for capturing daily or monthly mean sea level signals. However, the modeled RMSE values for monthly means also disagreed with the observed values when using the tide gauge as an input. Hence more work is required to understand the sources of uncertainty in daily and monthly means and extended periods of a year or longer should be analyzed at more sites to see if our results hold.

The elevation angle interval appears to be an important control on the precision of sea level measurements. If a large elevation angle interval is available for reflections at a particular site, choosing a low elevation angle interval will reduce the effect of noise, which is the dominant source of uncertainty when using the spectral analysis method. However, the effect of tropospheric delay will increase for low elevation angle intervals, especially at sites with a large tidal range. Both Williams and Nievinski (2017) and Santamaría-Gómez and Watson (2017) have provided methodologies to correct for the effect of tropospheric delay in sea level retrievals; however they rely on information about the temperature, pressure and humidity profiles of the lower atmosphere, which are generally unknown and must be estimated. Hence it is only possible to partially correct for the effects of tropospheric delay, unless additional instrumentation, such as a microwave radiometer profiler, is used to improve estimates of the state of the atmosphere above the sea surface.

While we have demonstrated that our model captures the most significant sources of uncertainty, future work could be done to improve the model by improving the characterization of noise, explicitly accounting for the effect of preferential reflections from wave troughs (Sun, 2017), by improving the modelling of the effect of tropospheric delay or by accounting for sea ice cover. Our analysis of the different sources of uncertainty could be improved by extending our analysis to sites with a large local tidal range or sites that are situated further above mean sea level (i.e., > 5 m), for which the effects of the dynamic surface and tropospheric delay would likely be more dominant. The *mpsim* model that forms the basis of our technique may be used to create synthetic SNR data for various GPS and GLONASS signals and hence our analysis may easily be extended to include multiple signals, which would likely improve the precision of sea level measurements (Strandberg et al., 2016; Tabibi et al., 2017). This forward model is also used for both soil moisture and snow depth measurements, hence we expect the developed technique to be applicable to such measurements as well.

2.6 Supplementary Information

To further support the error analysis technique outlined in the main article, we have extended our analysis to three additional GNSS sites that are all co-located with tide gauges. The three sites are BUR2 in Burnie and SPBY in Spring Bay near Triabunna, both in Tasmania, Australia and SCOA in Saint Jean de Luz, France. For the Australian sites, GNSS data is publicly available online from Geoscience Australia and hourly tide gauge data is publicly available from the Australian Government Bureau of Meteorology. For site SCOA, GNSS data is available from the Institut National de l'Information Géographique et Forestière (IGN) and tide gauge data is available from the Réseaux de référence des observations marégraphiques (REFMAR). We analyzed the observed GNSS and tide gauge data and produced synthetic SNR data following the technique outlined in the main article in order to obtain values for the observed and modeled RMSE for the month of May, 2019. Further details about the sites, which differ in instrumentation, tidal range and geometry, are given in Table 2.2.

The observed and modeled RMSE for the spectral analysis and inverse methods for the three sites are given in Table 2.3. The observed and modeled RMSE agree to within 1 cm for all sites and retrieval methods except for with the spectral analysis method at site SCOA. By inspection of the raw tide gauge data at Saint Jean de Luz (co-located with site SCOA), we noticed several periods of missing data in 2019, which could be indicative of less reliable tide gauge data at this site. The three sites have a narrow azimuth interval and therefore fewer sea level measurements per day in comparison to the sites SC02 and GTGU that are discussed in the main article. At site BUR2 we found periods of time with no GNSS-R sea level measurements, as can be seen in Figure 2.6. This site is in a commercial port hence the periods with no sea level measurements are probably due to ships docking in front of the GNSS antenna. The output from the inverse method was unstable when using both observed and modeled SNR data at site BUR2, which is likely due to the periods where the sea surface is fully or partially obstructed by boats. A comparison of observed and modeled sea level estimates at site SPBY is given in Figures 2.7 and 2.8. Figures 2.9, 2.10 and 2.11 show the mean LSP for observed and synthetic SNR data for the month of May 2019.

Site	Antenna	Receiver	Mean height above sea level (m)	Approx. tidal range (m)	Elevation interval	Azimuth interval
BUR2	LEIAT504GG	Septentrio PolaRx5	5.5	1.6	3 - 10	50 - 180
SPBY	LEIAT504GG	Leica GRX1200	4.0	0.7	1 - 7	280 - 360
SCOA	TRM55971.00	Leica GR25	10.6	2.4	3 - 10	155 - 240

Table 2.2: Details of the instrumentation and other parameters used at additional sites.

Site		Observed RMSE (cm)	Modeled RMSE (cm)
BUR2	Spectral analysis	9.7	9.7
	Inverse method		
SPBY	Spectral analysis	9.2	9.1
	Inverse method	4.8	3.8
SCOA	Spectral analysis	7.5	6.2
	Inverse method	7.0	7.6

Table 2.3: Observed and modeled RMSE at sites BUR2, SPBY and SCOA for the month of May 2019.

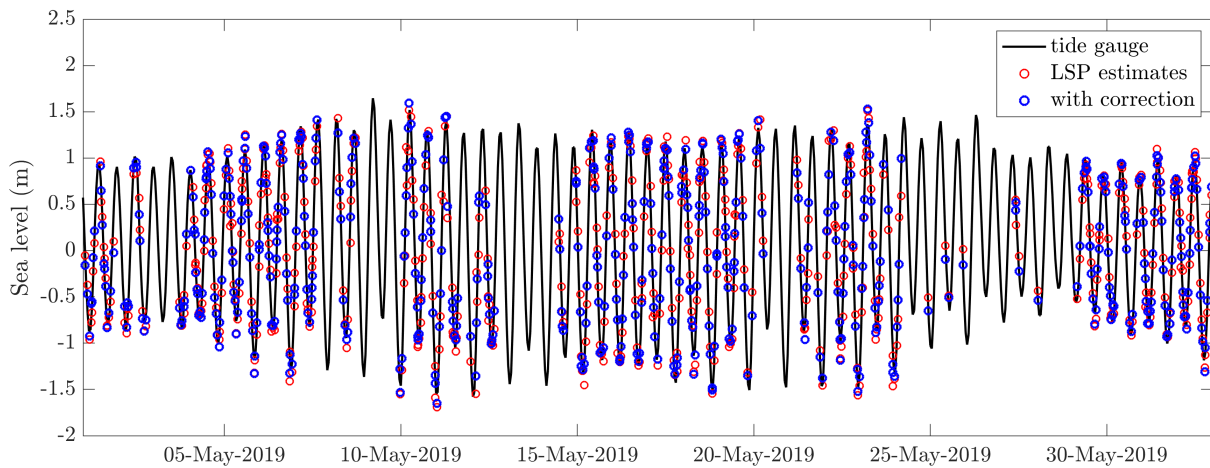


Figure 2.6: Comparison of tide gauge and GNSS-R sea level measurements at site BUR2 in May 2019.

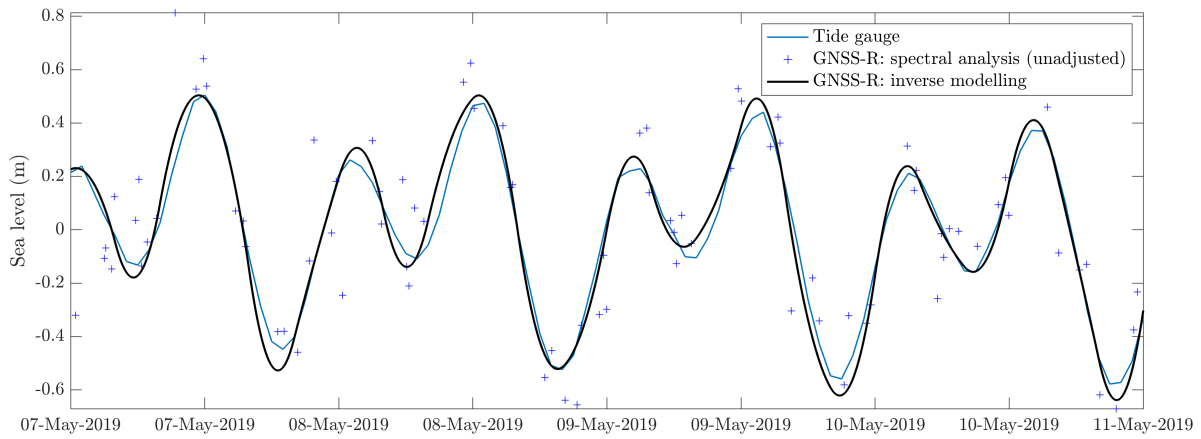


Figure 2.7: A comparison of observed tide gauge and GNSS-R sea level measurements at site SPBY.

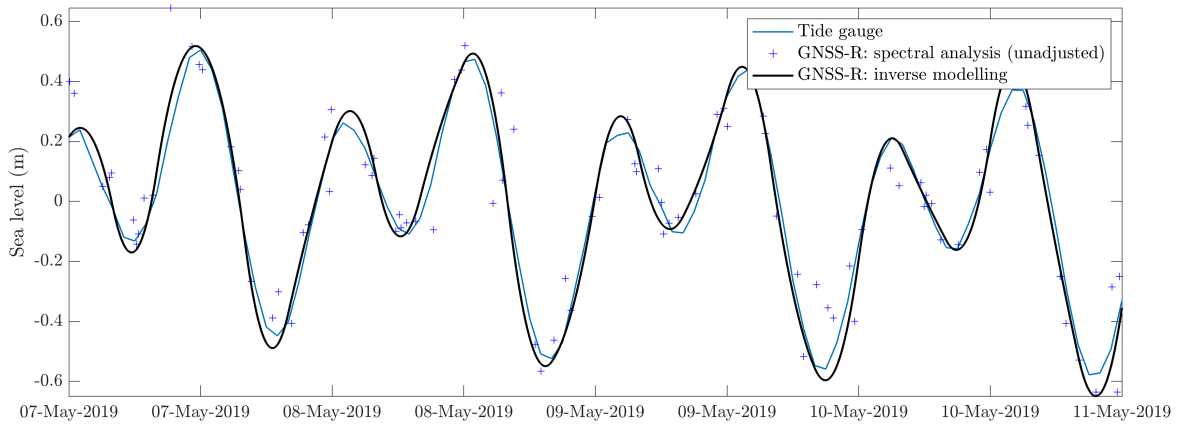


Figure 2.8: As in Figure 2.7 a but for modeled SNR data.

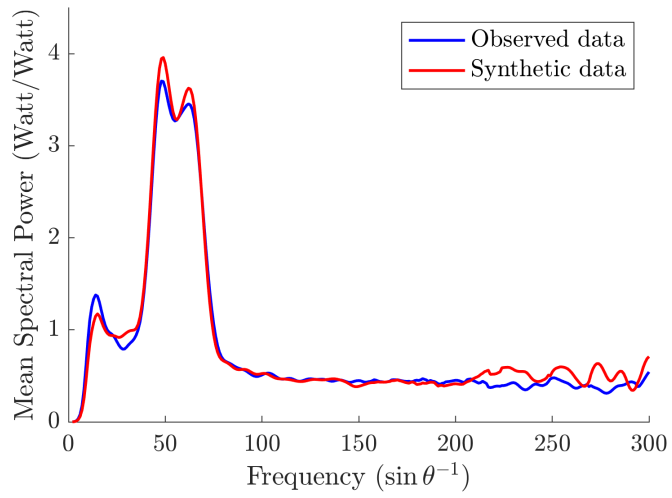


Figure 2.9: Mean values of the LSP for all observed and synthetic SNR arcs at site BUR2.

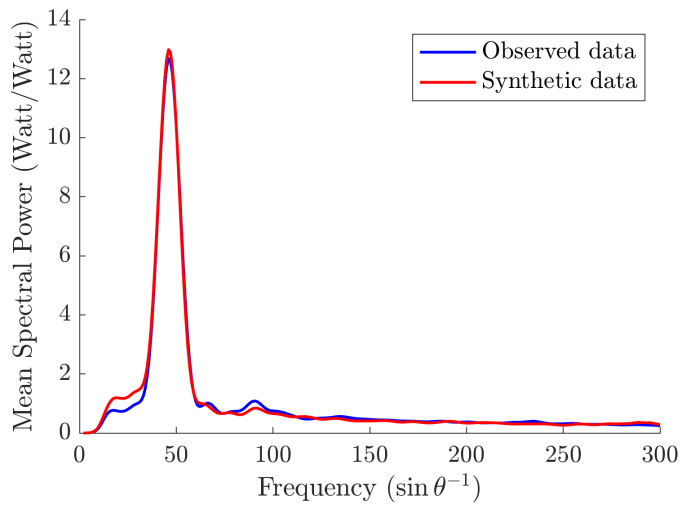


Figure 2.10: As in Figure 2.9 a but for site SPBY.

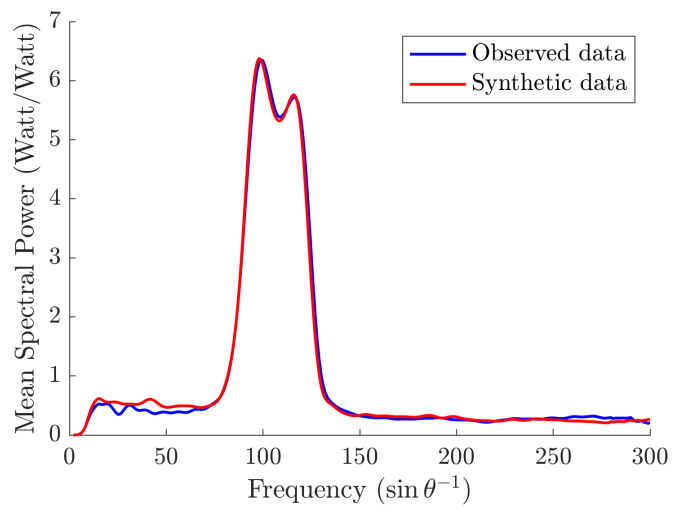


Figure 2.11: As in Figure 2.9 a but for site SCOA.

Chapter 3

Precise water level measurements using low-cost GNSS antenna arrays

One of the key results from Chapter 2 was that random noise is a dominant source of uncertainty in GNSS-R water levels. This result led to the hypothesis that multiple antennas in the same location could be used to obtain more precise water levels by reducing the effect of random noise. This chapter is focused on testing this hypothesis through field experiments with multiple co-located low-cost GNSS antennas at two locations in Québec, Canada and one location in New York, USA.

The missing link between Chapters 2 and 3 is some preliminary testing with a co-located low-cost and geodetic-standard antenna, where it was found that the low-cost antenna performed similarly to the geodetic-standard antennas for GNSS-R analysis. The preliminary testing was done during field work in June 2018 in Greenland, near Jakobshavn Glacier. A simple instrument was built from a single low-cost USB GPS antenna, connected a Raspberry Pi Zero to log the data. The low-cost unit was temporarily installed for 8 hours next to a Trimble TRM59800.00 antenna and a Septentrio PolaRx5 receiver. As shown in Figure 3.1, reflector height estimates were obtained by analyzing the SNR data from both geodetic-standard and low-cost antennas and then compared to local tidal predictions, using Padman and Erofeeva (2004). Visual inspection of the two GNSS-R water level data sets in Figure 3.1 does not reveal any obvious degradation in the precision of the water levels for the low-cost antenna. This result was significant in two key ways. First, it implied

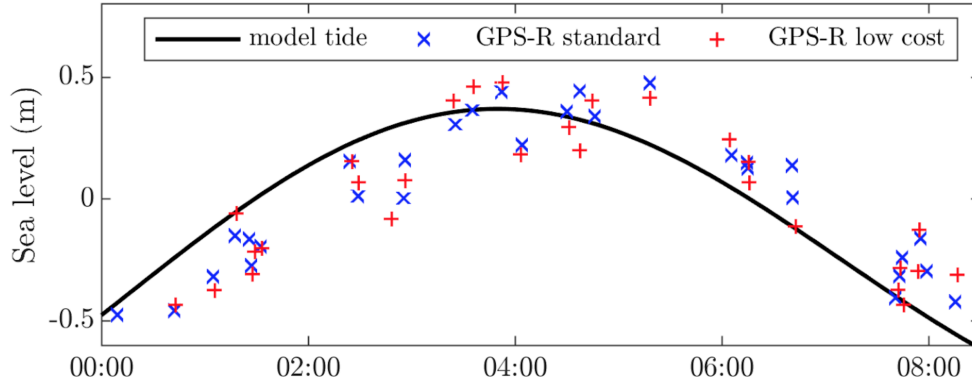


Figure 3.1: An 8-hour comparison of GNSS-R water levels using low-cost and geodetic-standard GPS antennas in Greenland in June, 2018. The water levels are plotted alongside a tidal prediction for reference (Padman and Erofeeva, 2004).

that low-cost antennas would be a suitable tool for testing the hypothesis that multiple co-located antennas could reduce the effect of random noise (it would be prohibitively expensive to co-locate multiple geodetic-standard antennas). Second, it signalled that a comparison between the two types of antennas for GNSS-R analysis merited further study.

3.1 Abstract

We have developed a ground-based Global Navigation Satellite System Reflectometry (GNSS-R) technique for monitoring water levels with a comparable precision to standard tide gauges (e.g., pressure transducers) but at a fraction of the cost and using commercial products that are straightforward to assemble. As opposed to using geodetic-standard antennas that have been used in previous GNSS-R literature, we use multiple co-located low-cost antennas to retrieve water levels via inverse modelling of signal-to-noise ratio data. The low-cost antennas are advantageous over geodetic-standard antennas not only because they are much less expensive (even when using multiple antennas in the same location) but also because they can be used for GNSS-R analysis over a greater range of satellite elevation angles. We validate our technique using arrays of four antennas at three test sites with variable tidal forcing and co-located operational tide gauges. The root mean square error between the GNSS-R and tide gauge measurements ranges from 0.69–1.16

cm when using all four antennas at each site. We find that using four antennas instead of a single antenna improves the precision by 30–50% and preliminary analysis suggests that four appears to be the optimum number of co-located antennas. In order to obtain precise measurements, we find that it is important for the antennas to track GPS, GLONASS and Galileo satellites over a wide range of azimuth angles (at least 140 degrees) and elevation angles (at least 30 degrees). We also provide software for analyzing low-cost GNSS data and obtaining GNSS-R water level measurements.

3.2 Introduction

Precise water level measurements are needed for monitoring the global oceans, lakes and rivers, all of which are vulnerable to anthropogenic climate change (Goudie, 2006; Adrian et al., 2009; Slangen et al., 2016). Sea level at any location is influenced by spatiotemporally variable processes such as tides, storm surges and glacial isostatic adjustment (Tamisiea et al., 2014; Kopp et al., 2015). Networks of coastal water level sensors are therefore necessary to validate models of these processes (Meysignac et al., 2017; Seifi et al., 2019; Dullaart et al., 2020) and satellite altimetry measurements (Gómez-Enri et al., 2018; Peng and Deng, 2020). The need for precise water level measurements was recently highlighted by Taherkhani et al. (2020), who showed that even a modest sea level rise of 1 cm in some regions could double the odds of a 50-year extreme water level event (i.e., a flooding event). The risk posed by extreme water level events is especially concerning given that current projections of globally averaged sea level rise by 2100 due to mass changes from the Antarctic ice sheet alone vary from 0 to 1.7 m (Pattyn and Morlighem, 2020), whilst projections of mass loss from Greenland’s largest outlet glaciers for the same period may be underestimated (Khan et al., 2020). Continuous records of sea level changes in the polar regions, that could be used to constrain the response of ice sheets to ongoing climate change, remain critically sparse (Baumann et al., 2020).

A range of different instruments are commonly used for monitoring water levels with variable cost and accuracy (GLOSS, 2012; Míguez et al., 2005; Pytharouli et al., 2018). With a budget of

approximately 1,000–10,000 USD, it is possible to buy an acoustic gauge or a pressure gauge to monitor water levels with sub-cm accuracy - the level of accuracy required for the Global Sea Level Observing System (GLOSS) network (GLOSS, 2012). However, pressure gauges may suffer from drift over multi-year timescales (Míguez et al., 2005; Pytharouli et al., 2018) and acoustic gauges are difficult to install in remote regions because they require a structure to hang over the water surface. Radar and bubbler gauges are also commonly used to monitor water levels (see Woodworth and Smith (2003) for a comparison) but these instruments are more expensive than pressure transducers or acoustic gauges. Global Navigation Satellite System Reflectometry (GNSS-R) is an alternative technique to monitor water levels using geodetic-standard antennas that were designed to monitor land deformation. These instruments can be purchased within the same budget as previously mentioned for acoustic or pressure sensors and do not suffer from the same issues. There are already many geodetic-standard antennas installed in remote regions to monitor earth deformation and a recent study demonstrated that coastal antennas in Greenland and Antarctica could also be used to monitor sea level (Tabibi et al., 2020). However, in previous studies the precision of GNSS-R water level measurements was found to be worse than 1 cm and the datum of measurements is generally undefined (Larson et al., 2013b; Strandberg et al., 2016; Tabibi et al., 2020; Purnell et al., 2020).

Recently, as part of a broader trend in environmental sensing, there has been interest in the use of mobile devices and low-cost instrumentation for monitoring water levels. For example, Sermet et al. (2020) used images captured on smartphones to make river stage measurements and Strandberg et al. (2019b) applied GNSS-R techniques to make sea level measurements using the built-in GNSS antenna on a tablet computer. The latter study found comparable precision to GNSS-R measurements from a co-located geodetic-standard antenna. Fagundes et al. (2021) applied GNSS-R techniques to monitor a lake in Brazil using instruments that cost approximately 200 USD and found a Root Mean Square Error (RMSE) of 2.9 cm when comparing with approximately one year of measurements from a co-located radar gauge. Similarly, Williams et al. (2020) mounted a low-cost GPS receiver and antenna near a tide gauge in Ireland and found an RMSE of 5.7 cm when comparing measurements taken over a 2-year period. The larger RMSE found by Williams

et al. (2020) compared to Fagundes et al. (2021) can be at least partly accounted for by the larger daily water level variations at the coastal site in Ireland due to ocean tides.

Low-cost GNSS antennas such as those used by Strandberg et al. (2019b), Fagundes et al. (2021) and Williams et al. (2020) have shown to be better suited for GNSS-R than geodetic-standard antennas because geodetic-standard antennas are designed to reduce multipath interference (the signal that is analyzed for GNSS-R measurements). Geodetic-standard antennas can only be used to make water level measurements at low elevation angles (often less than 20 degrees), whereas low-cost antennas are designed for mobile devices hence they are approximately isotropic in their gain pattern and can be used at larger elevation angles. The extra data at larger elevation angles is useful because the bias caused by tropospheric delay (or atmospheric refraction) is reduced at larger elevation angles (Santamaría-Gómez and Watson, 2017; Williams and Nievinski, 2017; Nikolaidou et al., 2020). According to Nikolaidou et al. (2020), the tropospheric altimetry bias varies from 5 cm to 3 mm for an antenna that is 10 m above a reflecting surface when using elevation angles larger than 20 degrees. Using data collected at elevation angles larger than 20 degrees could help to eliminate the need for complicated tropospheric delay corrections that rely on global models with poor spatial resolution (Williams and Nievinski, 2017) or additional instrumentation to make in-situ measurements (Santamaría-Gómez and Watson, 2017).

Purnell et al. (2020) recently showed that random noise in the Signal-to-Noise Ratio (SNR) is one of the dominant sources of uncertainty in GNSS-R water level measurements, particularly at high elevation angles. Their results suggest that multiple co-located antennas could be used to cancel out the effect of random noise in the SNR data and improve the precision of water level measurements. It would be prohibitively expensive to co-locate several geodetic-standard antennas for the purpose of cancelling out the effect of random noise, but multi-frequency, weatherproof GNSS antennas are commercially available online for 10-30 USD, meaning that multiple low-cost antennas are still a fraction of the cost of a single geodetic-standard antenna.

The purpose of this study is to test the hypothesis that multiple co-located antennas can be used to improve the precision of GNSS-R water level measurements and to demonstrate the effectiveness of low-cost antennas. We test this hypothesis by retrieving water level measurements from

arrays of four stacked low-cost antennas at three different locations with variable tidal forcing and compare the measurements with nearby operational tide gauges. Section 3.3 contains a summary of the technique that was developed by Strandberg et al. (2016) to retrieve sea level measurements using inverse modelling of SNR data and a description of how we adapted it for using multiple co-located antennas. In Section 3.4 we provide a description of the arrays of four stacked low-cost antennas that we used to retrieve water level measurements and in Section 3.5 we describe the three test sites. Finally in Section 3.6 we present our results from the test sites and in Section 3.7 we discuss a range of parameters related to the GNSS-R analysis in order to guide future installations.

3.3 Inverse modelling of SNR data using multiple antennas

An antenna with a view of a water surface simultaneously receives GNSS signals that travel directly from a satellite and signals that reflect off the water surface prior to reaching the antenna. As a satellite moves in orbit, the difference in path length between the direct and reflected signals changes and the signals arrive at the antenna periodically in and out of phase, thereby causing an oscillation in the SNR. For each period that a GNSS satellite is aligned with the water surface such that the antenna receives reflected signals, Larson et al. (2013b) showed that the SNR can be represented as a function of the elevation angle of the satellite and the height of the antenna above the reflecting surface;

$$\delta\text{SNR} = A \sin \left(\frac{4\pi h}{\lambda} \sin\theta + \phi \right), \quad (3.1)$$

where δSNR is the detrended SNR, A depends on the power of the reflected signal and the antenna gain pattern, h is the reflector height, λ is the wavelength of the GNSS signal, θ is the satellite elevation angle and ϕ depends on properties of the reflecting surface and the antenna phase response. The reflector height refers to the vertical distance between the antenna phase center and the reflecting surface, hence this value increases as the water level decreases. Observed SNR data (recorded in units of dB-Hz) is converted to detrended SNR data (in units of Watt/Watt) by converting to a

linear scale, taking the square root and removing a second order polynomial in $\sin \theta$ space. This last step removes the influence of the antenna gain pattern and the position of the satellite.

Given the relationship in Equation 3.1, Strandberg et al. (2016) showed that the water level (analogous to h) can be retrieved via inverse modelling of SNR data. First, Equation 3.1 is modified for numerical stability by representing the oscillation as a summation of a sine and cosine wave,

$$\delta\text{SNR} = \left(C_1 \sin \left(\frac{4\pi h}{\lambda} \sin \theta \right) + C_2 \cos \left(\frac{4\pi h}{\lambda} \sin \theta \right) \right) e^{-4k^2 s^2 \sin^2 \theta} \quad (3.2)$$

where $k = 2\pi/\lambda$ is the wavenumber of the GNSS signal, s is related to the standard deviation of the reflecting surface height and both C_1 and C_2 are related to A and ϕ . The damping factor at the end of equation 3.2 follows from Beckmann and Spizzichino (1987) and accounts for the loss of coherence of the reflected signal from a rough surface with standard deviation of s . For a predetermined period of consecutive data, referred to henceforth as a time window, the parameters C_1 , C_2 and s are assumed to be constant and h is represented by a b-spline curve,

$$h(t) = \sum_{j=1}^N h_j B_j(t) \quad (3.3)$$

where h_j are unknown scaling factors, B_j are basis functions and N is dependent on the chosen knot spacing. The scaling factors should be interpreted as control points (as opposed to points along the curve) with a temporal region of influence that depends on the knot spacing (and the b-spline order, which is fixed at 2 here). The b-spline curve is a continuous function that can be evaluated at any time, however the knot spacing controls the amount of scaling factors and hence limits the temporal scale over which features in the water level time series can be resolved. For more information on the b-spline formulation, refer to Strandberg et al. (2016)).

The parameters C_1 , C_2 , s and b-spline scaling factors (h_j) are estimated simultaneously by reducing the residual between observed and modelled δSNR using a least squares algorithm. The parameters C_1 , C_2 and s are to be estimated once for each GNSS signal and satellite constellation used. The analysis is repeated and parameters are re-retrieved for each consecutive time window

over the period of interest. As per Strandberg et al. (2016), only the scaling factors within the middle period of each time window (e.g., the middle day for a time window of 3 days) are used to form the final sea level time series in order to avoid instabilities at the ends of the b-spline curves.

As an additional step, we have found that it is important to normalize the observed SNR data prior to the least squares analysis. This is done by scaling each period of detrended SNR data for each satellite prior to the inverse modelling analysis such that the absolute maximum value is always 100 (the number 100 is chosen arbitrarily). This step is taken because the amplitude of the interference in the SNR data varies greatly between different satellite constellations; it is generally stronger for GLONASS satellites. The mean variance of the detrended SNR data for GLONASS satellite arcs is approximately 3 times larger than that of GPS satellites or 6 times larger than that of Galileo satellites. Therefore, if the SNR data is not normalized, the results will be biased towards matching the data from GLONASS satellites (any residual between observed and modeled SNR will be larger for GLONASS and hence will be prioritized over data from other satellites).

The inverse modelling approach using equations 3.2 and 3.3 is adapted to account for multiple GNSS antennas in the same location as follows. For multiple co-located antennas at fixed heights relative to each other, changes in the geometric (real) reflector height for each antenna are equal but they are offset by a constant value. These constant offsets can be estimated by measuring the distance between each antenna, but this distance does not take into account possible variations in the antenna phase center, i.e., the datum of the reflector height measurements. Instead, we retrieve a reflector height time series for each antenna and calculate the mean separation between each antenna. We then arbitrarily assign one antenna to be the reference antenna and remove the mean separation from the rest of the antennas to the reference antenna. With the adjusted reflector height solutions, we take a median of each b-spline scaling factor to produce the final, combined reflector height time series. It is also possible to use SNR data from all four antennas simultaneously as part of the inverse modelling to retrieve a single set of b-spline scaling factors. However, as discussed in the Supplementary information, we found this approach to be less effective.

The effectiveness of the inverse modelling approach is dependant on several factors identified by Strandberg et al. (2016). Firstly the initial choice of values for the parameters to be estimated in

the least squares algorithm is important to find the global minimum solution as opposed to a local minimum. In this regard, the initial estimates of scaling factors should be informed by performing spectral analysis on the SNR data. An initial estimate of the reflector height is obtained using the equation

$$f = \frac{2h}{\lambda}, \quad (3.4)$$

Where f is the frequency of oscillations and λ is the GNSS carrier wavelength. The median value of h can be used as an initial estimate for all the scaling factors if there are negligible tides at a location (< 0.1 m), as is the case for one of our test sites. For sites a greater daily tidal range, the scaling factor estimates should be obtained by reducing the residual between the left and right hand side of the following equation from Larson et al. (2013b)

$$\frac{\lambda f}{2} = h + \frac{\partial h}{\partial t} \frac{\tan \theta}{\partial \theta / \partial t} \quad (3.5)$$

Where h and $\frac{\partial h}{\partial t}$ are evaluated on the b-spline curve for each time there is a frequency estimate from spectral analysis. The initial estimates of the parameters C_1 and C_2 are less important and initially set to 0 for computational efficiency. We also found that it is efficient to use 1 mm as an initial guess for parameter s . The b-spline knot spacing (and hence the number of scaling factors) is constrained by any gaps in the observations: there should not be any gaps larger than the knot spacing as this may lead to instabilities and large errors. A sea level time series at a site with large tidal forcing should theoretically be better captured by a b-spline curve with more frequent knot spacing. However, decreasing the knot spacing also decreases the amount of SNR data that is used to determine the scaling factors. The influence of the b-spline knot spacing and time window length is investigated in the results Section 3.7.3.

The reflector height time series that is output from the inverse modelling is converted to a water level time series by taking the negative of the time series (reflector height increases as water level decreases), whereby it can be compared with measurements from other water level sensors. The datum could be determined either by installing antennas next to a tide gauge with a visible bench

mark or by installing the antennas on a fixed, flat surface and using a levelling device to measure the distance between some mark on the reference antenna and the fixed surface or bench mark.

3.4 Instrumentation

We tested two different types of low-cost GNSS antennas that record data from GPS, GLONASS and GALILEO satellites: TOPGNSS GNSS100L and Beitan BN-84U. These antennas are currently available commercially online for 15–20 USD each. Arrays of four antennas are connected to a Raspberry Pi Zero to log data via USB. To maximise the strength of the multipath interference and to reduce noise from signals received from the coastline, the antennas are attached to a ground plane and oriented sideways, facing outwards from the coast. It should be noted that this configuration would likely limit the azimuthal range of measurements at a site where there is an azimuthal view of the water surface greater than 180 degrees. Information on how to build and program a similar installation is presented in a separate contribution. The SNR data that is processed for water level measurements is recorded at a frequency of 1 second at a resolution of 1 dB-Hz. A description of the data from the low-cost GNSS antennas and how it is processed for GNSS-R analysis is given in the Supplementary information. Codes written in MATLAB and Python for processing the raw GNSS data and retrieving water level measurements are provided along with this article (See Section Code Availability).

The key aim of using multiple GNSS antennas is to cancel out noise in the SNR data to improve the precision of water level measurements. It is most convenient and structurally stable to build an antenna array where the antennas are placed side-by-side, but the spacing of the antennas may be important for cancelling out noise. If the source of the noise in the SNR data is due to the local multipath environment, then the spacing of antennas should be large enough such that the signal associated with the local environment differs between antennas and cancels out when averaged and the water level signal remains. Conversely, if the noise in the SNR data is random instrument noise then the placement of the antennas is likely not important. We therefore tested two different configurations with the antennas spaced apart vertically in a line: two 'wide' configurations where

antennas were spaced apart by approximately 25 cm and one 'narrow' configuration where they were spaced apart as close together as possible (approximately 10 cm). It is not clear exactly where the antennas are located within the plastic casing, hence these distances were measured from the center of one antenna case to the next (using a ruler). We found that the mean differences between the reflector height time series for each antenna obtained using inverse modelling varied by ± 1 cm compared to the distances measured using a ruler. The distance of 25 cm between antennas for the wide configuration was chosen because it is larger than the expected standard deviation of reflector height measurements from each antenna and therefore the water level measurements from different antennas should occupy a different multipath frequency region at any given time. We note that the distance of 25 cm may not be large enough to avoid interference between antennas. We also installed both narrow and wide configurations several meters apart from each other at the same site in order to test if a larger spacing between antennas is important and to test if more than 4 antennas at the same site is advantageous.

As already discussed in Section 3.2, low-cost antennas that are used in this study are advantageous over geodetic-standard antennas in that they can be used for reflectometry at larger elevation angles. To illustrate this point, we have provided a comparison of the observed interference pattern using a GNSS100L antenna and a Leica AR25 antenna positioned at a similar height above sea level in Figure 3.2. Whilst the interference pattern is heavily dampened for more than 10 degrees for the geodetic-standard (Leica AR25) antenna, the oscillations are clear throughout 0 – 80 degrees for the low-cost (GNSS100L) antennas. One disadvantage of the GNSS100L antennas used here and of low-cost antennas in general is that they tend to only record the L1 C/A signal for GPS and GLONASS or the E1 signal for GALILEO and they do not record other signals such as the modernised L2C and L5 signals that have been shown to be better suited for reflectometry purposes (Tabibi et al., 2015, 2020). Similar GNSS receivers that also utilize the L2C signal are available for approximately six times the cost; these may be investigated in the future.

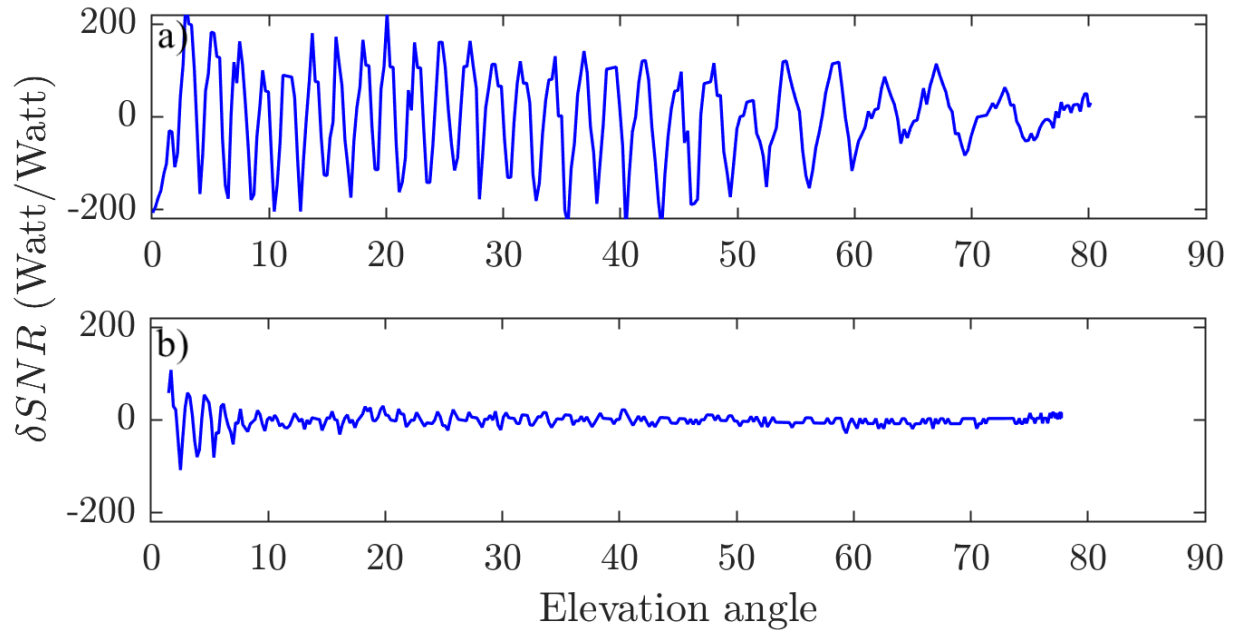


Figure 3.2: Examples of the interference pattern observed in detrended SNR data as a function of satellite elevation angle for a) one of the GNSS100L antennas used in this study placed approximately 3 m above a water surface and b) a Leica AR25 antenna at site GTGU in Onsala, Sweden situated approximately 4 m above a water surface. The data for site GTGU is available online as part of the study Geremia-Nievinski et al. (2020). The oscillations in b) are dampened with increasing elevation angle whereas in a) the dominant oscillations have an approximately constant amplitude. It should be noted that the low-cost antenna is tilted towards the horizon to maximize its sensitivity to reflected GNSS signals whereas the geodetic-standard antenna is pointed vertically.

3.5 Test sites

Our experimental antenna arrays were tested at two locations along the Saint Lawrence River in Québec, Canada and one location on the Hudson River in Piermont, NY, USA. Pictures of the three installations are given in Figure 3.3. There is a water level sensor at each site near to where the antennas were installed. For clarification, we will refer to these water level sensors as tide gauges henceforth. The Saint Lawrence River is an ideal testing ground in that water level variations are forced by a range of different signals. From Lake Ontario to the island of Montreal water level variations are dominated by drainage of precipitation, seasonal snow melt and dam activity,



Figure 3.3: Pictures of antenna arrays a) at Trois-Rivières, b) and c) show different angles at Sainte-Anne-de-Bellevue and d) at Piermont. The antenna array showed in b) and c) was also temporarily installed at Trois-Rivières. The antennas are closer together in a) in comparison to the other two setups.

Location	Tidal range (m)	Antenna model	Azimuth angle limits	Elevation angle limits	Length of data set	Antenna heights (m)	Tide gauge	Distance from GNSS-R to tide gauge (m)
Trois-Rivières	0.6	GNSS100L	80–220°	0–50°	29 d	4–6	pressure	5–10
SAB	negligible	GNSS100L	100–240°	0–80°	17 d	2–3	pressure	500
Piermont	0.8	BN-84U	180–280°	0–50°	2 d	3–5	bubbler	0 (directly above)

Table 3.1: Information about the three test sites. 'SAB' refers to Saint-Anne-de-Bellevue. Antenna heights refer to mean heights above the water surface.

whilst tidal forcing becomes progressively more dominant from Montreal to Québec city, where the Estuary to the Atlantic Ocean begins. Daily water level variations at Piermont are also dominated by tides. Key information for the three sites used is summarized in Table 3.1. The azimuth and elevation angle limits correspond to the region from which the antenna is receiving reflected signals on the water surface and were determined based on visual inspection of oscillations in the SNR data.

The site at which we collected the longest continuous data set is at the Port of Trois-Rivières. This site is on the north shore of the Saint Lawrence river, west (upstream) of the confluence with the Saint Maurice river. Trois-Rivières is approximately midway between Montreal and Quebec

City, hence daily water level variations are dominated by tides. There are three OTT Hydromet PLS pressure tide gauges at this site. The average of water level measurements from the three sensors is provided at intervals of 3 minutes from the Canadian Hydrographic Service. According to the instrument handbook, the accuracy is 0.5 cm or less. The narrow GNSS100L antenna array collected data for a continuous four week period from September 11 to October 9, 2020. Both narrow and wide GNSS100L antenna arrays were also installed for a 5 day period in August, 2020. The antenna arrays at this site were installed approximately 5 – 10 meters away from the tide gauges.

The second site in Québec is in Sainte-Anne-de-Bellevue, at the western tip of the island of Montréal. The stretch of coast where the antennas were situated is part of the northern border of Lake Saint-Louis, which is at the meeting point of the Saint Lawrence and the Ottawa rivers. We installed the antennas on a tree looking over the lake (Figure 3.3b). The antennas were installed between February and June 2020, however the lake was frozen for the first two months of this period and the antennas were not continuously recording data due to logistical issues associated with the COVID-19 pandemic. Here we focus on a continuous period of data from May 17th to June 2nd. We used data from a nearby Environment and Climate Change Canada tide gauge to validate our GNSS-R measurements. The tide gauge is a Campbell Scientific CS450 pressure transducer and data is available online at 6 minute intervals from the Government of Canada. It is not clear what specific model of the CS450 sensor is installed at this site, but if we assume that it is a standard accuracy model with 10 m range, the accuracy is at most 1 cm. The tide gauge is situated approximately 500 m west of where the antenna array was installed, just south of a canal and the Sainte Anne Rapids that flow from the Lake of Two Mountains to Lake Saint Louis (see Figure 3.4). We are cautious that differences between the tide gauge and GNSS-R measurements at site could be partly accounted for by differences in the local flow regimes.

At the site on the Hudson River in New York, the antenna array was installed at the end of a large pier. The antennas were mounted on a pole directly above a Sutron Constant Flow Bubbler for an approximately 48-hour period from 8–10th September, 2020. Data from the bubbler tide gauge at intervals of 15 minutes was downloaded online from the United States Geological Survey.

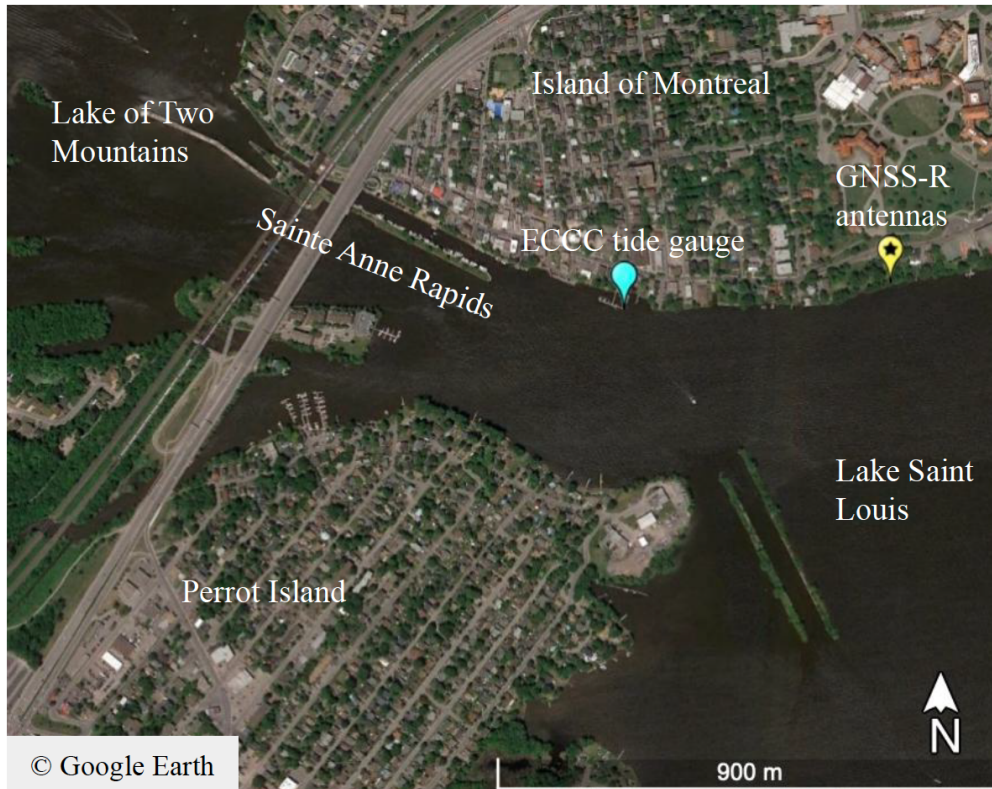


Figure 3.4: The area surrounding the antenna array and tide gauge at Sainte-Anne-de-Bellevue.

According to the instrument specifications, the accuracy of this sensor is approximately 0.3 cm (0.01 ft).

The RMSE between GNSS-R and tide gauge measurements is used henceforth as a proxy for the precision of the GNSS-R measurements. If we assume that errors from the tide gauge and GNSS-R measurements are not correlated then the RMSE is actually an upper limit for the precision. It is not a focus of this study to calculate the datum of the GNSS-R measurements relative to that of the tide gauges, hence the mean is removed from each time series and the RMSE is then calculated by evaluating the b-spline curve from inverse modelling at each time that a measurement from the tide gauge exists.

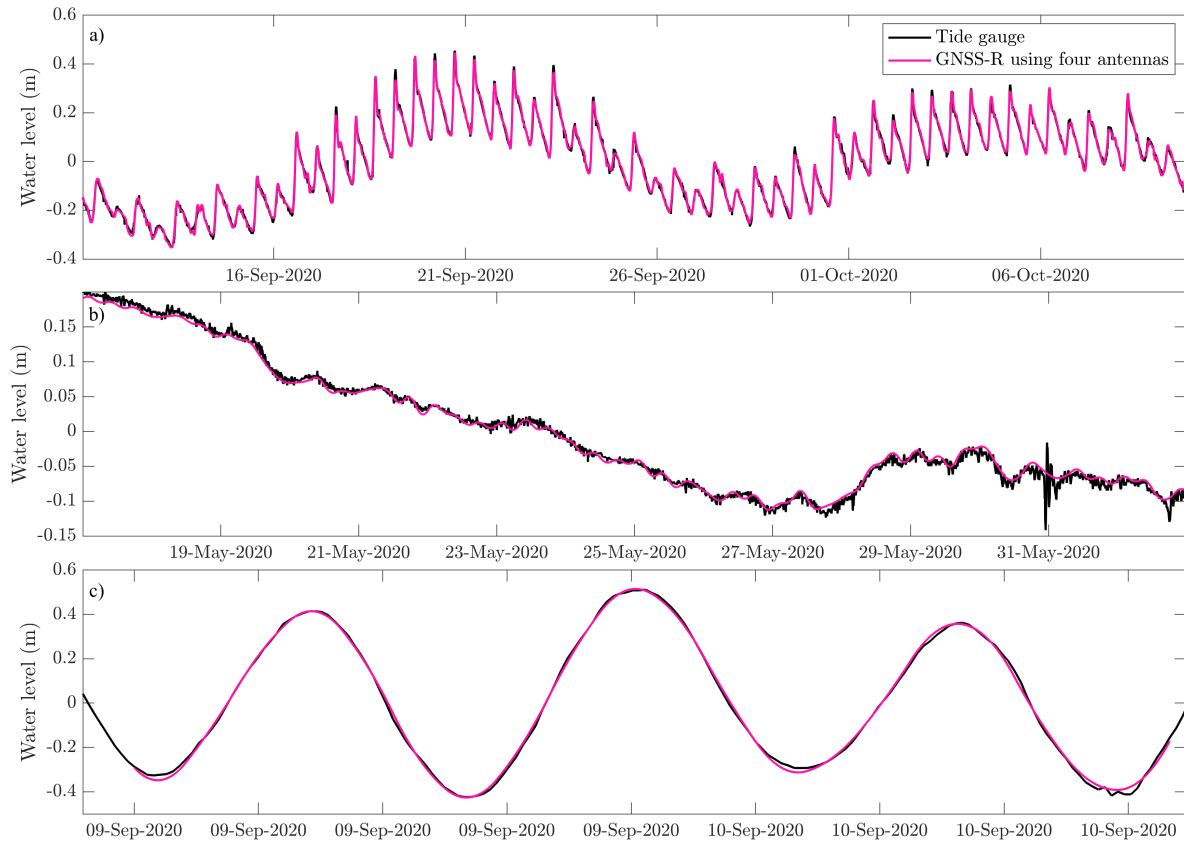


Figure 3.5: A comparison of GNSS-R and tide gauge measurements at a) Trois-Rivières, b) Sainte-Anne-de-Bellevue and c) Piermont. The mean of each time series is removed before plotting.

3.6 Results

The GNSS-R water level measurements obtained using inverse modelling of SNR data from four low-cost antennas are plotted alongside tide gauge measurements at all three sites in Figure 3.5. There is a good agreement between the GNSS-R and tide gauge measurements at all sites; for the 29-day period at Trois-Rivières the RMSE is 1.02 cm, for the 17-day period at Sainte-Anne-de-Bellevue the RMSE is 0.69 cm and for the 2-day period at Piermont the RMSE is 1.16 cm. To help visualize the data that is obtained from the arrays of four antennas, an example of the reflector height solutions from each antenna at Sainte-Anne-de-Bellevue is given in Figure 3.6. There is also a shorter period of data for each site plotted with GNSS-R minus tide gauge measurement residuals given in the supplementary information, Figure 3.7.

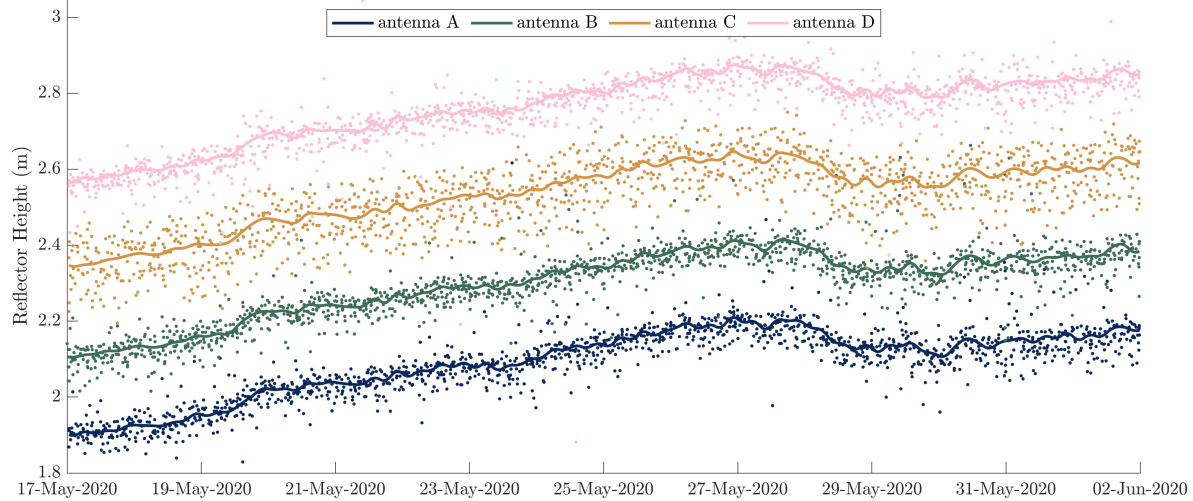


Figure 3.6: Reflector height measurements from four antennas at Sainte-Anne-de-Bellevue. The solid lines represent the b-spline solutions from inverse modelling and the dots are estimates from spectral analysis. The b-spline parameters that are used to plot the solid lines in this figure are averaged to form the single solution in Figure 3.5b. The curves are inverted because reflector height increases as water level decreases.

The daily water level variations at Trois-Rivières (in Figure 3.5a) and Piermont (in Figure 3.5c) are dominated by the principal lunar semidiurnal tides. However, tidal waves are modified in the shallow river channel at Trois-Rivières such that the crests travel faster than the troughs, which gives rise to the sawtooth-like pattern at Trois-Rivières as opposed to the smoothly varying sinusoid that dominates the signal at Piermont. Daily water level variations at Sainte-Anne-de-Bellevue (in Figure 3.5b) are of much smaller magnitude as there are negligible tides, but high frequency variations in water levels associated with local weather can be seen in the tide gauge record. The water level variations at this site are driven by drainage of precipitation and other hydrological effects, for example it rained upstream of Montreal on May 28, which corresponds with a rise in the observed water level on this day at Sainte-Anne-de-Bellevue.

3.6.1 Influence of multiple co-located antennas

There is an improvement in the precision of water level measurements when using four antennas as opposed to using just one antenna at all three sites. Reading values from Table 3.2, if the RMSE

Site	RMSE (cm) obtained using inverse modelling with:			
	One antenna	Two antennas	Three antennas	Four antennas
Trois-Rivières	1.24–2.25	1.26–1.64	1.04–1.10	1.02
Sainte-Anne-de-Bellevue	0.63–0.95	0.64–0.81	0.65–0.73	0.69
Piermont	1.08–1.67	1.07–1.44	1.10–1.25	1.16

Table 3.2: Summary of results obtained using different combinations of antennas to retrieve water level measurements. For 1–3 antennas, the RMSE for every combination of antennas at each site was calculated but only the lowest and highest values are shown in the table.

obtained with four antennas is compared to the maximum RMSE obtained with one antenna, there is a reduction of 1.23 cm (or 50%) at Trois-Rivières, 0.26 cm (or 30%) at Sainte-Anne-de-Bellevue and 0.51 cm (or 30%) at Piermont. The results from Table 3.2 indicate a significant improvement (up to 0.62 cm) when using four instead of two antennas, but minimal improvement between three and four antennas. Four antennas is also recommended over three antennas in case of redundancy. Note that whilst the difference between the minimum RMSE obtained with one antenna is comparable to that obtained with four antennas, our analysis suggests that the relative performance of each antenna appears to be random, which in turn implies that the upper limit should be used for comparison. For example, if the data from Trois-Rivières is split into two two-week periods and analyzed separately, the antennas that give the most and least precise results are not the same for both periods, and neither of these sets in turn match those for the total four week period.

During a period of four days, we performed an experiment with two arrays of four antennas (8 in total) installed at different heights and found that there is no advantage in installing more than four antennas at the same site. For this four day period there is an RMSE of 1.06 cm when using just the narrow configuration, 1.32 cm when using just the wide configuration or 1.14 cm when using both narrow and wide simultaneously. Given that the configurations were installed several meters apart, we tested different combinations of antennas across both configurations to see if the spacing of antennas influences the precision when using multiple antennas and found that there is no advantage in using antennas spaced further apart than the narrow configuration. These findings together with our analyses at all three sites also indicate that there is no clear dependence on the heights of the antennas above the water surface. These results also suggest that the source of noise

in the SNR data is likely due to random instrument noise as opposed to interference from the local environment.

Our results so far have focused on inverse modelling of SNR data, but spectral analysis estimates, shown as dots in Figure 3.6, can also be compared with the tide gauge measurements. The RMSE of hourly means of spectral analysis estimates at Sainte-Anne-de-Bellevue varies from 2.40 – 3.90 cm for each antenna. The hourly means can then be combined into a single time series by removing the height offset from each antenna and taking the median of the hourly values, which gives an RMSE of 1.94 cm. The maximum improvement of 1.96 cm when using four antennas as opposed to a single antenna for spectral analysis estimates is much larger than the 0.26 cm maximum improvement when using inverse modelling at this site. These differences between inverse modelling and spectral analysis suggest that random noise is a larger source of uncertainty when using spectral analysis, thus supporting the results from Purnell et al. (2020). These results demonstrate that using multiple antennas in the same location is an effective technique for improving the precision in GNSS-R water level measurements, regardless of the technique that is used.

3.7 Discussion of GNSS-R parameters

The results described above were obtained after exploring a large parameter space related to the inverse modelling and experimental setup. The most important parameters to consider are the elevation angle limits, the azimuth angle limits, the b-spline knot spacing and time window length, the satellite constellations used and the temporal resolution of data. We discuss the results of tests with these parameters below. The results discussed in this section were all obtained using the inverse modelling technique given in Section 3.3.

Note that elevation and azimuth angle limits are constrained by the site surroundings and the discussions in Sections 3.7.2 and 3.7.1 refer to investigating optimal limits within these pre-defined constraints. A given azimuth and elevation angle corresponds to a Fresnel zone on the reflecting surface where the power of the signal is concentrated. Software for calculating and visualizing Fresnel zones is given by Roesler and Larson (2018). As the elevation angle decreases, the Fresnel

zone increases in size and moves away from the antenna, whereas changing the azimuth angle rotates the Fresnel zone laterally around the antenna. The limits given in Table 3.1 correspond roughly to the region in which the Fresnel zones are on the water surface and where there are no objects obstructing the view of the water surface (e.g., moored boats).

3.7.1 Elevation angle limits

Using low-cost antennas we retrieved water level measurements over a range of elevation angles up to 50 degrees at Trois-Rivières and Piermont and up to 80 degrees at Sainte-Anne-de-Bellevue, whereas previous ground-based GNSS-R studies have been limited to the use of elevation angles up to 35 degrees. Due to a number of trade-offs between low and high elevation angles, we found optimal limits of 10–50 degrees at all three sites. For sites located at mid to high latitudes (such as our sites), satellites are more prevalent towards the equator (i.e. to the south of our instruments) at lower elevation angles, and therefore using lower elevation angles increases the amount of SNR data that is available for analysis. We find that reflector height measurements are generally less precise at elevation angles greater than 30 degrees, in agreement with previous work using geodetic-standard antennas that found the effect of random noise in SNR data leads to a greater uncertainty at larger elevation angles (Purnell et al., 2020). However, the effect of tropospheric delay increases with decreasing elevation angle and leads to an underestimation of the reflector height (Williams and Nievinski, 2017). For our sites, tropospheric delay has a minor effect on the precision, but aforementioned literature (Nikolaidou et al., 2020) suggests that this effect is more important at sites where the antennas are at a greater height above the water surface (e.g., ≈ 5 m) or where there is a large tidal range (e.g., ≈ 2 m) and especially when attempting to find the datum of reflector height measurements (not done here). In general, we find that it is most important to use a large range of elevation angles (e.g., 30 degrees or more) to eliminate any gaps in time in the SNR data and this is especially important at sites with daily tidal variations, such as at Trois-Rivières and Piermont. We initially tried to use a lower limit of 20 degrees, where the effect of tropospheric delay becomes negligible (Nikolaidou et al., 2020), but found more precise measurements using a

lower limit of 10 degrees at Trois-Rivières and Piermont. Limits of 20–50 degrees can be used to make equally precise measurements as 10–50 degrees at Sainte-Anne-de-Bellevue.

3.7.2 Azimuth angle limits

In general, azimuth angle limits should be fixed to match the widest unobstructed view of the water surface. In contrast with elevation angles, there are no complicated azimuth angle-dependent effects; the larger the range of azimuth angle limits, the more data for GNSS-R analysis. The only complicating factor is that some azimuth angles yield more data per day than others because satellites are more prevalent towards the south at mid to high latitudes in the northern hemisphere or vice versa in the southern hemisphere. To demonstrate the importance of maximising the azimuth angle range, we retrieved water level measurements at Trois-Rivières and Sainte-Anne-de-Bellevue with the azimuth angle range reduce from 140° to 100° . The RMSE increased by approximately 50% (from 1.02 cm to 1.49 cm) at Trois-Rivières and 15% (from 0.69 cm to 0.79 cm) at Sainte-Anne-de-Bellevue when using the reduced azimuth angle ranges.

3.7.3 B-spline knot spacing and time window

For the results described in the previous section, the b-spline knot spacing and time window length vary for each site: at Trois-Rivières we use a knot spacing of 1 hour and a time window of 6 hours, at Sainte-Anne-de-Bellevue we use a knot spacing of 4 hours and a time window of 24 hours and at Piermont we use a knot spacing of 2 hours and a time window of 6 hours. In general, the knot spacing should be set to 1 hour at a site with large daily tidal variations or a site with a complicated signal (such as the sawtooth-like signal at Trois-Rivières). Note that there is automatically a lower limit on the precision that can be achieved using inverse modelling because a b-spline curve cannot perfectly represent the time series. This lower limit on the precision increases with increasing knot spacing. For example, if we directly fit a b-spline curve to the tide gauge measurements at Trois-Rivières shown in Figure 3.5a, we find an RMSE of 0.5 cm if using a knot spacing of 1 hour or 1.6 cm if using a knot spacing of 2 hours. However, decreasing the knot spacing for inverse

modelling also decreases the amount of SNR data that is used to compute each b-spline scaling factor, potentially leading to less precise results, hence we do not recommend using a knot spacing of less than 1 hour.

The time window should be at least 3 times the length of the knot spacing. Provided that this minimum is met, the length of the time window does not appear to impact the precision in our experiments. However, both increasing the window length or decreasing the knot spacing greatly increases the computation time for the inverse modelling.

3.7.4 Satellite constellations

Using data simultaneously from all three satellite constellations that are tracked by our low-cost antennas (GPS, GLONASS and Galileo) is important to achieve the most precise results. For example, when using only GPS data at Trois-Rivières, the RMSE increases by over 200% compared to the results obtained using all three constellations (the RMSE is 3.11 cm with just GPS compared to 1.02 cm with all three constellations). Using any combination of two constellations also leads to less precise results than using all three constellations: The RMSE increases by approximately 30% (to 1.27 cm) when using just GPS and GLONASS together or 170% (to 2.69 cm) when using just GLONASS and Galileo together. It is not clear if these differences are due to the prevalence of satellites (there are more GPS satellites) or differences in the signals themselves.

3.7.5 Temporal resolution of SNR data

The temporal resolution of SNR data greatly affects the computation time for inverse modelling. Data was recorded at our sites every second but we found that it was most efficient to resample the data to intervals of 15 seconds prior to analysis. When varying the temporal resolution between 1 and 15 seconds at Trois-Rivières, we found that the RMSE varies by less than 1 mm but the computation time increases greatly when using an interval time of one second. The RMSE increases by approximately 70% when decimating the data to intervals of 30 seconds or 60 seconds. Recording data at intervals of 5, 10 or 15 seconds is therefore advantageous for data storage and efficient

analysis. It is important to note, however, that the temporal resolution provides a limitation on the maximum reflector height that can be resolved due to the Nyquist frequency. See Roesler and Larson (2018) for a discussion on this Nyquist limit.

3.8 Conclusions

We presented a technique for retrieving precise water level measurements using arrays of four low-cost GNSS antennas and validated our technique at three sites with variable tidal forcing. By comparing with nearby operational tide gauges, we found an upper limit on the precision of water level measurements of 0.69–1.16 cm at all sites, whereas previous studies using geodetic-standard antennas have found an RMSE of 2–50 cm. The RMSE values obtained are likely upper limits on the precision because they also contain error from the tide gauge measurements. The amount of error from the tide gauge measurements is also likely to differ between sites because there are different types of instruments at the sites in Québec (pressure transducers) and Piermont (bubbler gauge). While pressure transducers are more susceptible to errors over multi-year timescales due to instrument drift (Míguez et al., 2005; Pytharouli et al., 2018), bubbler gauges are more susceptible to errors during wavy conditions (Woodworth and Smith, 2003). The results presented here are significant in that an accuracy of 1 cm is the benchmark set by (GLOSS, 2012) for studying multi-year trends in sea level. We found an improvement in the precision of 30–50% when using four co-located antennas instead of one, which suggests that random noise is one of the key sources of uncertainty in GNSS-R measurements and supports the results from Purnell et al. (2020). In addition to the reduction in cost (on the order of several thousand USD or more), we found that the low-cost antennas are better suited for reflectometry than geodetic-standard antennas because they can be used to obtain water level measurements over a much larger range of elevation angles.

Our results provide a strong proof of concept, but work remains to be done to further validate and improve our technique. Most importantly, an array of antennas should be installed with a co-located tide gauge for a longer time period (e.g., for at least several months) and at a site with a larger tidal range. It is also necessary to attempt a levelling procedure so that the datum of the

water level measurements can be defined. To place measurements on a global reference frame and simultaneously monitor local land deformation, an array of low-cost antennas could then be co-located with a geodetic-standard antenna with the aim of using the low-cost antennas to obtain precise water level measurements and the geodetic-standard antenna to perform precise positioning. More models of low-cost antennas should also be tested, preferably in the same location (we do not recommend one of the types of antennas used in this study over the other type because we have not had the opportunity to test them at the same location). Whilst our results suggest that the spacing apart of antennas is not important, we cannot rule out the possibility of interference between antennas at the separation distances used in this study. A rigorous investigation of the clearance distance required to ensure that antennas are not interfering should guide a future study. A vertical array of low-cost antennas such as those used in this study could be used to test the technique for obtaining high-rate sea level measurements recently proposed by Yamawaki et al. (2021).

For future installations of low-cost antennas, we propose the following guidelines:

- at least four co-located antennas
- the antennas should record data from GPS, GLONASS and Galileo satellites
- the antennas should be positioned within 1–5 m above the water surface
- the antennas should have an unobstructed view of the water surface that extends 140 degrees or more laterally and at least 50 metres outwards (this corresponds to the edge of the Fresnel zone for an antenna 5 m above the water surface and a satellite at 10 degrees elevation)
- data should be recorded at intervals of 5 seconds (or more, depending on the mean height of the antennas above the water surface and the associated Nyquist limit).

Upon obtaining data, the following inverse modelling parameters should be used to extract precise water level measurements:

- a large range of elevation angles (e.g., 10–50 degrees)

- a b-spline knot spacing of 1 hour at a site with tides (or larger would be more efficient at a site with negligible tides)
- a b-spline time window length of at least three times the knot spacing.

The above guidelines may be refined following further field work. For example, we found that four antennas is optimal when we tested eight co-located antennas for a short period of four days - more data is needed to support this result. Additional data from other satellite constellations (such as BeiDou) and from other signals (such as L2C and L5) may also be useful.

Our technique for monitoring water levels with arrays of low-cost antennas could be applied to address the need for widespread, accessible water level measurements in the face of future climate change. The antenna arrays are relatively simple to build and therefore suited to citizen science efforts. They could be used to obtain sea level measurements in remote coastal regions as well as lake level or river stage measurements at a lower cost than commercially available sensors and with comparable precision. Such measurements could be used to validate satellite measurements and to better constrain tidal models in the polar regions, where there are few coastal sea level measurements. A dense network of sensors could also be installed to detect spatially variable sea level signals, for example near tidewater glaciers to detect so-called sea level fingerprints (Mitrovica et al., 2011).

3.9 Supplementary Information

3.9.1 Combined inversion of SNR data from multiple antennas

Instead of using the methodology described in Section 3.3 in the main text for combining data from co-located antennas by averaging b-spline scaling factors, we also tried performing inverse analysis using data from all co-located antennas simultaneously. This combined inversion is performed by adapting equation 3.2 in the main text, such that h is written in terms of the reflector height for a chosen reference antenna and the predetermined vertical separation between each antenna and the reference antenna. The RMSE increases from 1.02 to 1.24 cm when performing the combined

inversion with all four antennas at Trois-Rivières as opposed to averaging b-spline scaling factors from different antennas. This result suggests that there is no advantage in performing a combined inversion using data from multiple co-located antennas.

3.9.2 Data processing

The signals received by the GNSS100L and BN-84U antennas are internally processed and recorded into the National Marine Electronics Association (NMEA) 0183 format, which contains processed GNSS data such as the estimated position of the antenna, number satellites in view and position and strength of signal received from the satellites. This is in contrast to the standard receiver independent exchange (RINEX) format, standard for geodetic receivers, which contains information about the carrier phase of received signals that can be processed to obtain precise positioning data. Whilst precise positioning is not possible with the low-cost antennas used herein, the key parameter of interest for reflectometry applications is the SNR data, which is recorded in the NMEA file format.

The azimuth and elevation angle of satellites relative to the antenna is also recorded in the NMEA file format at a resolution of 1 degree. This resolution is not good enough for obtaining reflector height estimates. Instead, we use the Center for Orbit Determination in Europe (COD) orbit solutions that are available online from the Multi-GNSS Experiment and Pilot Project (MGEX) and Crustal Dynamics Data Information System (CDDIS) archive. These orbit solutions give the location of each GNSS satellite every 5 minutes, which can then be interpolated to every second and converted to an azimuth and elevation angle at the antenna. Codes that were used to obtain and process this data are provided along with this article.

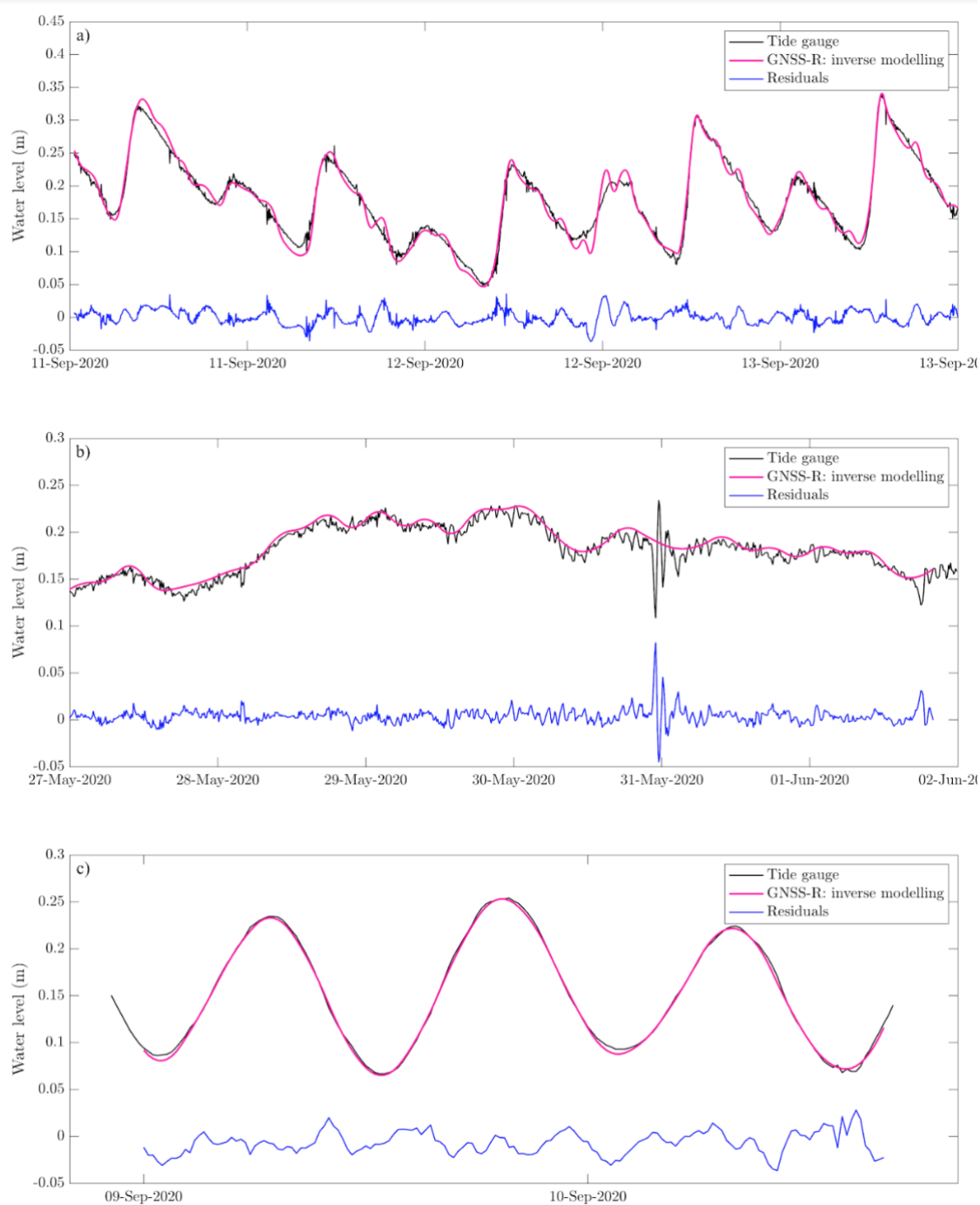


Figure 3.7: Comparison of GNSS-R and tide gauge measurements with residuals at a) Trois-Rivières, b) Sainte-Anne-de-Bellevue and c) Piermont, as in Figure 3.5 in the main text but for reduced periods. In each of these figures, the GNSS-R and tide gauge measurements are offset by an arbitrary amount from the residuals. In c), the GNSS-R and tide gauge measurements have been scaled by 0.2 for an easier comparison with the residuals.

Chapter 4

Near real-time water levels for flood monitoring using GNSS-R with multiple low-cost antennas

In Chapter 3, a promising, novel GNSS-R technique was presented for obtaining precise GNSS-R water levels. This technique is further developed in this chapter, with the aim of developing software for in-situ, real-time processing of GNSS-R water levels using multiple co-located low-cost antennas. The motivation for developing this software is to broaden the range of applications of GNSS-R water level monitoring and to make the technique more accessible for non-experts. In order to achieve these goals, this chapter focuses on the technical details of the data processing and provides guidance on the precision that can be achieved for near real-time water levels. This chapter also contains results from additional field work at Saint-Joseph-de-la-Rive, Québec, where we found that using multiple co-located antennas significantly improves the precision of GNSS-R water levels, thereby further supporting the results from Chapter 2 (that random noise is a dominant source of uncertainty in GNSS-R water levels).

4.1 abstract

Global Navigation Satellite System Reflectometry (GNSS-R) using low-cost antennas is a practical solution for monitoring water levels from rivers, lakes or coastlines that does not require submerging any instruments in water. It was shown in a previous article that multiple low-cost GNSS antennas installed on the shore of a river could be used to obtain water level measurements with a precision of approximately 1 cm. Real-time water levels are critical for a range of applications such as flood and storm surge monitoring, marine navigation and reservoir management, however, the water level measurements in previous work have been obtained by processing the GNSS data weeks after it was initially recorded. Here we present, for the first time, a novel method for obtaining near real-time water levels using multiple low-cost antennas. We develop an efficient moving window algorithm for real-time data processing and test it at one site with high amplitude tides and one site with low amplitude tides (Saint-Joseph-de-la-Rive and Trois-Rivières, Quebec, respectively). Unlike previously developed techniques, the moving window algorithm does not rely on external data sets (i.e., no internet connection is required) and it can be implemented for in-situ water level monitoring using a microcomputer or microcontroller with limited memory. By comparing near real-time GNSS-R water levels (post-processed with 1 hour delay) with a co-located pressure gauge, we find an RMSE of 1.76 cm at the site with smaller tides and 6.85 cm at the site with larger tides. The optimal results when using the moving window algorithm are found for measurements post-processed 4 hours into the past, with an RMSE of 1.59 cm and 4.93 cm at the site with smaller and larger tides, respectively. When compared to the optimal results from a previously developed post-processing technique that relies on external data sets, the moving window algorithm is more accurate at the site with large tides (more than 2 cm reduction in the RMSE) and marginally less accurate at the site with smaller tides (less than 1 cm greater RMSE). We also assess the bias in the GNSS-R water levels at the site with larger tides by using an optical survey to independently measure the vertical separation between the antennas and the water surface. By using a correction for the effect of tropospheric delay, we effectively remove the mean bias in the GNSS-R measurements, from 6.9 cm to less than 1 cm. We conclude that GNSS-R water level sen-

sors could be a powerful tool for more accessible flood monitoring and for improving the spatial coverage of sensors in remote regions.

4.2 Introduction

The global average of economic losses associated with flooding are estimated at over 100 billion USD per year (UNISDR, 2015). These losses are expected to increase as populations in flood-prone areas grow and floods become more frequent under climate change (Jongman et al., 2012; Dottori et al., 2018; IPCC, 2021). Water levels are a crucial component of flood forecasting and monitoring (Jain et al., 2018; Merkurjeva et al., 2015). For example, water level sensors are often installed along rivers upstream of populated areas in order to forecast the potential for costly and life-threatening flooding downstream (Cools et al., 2016). However, the most common instruments for water level monitoring (pressure gauges) are flawed in their capacity for flood monitoring in that they need to be submerged in water, where they are vulnerable to being destroyed or moved during flooding conditions, for example by debris or ice (Asante et al., 2007; Pomeroy et al., 2016; Apel et al., 2022). Other commonly used instruments such as radar gauges or acoustic sensors need to hang directly over the water surface, which is impractical outside of populated areas if there is no infrastructure to hang them off (such as bridges or piers).

Global Navigation Satellite System Reflectometry (henceforth GNSS-R) is a technique for obtaining water levels using antennas that can be positioned up to tens of meters away from a shoreline (horizontally and vertically), where they are less likely to be destroyed during flooding conditions. This technique is also known as GNSS Interferometric Reflectometry (GNSS-IR). The potential for GNSS antennas to be used as water level sensors has been studied in detail using geodetic-standard antennas (Anderson, 2000; Larson et al., 2013b; Strandberg et al., 2016; Purnell et al., 2020; Liu and Zhang, 2021; Wang et al., 2019) and large global networks of these instruments already exist for monitoring land motion. The GNSS-R technique is therefore appealing for obtaining additional environmental information from these networks, especially from sites in remote regions such as Greenland and Antarctica (Tabibi et al., 2020; Dahl-Jensen et al., 2021b).

Perhaps the main disadvantage of the GNSS-R technique is that the process of obtaining water levels is complex, although there have been several recent notable efforts to make GNSS-R analysis techniques more accessible to non-experts (Roesler and Larson, 2018; Altuntas and Tunalioglu, 2021; Martín et al., 2020) (also see <https://github.com/kristinemlarson/gnssrefl>). Another disadvantage of the GNSS-R technique is that the estimated precision of water levels from GNSS-R is cm-scale (Geremia-Nievinski et al., 2020; Purnell et al., 2020), which is an order of magnitude less precise than most pressure or radar gauges (according to product specification manuals).

Recently it has become clear that compact, low-cost (or mass-market) GNSS antennas and receivers, such as those that are embedded in mobile devices, may be better suited for water level monitoring than geodetic-standard antennas (Fagundes et al., 2021; Karegar et al., 2021; Purnell et al., 2021; Williams et al., 2020). Geodetic-standard antennas are designed to reduce the interference from reflected GNSS signals (the interference that is used for GNSS-R analysis), while the low-cost antennas are not. In Purnell et al. (2021) (henceforth DP21), the authors used GNSS-R with low-cost antennas to obtain a similar level of precision to commercial sensors such as pressure gauges. The authors found that using multiple antennas in the same location is an effective way to reduce the effect of random noise and hence improve the precision of water levels. This result followed from (Purnell et al., 2020), in which the authors showed that random noise was a dominant source on uncertainty in GNSS-R measurements.

A key limitation of the technique presented in DP21 is that the GNSS-R water levels were not recorded in-situ and hence could not be sent remotely in real-time i.e., using telemetry. Instead, the GNSS data was retrieved and then analyzed weeks after it was initially recorded. Yet, for the majority of operational water level monitoring applications, real-time water levels are either preferred or required. For example, real-time water levels are required near ports to ensure that the water is deep enough or that there is enough space under bridges for ships to pass. For flood monitoring, real-time river discharge estimates (that are generally derived from water levels) are used to drive hydrological models that predict floods and real-time water levels are also directly used to estimate flood extent, thereby aiding with flood preparedness and emergency response efforts. Real-time GNSS-R levels also have the potential to be useful for reservoir management,

rapid deployment for storm surge monitoring, ice jam monitoring and snow depth monitoring. It should also be noted that an instrument that processes GNSS-R data in-situ (i.e., an instrument that does not require any GNSS-R expertise to operate) would likely be appealing for research in a range of scientific fields, including sea level and coastal change, geodesy, hydrology and cryospheric sciences.

The water levels were not processed in-situ in DP21 due to a combination of two issues. The first issue was that the GNSS-R analysis is computationally demanding and it would require a powerful microcomputer to process the data in-situ. Such a microcomputer would have large power requirements, which would make the system expensive to run using solar power (there were no power outlets available for two out of three of the sites in DP21). The second issue was that the analysis relied on precise GNSS orbit solutions that were published online and there was no available internet connection at the sites in DP21. One potential solution to these issues would be to install a GNSS-R sensor at a location where there is a power outlet and an internet connection. However, the major advantage of the GNSS-R technique is that the associated field work is less expensive and time-consuming in remote regions, where power outlets and internet connections are either unavailable or prohibitively expensive. Another potential solution would be to send the GNSS data remotely to be processed via cloud-based software. This solution is also not suitable for remote regions because the raw GNSS data is large and sending the data remotely, much like maintaining an internet connection, would be expensive. On the other hand, it would be feasible to send processed data from remote regions using satellite telemetry. In less remote regions, where cellphone networks could be used for telemetry, it would also be much more efficient to send processed data than unprocessed data.

Another limitation of the results from DP21 is that the datum of the GNSS-R water levels (the zero point) was not independently measured. For hydrological applications, it is important to monitor the datum of water levels because any errors will translate to erroneous discharge estimates and hence to forecasting errors. It is equally important to monitor the datum of water levels for studies of sea level change to ensure that there is no instrument drift that could be misinterpreted as a climate signal (Pérez et al., 2014; Pytharouli et al., 2018). In theory, the datum of GNSS-R

water levels is the antenna phase center, which can be independently monitored relative to a global reference frame with a geodetic-standard antenna by using precise point positioning. The combination of precise point positioning and GNSS-R water levels can therefore be used to compare with satellite altimetry measurements (Lee et al., 2019) or for levelling with co-located tide gauges (Santamaría-Gómez and Watson, 2017). It may not be possible to perform precise point positioning analysis with low-cost antennas because vertical errors can be on the order of tens of meters, but the vertical separation between the antennas and water surface can be independently measured using standard surveying techniques. A bias in GNSS-R levels (an underestimation of the separation between the antennas and water surface) is expected due to the effect of tropospheric delay (Santamaría-Gómez and Watson, 2017; Williams and Nievinski, 2017; Nikolaidou et al., 2020, 2021).

With the application of flood monitoring as motivation, the goal of this article is to develop a GNSS-R instrument for real-time data processing that is practical, affordable, and suitable for obtaining water levels in remote regions. We seek to develop an algorithm for efficient real-time data processing without any reliance on external data sets or instrumentation. In order to make the data accessible to non-experts, water levels should be recorded in-situ with the capability of sending them remotely. Whilst we do not have data from a flooding event to test the technique, we use data from a site with large tides (up to nearly 6 m daily variations), which acts as a proxy for an extreme flooding event. We use additional data from a site in DP21 to further validate the real-time processing technique. Finally, we assess the datum of GNSS-R water levels by using an optical survey to measure the vertical separation between antennas and water surface.

4.3 GNSS-R theory

Water level measurements can be obtained by analyzing the Signal-to-Noise Ratio (SNR) of GNSS signals recorded by coastal antennas. If a satellite is positioned such that some signals reflect off the water surface prior to reaching the antenna, then these reflected signals will interfere with direct signals from the satellite as the satellite moves in its orbit. In this case, the SNR will exhibit

an oscillation that can be approximately described by the following equation from Larson et al. (2013b),

$$\delta\text{SNR} = A \sin\left(\frac{4\pi h}{\lambda} \sin\theta + \phi\right), \quad (4.1)$$

where h is the vertical separation between the antenna phase centre and the water surface (henceforth, the reflector height), λ is the wavelength of the GNSS signal and θ is the satellite elevation angle. Water level variations are equal but opposite to reflector height variations, i.e., as the water level increases, the reflector height decreases. The parameters A and ϕ describe the amplitude and phase offset of the oscillation. The SNR is also affected by the changing distance between the antenna and the satellite but this effect is not of interest for GNSS-R analysis and can be removed by detrending the SNR, as denoted by δSNR . If spectral analysis is performed on δSNR in $\sin\theta$ coordinates, then the dominant frequency should theoretically be related to h using the following equation, first presented in Larson et al. (2013b),

$$\frac{\lambda f}{2} = h + \frac{\partial h}{\partial t} \frac{\tan\theta}{\partial\theta/\partial t} \quad (4.2)$$

where f is the peak frequency retrieved from spectral analysis. An estimate of h , or equivalently a water level measurement, can therefore be obtained for each time a satellite is positioned such that signals reflect off the water surface prior to reaching the antenna (referred to henceforth as a satellite arc).

4.4 Real-time data processing

Obtaining accurate GNSS-R water level measurements in real-time using multiple antennas requires an algorithm that can efficiently process a large amount of data. A single water level estimate from one satellite arc requires a time series of many SNR measurements (approximately 100 measurements will give a strong peak from spectral analysis, depending on the height of the antenna) and accurate water levels are obtained from averaging many arcs because each arc con-

tains random noise (Purnell et al., 2020). Here we develop a moving window type technique for real-time data processing that is adapted from the spline-fitting technique used in DP21. The data processing, as outlined in Figure 4.1, is performed in stages to incrementally reduce the size of the data and increase the efficiency of the algorithm. An example of one time step of the moving window algorithm is visualized in Figure 4.2. More details about the stages of data processing are given in the following sections.

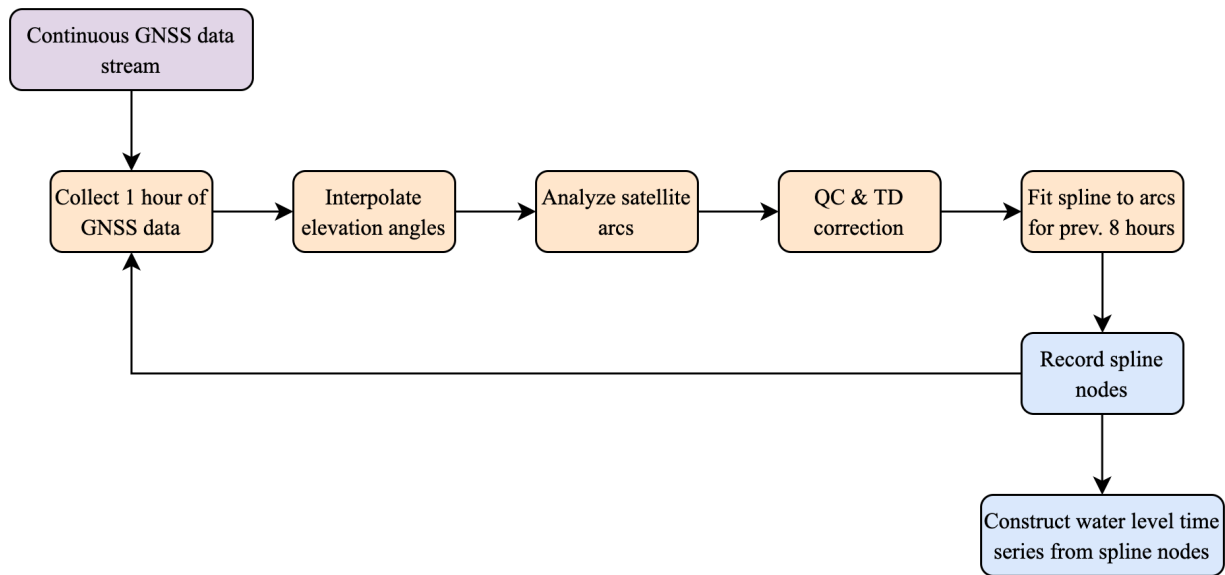


Figure 4.1: Flow chart showing the stages of data processing to obtain water level measurements from the low-cost GNSS antennas using a moving window algorithm. 'QC' stands for quality control and 'TD' stands for tropospheric delay. The details of each step are discussed in Sections 4.4.1 – 4.4.5 and the step 'fit spline to arcs' is visualized in Figure 4.2. For each iteration, water levels (spline nodes) are computed for the previous 8 hours and a water level time series can be constructed from any of these nodes. The most recent node is considered to be a real-time measurement, whilst the other nodes are considered to be post-processing, with up to 8 hours delay from real-time.

The real-time algorithm must be efficient not only to avoid latency issues but also so that it can be implemented in-situ, for example using a microcontroller with limited memory. With the goal of in-situ data processing, it is also beneficial to avoid reliance on an internet connection to download external data sets because an internet connection is likely unavailable (or very expensive)

in remote locations. Similarly, additional instrumentation should also be avoided to reduce the cost and power requirements of the system.

4.4.1 Initial GNSS data processing and elevation angle interpolation

Low-cost antennas provide data in the National Marine Electronics Association (NMEA) 0183 format. This format consists of a stream of lines that begin with an identifier that contains information about the position of the antenna or the GNSS satellites in view. The data of interest for GNSS-R processing is the time of the measurements, the GNSS satellite constellation and pseudorandom noise (PRN) identifier, satellite azimuth, satellite elevation and SNR. The first step of processing the NMEA data is therefore to extract and organize this data.

Satellite elevation angles are recorded with a precision of 1 degree in the NMEA format, which is not good enough for spectral analysis, so the second step is to improve the precision of the satellite elevation angles. In DP21, the elevation angles were re-calculated using published final orbit solutions from the center for orbit determination in Europe (CODE) multi-GNSS experiment (MGEX) (Prange et al., 2016). This approach is not possible in real-time because the orbit solutions are published several days after the period that they refer to. There are also real-time orbit solutions and forecasts, however we seek to avoid reliance on external data sets. Instead, we fit a spline to the elevation angles recorded in the NMEA format for each satellite and read more precise elevation angles from the spline (note that this is a separate spline fitting process to the one outlined in Section 4.4.5).

4.4.2 Analyzing satellite arcs

The next step is to perform spectral analysis on the SNR data to obtain estimates of the reflector height (the grey dots in Figure 4.2). The SNR data must be organized into satellite arcs, detrended by removing a low order polynomial (here we use a second order polynomial) and then a lomb-scargle periodogram (LSP) algorithm is used to retrieve the frequency content of the SNR data in $\sin\theta$ space. The dominant frequency from the LSP is related to the reflector height using Equation

4.2. For the purpose of visualising the satellite arcs, Equation 4.2 can be simplified to

$$h = \lambda f/2. \tag{4.3}$$

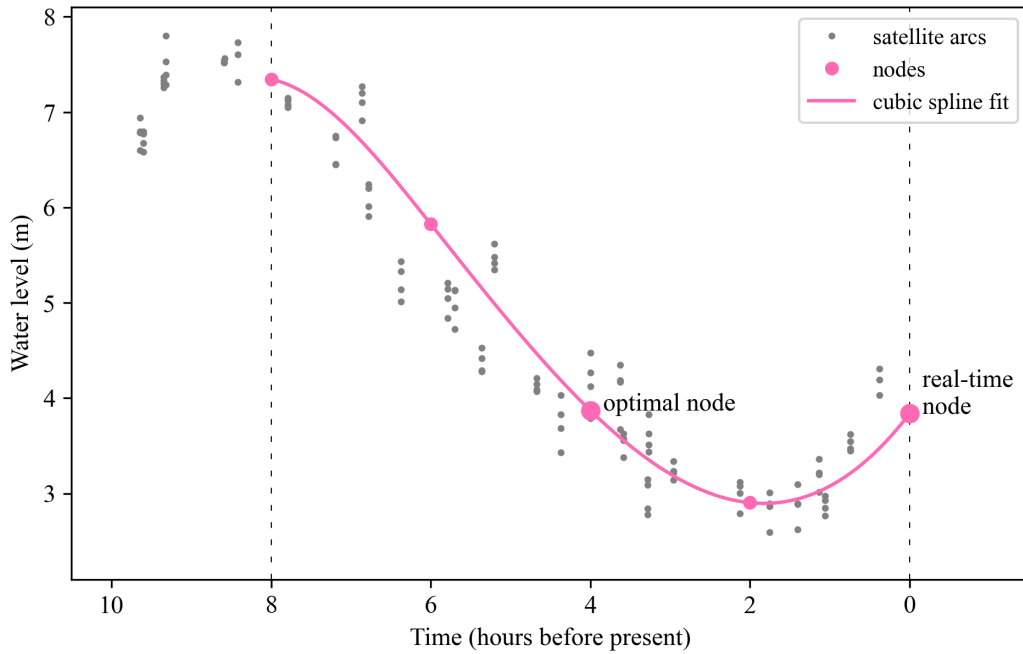


Figure 4.2: An example to show the parameters and outputs for one time step of the moving window algorithm. A spline is used to represent 8 hours of water level changes and is fit to the data from satellite arcs (represented as grey dots by using equation 4.3). The spline is defined by 5 nodes and the water levels between these nodes are obtained using cubic spline interpolation. The dotted black lines mark the beginning and end of the moving window. The node on the leading edge of the moving window is considered to be a real-time measurement, whereas the other points along the spline are considered to be post-processing. A water level time series could be formed by taking a measurement from the same point along the spline at each time step. The moving window algorithm is explained in more detail in Section 4.4.5.

4.4.3 Quality control

There are many outliers in GNSS-R water levels and numerous approaches have been proposed for removing them, as summarized in Song et al. (2019). These outliers are likely associated with random instrument noise in the SNR data and reflections from other nearby objects (Purnell et al., 2020). Two quality control steps are taken to remove outliers from the reflector height measurements. First, as suggested by Larson et al. (2013b), reflector heights with a peak-to-noise ratio of less than 3 are removed. Here the peak-to-noise ratio is defined as the ratio of the dominant peak to the mean of the periodogram within a frequency range that corresponds to reflections from the water surface. Second, the reflector heights are adjusted by their measured vertical separation so that they have a common datum (we use the lowest antenna) and then reflector heights that differ by more than 3 m from the mean of the adjusted reflector height within a 1-hour window are considered outliers and removed. The value of 3 m is chosen arbitrarily and could be adjusted on a site-by-site basis given the expected tidal range. This second step takes advantage of the large amount of reflector height measurements from multiple co-located antennas.

4.4.4 Tropospheric delay correction

Tropospheric delay is the effect of satellite signals being bent and slowed in the atmosphere before they reach the antenna. The tropospheric delay effect increases exponentially for lower elevation angles and causes an underestimate of the reflector height. This effect has been studied in the context of ground-based GNSS-R by Williams and Nievinski (2017) and recently in more detail by Nikolaidou et al. (2020, 2021). Here we use the altimetric height correction from Nikolaidou et al. (2021),

$$h^* = \Delta h_a + \Delta h_g \tag{4.4}$$

where h^* is the corrected reflector height and the tropospheric delay effect is split into two components; the along-path delay factor, represented by Δh_a , and the geometric delay factor, Δh_g . Both

of these factors depend on the uncorrected reflector height, h , using

$$\frac{\Delta h_a}{h} = \frac{N}{\sin^2 \theta'} \frac{\cos \theta'}{\cos \theta} (1 + \xi), \quad (4.5)$$

$$\frac{\Delta h_g}{h} = -\xi + (\sin \delta\theta \tan \theta + 1 - \cos \delta\theta)(1 + \xi) \quad (4.6)$$

and

$$\xi = \frac{\partial \delta\theta}{\partial \theta}, \quad (4.7)$$

where N is the refractivity of the atmosphere at the height of the antennas and is calculated using equations from Hobiger et al. (2008). The elevation angles are related by $\theta' = \theta + \delta\theta$, where $\delta\theta$ is the elevation bending (or refraction), calculated from Bennett (1982).

The equations for $\delta\theta$ and N depend on atmospheric pressure, temperature and water vapor pressure, which could be obtained from observations or estimated using a climatological model. The climatological estimates are more convenient because they do not require additional instrumentation. Here we try using both observations from a local weather station and estimates from the Global Pressure and Temperature (GPT) model (Böhm et al., 2015), which provides a climatological estimate of atmospheric parameters for a given location and time of year.

4.4.5 Spline fitting using a moving window

It was initially shown by Strandberg et al. (2016) that using a spline to represent a GNSS-R water level time series is an effective way to combine data from multiple satellites and improve the precision of water levels. Rather than fitting a spline directly to the reflector height estimates from spectral analysis, the SNR is modeled using an equation that depends on the reflector height and the spline parameters are obtained by using a least squares algorithm to reduce the residual between observed and modeled SNR. In DP21, it was found that precise water levels could be obtained by

collecting the spline parameters from the middle of a 6-hour moving window and then averaging the spline parameters for the co-located antennas.

In this study, with the aim of improving both the accuracy and computational efficiency of the GNSS-R data processing, we have made three key adjustments to the spline fitting technique used in DP21. First, the spline is no longer fit to modeled SNR data, rather it is fit directly to the reflector heights using equation 4.2, as shown in Figure 4.2. This adjustment greatly reduces the computation time for each time window, with minimal impact on the results. Second, the spline is now represented by a series of nodes and the water levels between the nodes are obtained using cubic spline interpolation, as shown in Figure 4.2. This simple formulation differs from the b-spline formulation used by Strandberg et al. (2016) and in DP21, in which the spline is formed from scaling factors that do not represent any point along the spline. This adjustment reduces the number of parameters calculated at each time step and also means that the output spline nodes can also be used as hourly water level measurements. Third, the reflector height estimates from each antenna are adjusted to the same datum prior to the spline fitting. This differs from the technique in DP21, in which a spline was obtained for each antenna and a final solution was formed by averaging the spline parameters. This third adjustment is necessary for the quality control step described in Section 4.4.3.

The output of the moving window algorithm at each time step is not a single water level but an 8 hour long spline that is defined by 5 nodes, shown as pink dots in Figure 4.2. The most recent node is considered to be a real-time measurement, whereas the other nodes (or other points along the spline) are considered to be post-processing as they refer to estimates of water levels at some time in the past. A water level time series can be constructed by repeatedly taking measurements from the same point along the spline at each time step. The accuracy of real-time measurements can therefore be assessed by constructing a water level time series using only the real-time nodes. However, any spline-fitting algorithm, such as the one used in DP21 or Strandberg et al. (2016) and further developed here, may be unstable if there is a gap between the leading edge of a time window (the real-time node) and the most recent measurements (satellite arcs) used to fit the spline. This issue was first raised in Strandberg et al. (2019a), who used an unscented Kalman filter to improve

the precision of real-time measurements. In this study, we investigate the post-processing delay that is required to avoid leading edge instabilities by constructing a time series from different points along the spline. For example, the accuracy of post-processed water levels with four hours delay from real-time can be assessed by constructing a time series using only the nodes from the middle of the time window. Likewise, the accuracy of post-processed water levels with 30 minutes delay from real-time can be assessed by constructing a time series using only the points along the spline that are 30 minutes behind the real-time node. The node in the middle of the time window is referred to as the optimal node (see Figure 4.4.5) because it is surrounded by data and therefore less likely to be influenced by any gaps.

There are two key parameters to describe the moving window algorithm: the node spacing and the number of nodes. The node spacing is chosen based on the frequency of satellite arcs. If the satellite arcs are less frequent, then the node spacing must be large enough to avoid periods where there are no arcs between consecutive nodes. We have found that 5 nodes is the most efficient configuration for the moving window algorithm (more than 5 nodes does not appear to improve the accuracy).

4.5 Instrumentation

The instrumentation and design of the low-cost antenna array is similar to that used in DP21 (see Figure 4.3). It consists of four Beitan BN-808 antennas (with UBLOX UBX-M8030 chips), connected to a Raspberry Pi Zero to record data. The antennas are programmed to record data from GPS, GLONASS and GALILEO satellites at a frequency of 5 seconds. The antennas are fixed to ground planes, spaced 10 cm apart and oriented vertically facing the water surface.

4.6 Field work at Saint-Joseph-de-la-Rive

For this study we chose the site with the largest tidal range along the Saint Lawrence River, Saint-Joseph-de-la-Rive in Quebec, Canada. This site is approximately 100 km downstream of Québec

City, where the river begins to widen before it meets the Atlantic Ocean. We installed our low-cost antenna array for a period of more than two weeks, from November 10 until November 27. During this period, there was a maximum rate of water level change of approximately 5 meters per hour, providing a rapid rise in water levels analogous to an extreme flood event.

The antenna array was installed next to a pressure gauge maintained by the Canadian Hydrographic Service, as can be seen in Figure 4.3a. The pressure gauge is a Campbell Scientific CS450 and it is installed in a stilling well. Data is available to download at 1-minute intervals from <http://tides.gc.ca>. The water level heights from this tide gauge are linked to a local benchmark network. We used an optical survey and a levelling staff to find the vertical separation between the antennas, a local benchmark and the water surface. This standard surveying technique involves aiming the optical survey at the levelling staff in different locations in order to infer the relative heights of different points of interest. The optical survey is then moved to a different position and the measurements are repeated for verification. The height of the benchmark is known relative to the chart datum, hence the heights of the antennas can be inferred from the benchmark. The antenna heights agreed to within 1 cm over the two visits. The GNSS-R reflector heights are converted to the same datum as the pressure gauge using the following equation

$$wl = h_{\text{datum}} - h \quad (4.8)$$

where wl is the GNSS-R measured water level and h_{datum} is the vertical separation between the reflector height datum (the antenna phase center for the lowest antenna) and the pressure gauge datum (chart datum).

In comparison to the sites used in DP21, the extent of the water surface area used to make GNSS-R water level measurements is quite limited, as shown in Figure 4.3b. This area is defined by satellite elevation and azimuth angle limits of 5 – 20 degrees and 190 – 250 degrees, respectively. In order to avoid instabilities in the moving window algorithm caused by periods where there are no satellite arcs between consecutive nodes, the node spacing is set to 2 hours at this site. The azimuth range is constrained by the dock directly south of the instruments, where a ferry is



Figure 4.3: a) A Picture of the site at Saint-Joseph-de-la-Rive and b) a top-down view of the reflection zones from <https://gnss-reflections.org/rzones> (Roesler and Larson, 2018). In the left picture, the stilling well that contains the pressure gauge can be seen to the left of the tripod, with a padlock attached to it. The different coloured ellipses refer to reflection zones from satellites at an elevation of 5, 10 and 15 degrees (yellow, blue and red, respectively).

frequently picking up passengers. To the north-west direction from the antennas, the shoreline is changing rapidly during the day. The antennas are found to vary between approximately 2 – 8 m above the water level during tidal variations.

4.7 Additional data from Trois-Rivières

In order to further validate the real-time data processing, we use previously collected data from DP21, from the site at the Port of Trois-Rivières. This site is also on the Saint Lawrence River, approximately 200 km upstream of Saint-Joseph-de-la-Rive, where the tidal amplitude is much smaller (approximately 0.6 m). The GNSS-R setup was almost identical to that from Saint-Joseph-de-la-Rive, except that the antennas are of the type TOPGNSS GNSS100L (they contain the same

UBLOX UBX-M8030 chips as the Beitan BN-808 antennas and are expected to perform similarly). This site is more ideal for water level measurements than the site at Saint-Joseph-de-la-Rive because the extent of the water surface area that can be used for GNSS-R analysis is relatively large. The elevation and azimuth angle limits used are 5 – 30 and 80 – 220 degrees, respectively. These expanded limits mean that a node spacing of 1 hour can be used for the moving window algorithm. For validation of the GNSS-R levels, there are three OTT Hydromet pressure level sensors maintained by the Canadian Hydrographic Service and data can be retrieved online at <http://tides.gc.ca>. The antennas were not surveyed at this site hence the datum of the GNSS-R water levels was not determined and compared with the pressure gauge. The GNSS antenna array was installed for approximately one month from September to October 2020. More information about this site can be found in DP21.

4.8 Results

The results are split into two sections. Section 4.8.1 includes results from running the moving window algorithm on the data from Saint-Joseph-de-la-Rive and Trois-Rivières, while section 4.8.2 focuses on the mean bias between the pressure gauge and GNSS-R at Saint-Joseph-de-la-Rive (i.e., the mean difference between the two water level time series). Note that the bias cannot be assessed at Trois-Rivières because the GNSS-R levels were not surveyed. It should also be noted that the tropospheric delay correction discussed in the Section 4.8.2 is applied to the results at both sites presented in Section 4.8.1.

4.8.1 Performance of moving window algorithm

The GNSS-R sensor captures the full range of the tidal signal at Saint-Joseph-de-la-Rive (Figure 4.4 a). The sensor functioned in sub-zero temperatures and through significant snowfall in November without any issues. The RMSE between the GNSS-R water levels when using the optimal node from the moving window algorithm (post-processed with 4 hours delay) and the co-located pressure gauge for the continuous 16-day period at this site is 4.93 cm, with a mean bias revealed

by the surveying of less than 1 cm after correcting for the effect of tropospheric delay. The RMSE between the GNSS-R water levels and pressure gauge at Trois-Rivières is 1.59 cm when using the optimal node from the moving window algorithm (a comparison can be seen in Figure 4.4 b). As discussed below, the greater RMSE at Saint-Joseph-de-la-Rive compared to Trois-Rivières is likely due to the reduced azimuth angle range at this site. The results from Saint-Joseph-de-la-Rive also support the main result from DP21 - that using multiple co-located antennas improves the accuracy of water level measurements. For the period shown in Figure 4.4 a, using four antennas reduces the RMSE by 59 – 68% compared to one antenna, 22 – 41% compared to two antennas or 10 – 17% compared to three antennas.

The moving window algorithm described in Section 4.4.5, is similarly accurate and less computationally demanding than using an inverse model of SNR data (the approach developed by Strandberg et al. (2016) and adapted for use with multiple antennas in DP21). For the data at Saint-Joseph-de-la-Rive, the RMSE between pressure gauge and GNSS-R water levels increases by over 2 cm (from 4.93 to 7.0 cm) when using the inverse modelling approach in comparison to the moving window algorithm. Whereas, at Trois-Rivières, the RMSE obtained using the moving window algorithm (1.59 cm) is larger than the value obtained with post-processing in DP21 (1.02 cm). The computation time when using a laptop computer may be more than 5 minutes for the inverse modelling approach as opposed to less than a tenth of a second for the moving window algorithm. This algorithm is more efficient because less data is being used to fit the spline. For example, for an 8-hour window of data from the four antennas at Saint-Joseph-de-la-Rive, there are approximately 40 – 90 reflector heights as opposed to 15,000 – 30,000 individual SNR measurements. Recall from Section 4.4.5 that the reflector heights are initially obtained from the individual SNR measurements, but they are analyzed arc by arc as opposed to all being analyzed at the same time (as is the case for the inverse modelling approach).

The GNSS-R levels from both sites are less accurate in real-time than post-processing, as shown in Figure 4.5. The RMSE between pressure gauge and GNSS-R water levels is 24.6 cm and 3.93 cm for real-time measurements at Saint-Joseph-de-la-Rive and Trois-Rivières, respectively. Figure 4.5 shows that the RMSE improves rapidly at both sites for a post-processing delay

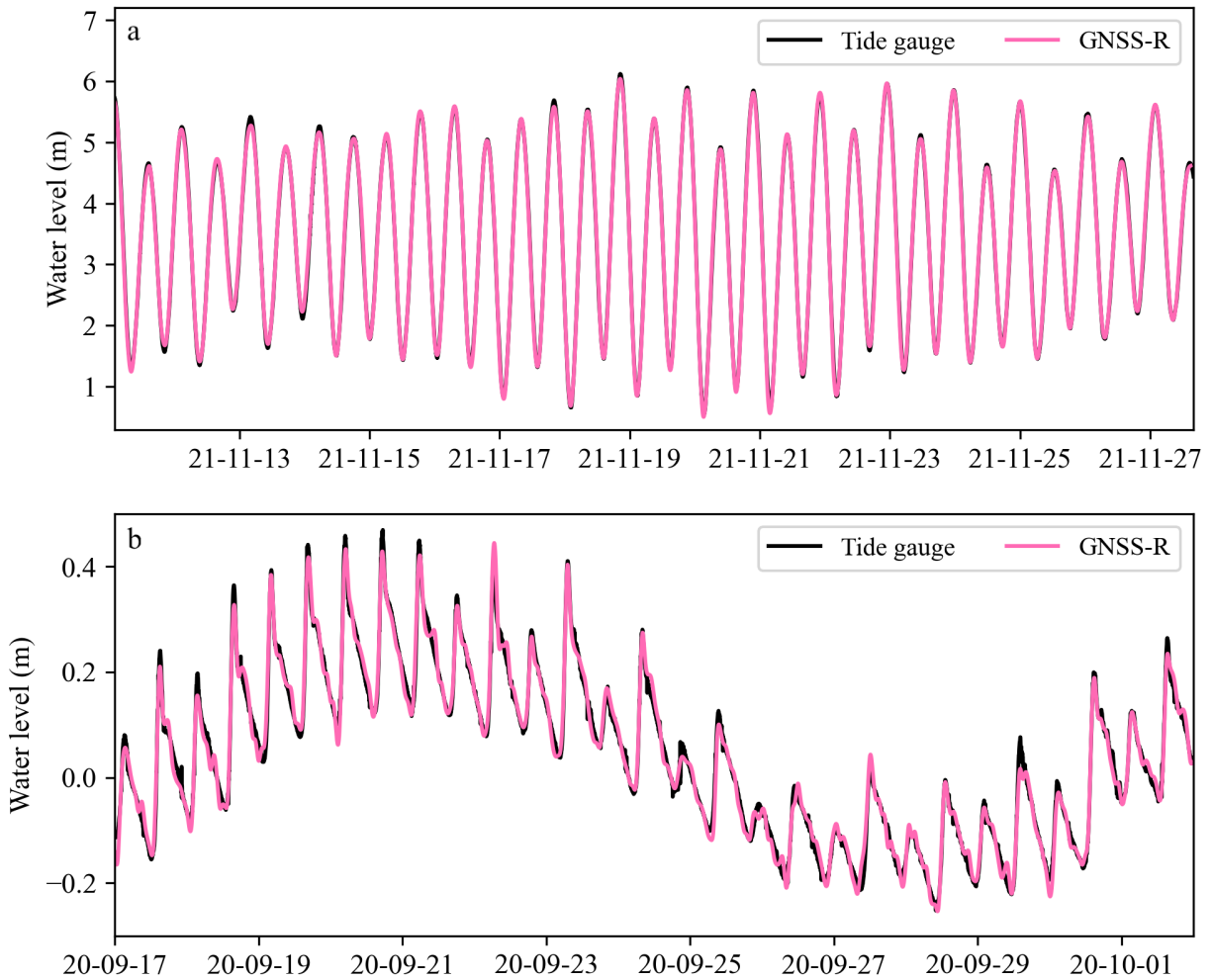


Figure 4.4: Water levels from GNSS-R and co-located pressure gauge at Saint-Joseph-de-la-Rive and Trois-Rivières. The GNSS-R water levels are constructed from the "optimal node" of the moving window algorithm labelled in Figure 4.2 (4 hours delay from real-time). At Saint-Joseph-de-la-Rive, the water levels are relative to chart datum and at Trois-Rivières, the datum is arbitrary as both pressure gauge and GNSS-R levels have had the mean removed for comparison.

between 0 and 1 hour in contrast with a minimal improvement in the RMSE for a delay greater than 1 hour. The RMSE for a post-processing delay of 1 hour (referred to henceforth as near real-time) is 6.85 and 1.76 cm at Saint-Joseph-de-la-Rive and Trois-Rivières, respectively. The advantage of using near real-time water levels is presented in Figure 4.6, which shows a three day period with large deviations between real-time and near real-time water levels. At Saint-Joseph-de-la-Rive, the

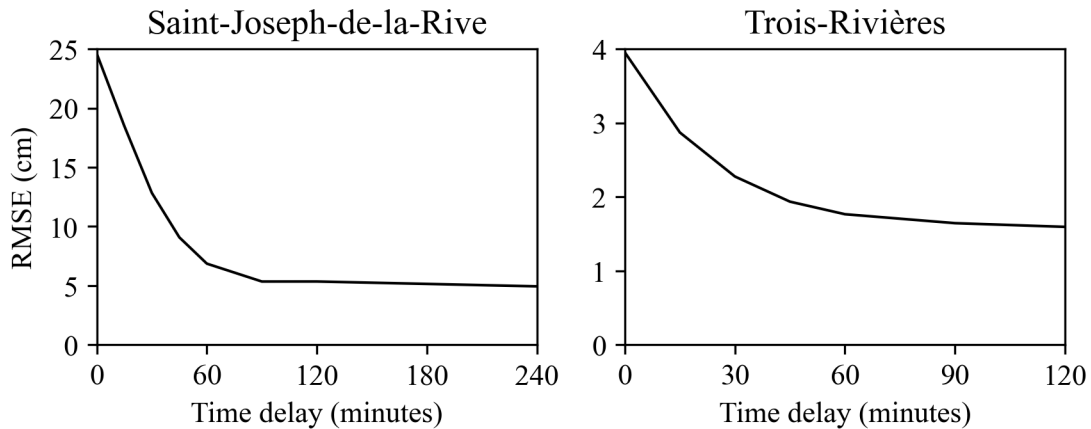


Figure 4.5: The RMSE of GNSS-R water levels when compared to co-located pressure gauges at Saint-Joseph-de-la-Rive and Trois-Rivières as a function of the time delay after which the GNSS-R water levels are processed. The time delay of 0 minutes corresponds to the a time series being formed using the "real-time node" labelled in Figure 4.2. Whereas, a time delay of 240 minutes at Saint-Joseph-de-la-Rive corresponds to the "optimal node" labelled in Figure 4.2. The limits on the x-axis are different between the two sites because the node spacing is different between the two sites, as explained in Sections 4.6 and 4.7.

largest error between GNSS-R and pressure gauge water levels is 1.15 m in real-time or 48 cm in near real-time, hence large instabilities are at least partially avoided by using the near-real time measurements. The largest errors in real-time water levels tend to occur when there are large gaps between satellite arcs and during a rapid rise or fall in water levels.

The larger tidal range and RMSE for GNSS-R water levels at Saint-Joseph-de-la-Rive compared to Trois-Rivières could lead to the assumption that the tidal range is an important controlling factor on the accuracy of GNSS-R water level measurements. However, the azimuth angle limits are also significantly different between the two sites - the azimuth angle range at SJDLR is 80 degrees larger than that at Saint-Joseph-de-la-Rive. If we limit the azimuth range at Trois-Rivières to the same as that at Saint-Joseph-de-la-Rive, then the RMSE increases from 1.59 cm to 4.03 cm. This increase in the RMSE suggests that the azimuth angle range is a more important control on the accuracy than the daily tidal range. A larger azimuth angle range gives more frequent

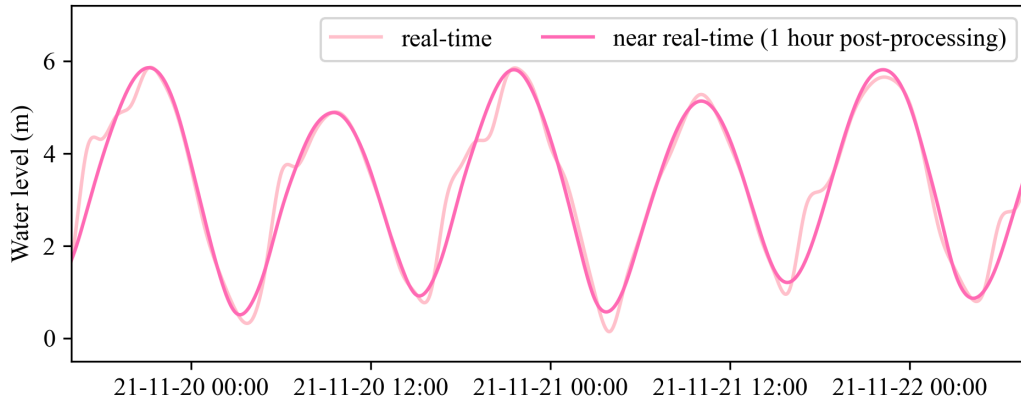


Figure 4.6: GNSS-R water level measurements at Saint-Joseph-de-la-Rive from the moving window algorithm. The real-time water levels are constructed from the "real-time node" labelled in Figure 4.2, while the near real-time water levels are post-processed with an hour delay from real-time.

satellite arcs (there are approximately twice as many arcs per day at Trois-Rivières compared to Saint-Joseph-de-la-Rive) and this limits the likelihood of instabilities in the spline algorithm.

4.8.2 Bias and tropospheric delay

The bias in GNSS-R water levels was assessed by measuring the vertical separation between the GNSS antennas, the water surface and a local benchmark using an optical survey on two separate occasions (when installing and uninstalling the GNSS-R sensor). Assuming no bias in the pressure gauge measurements, the mean bias for GNSS-R measurements with no tropospheric delay correction is 6.9 cm (i.e., water levels are overestimated by 6.9 cm for GNSS-R measurements). The bias in uncorrected GNSS-R measurements is negatively correlated with increasing water levels, as shown in Figure 4.7 and as expected from Williams and Nievinski (2017); Nikolaidou et al. (2021). The tropospheric delay correction described in Section 4.4.4 removes the bias in GNSS-R measurements to under 1 mm (albeit with a survey error of 1 cm) and improves the RMSE of water levels from 8.73 cm to 4.93 cm. We tried using data from the GPT model as well as data from a local weather station to inform the tropospheric delay corrections and found that there was no significant difference between using the model and observations at this site (less than 1 mm change

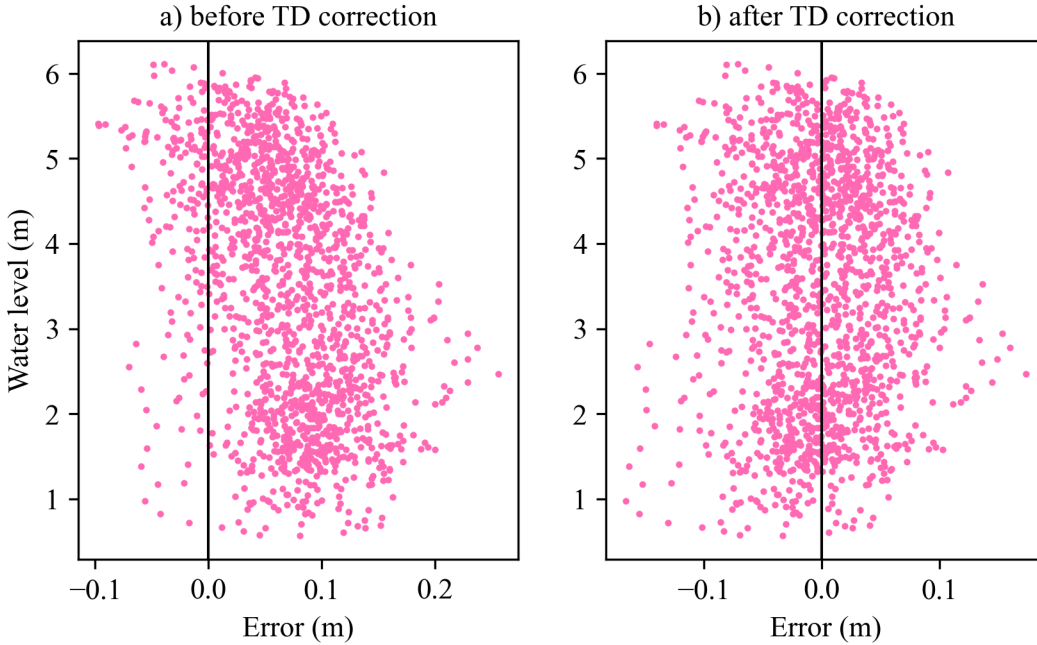


Figure 4.7: Van de Castele diagrams showing the effect of tropospheric delay (TD) on the GNSS-R water level measurements (pink dots) at Saint-Joseph-de-la-Rive. The error is the difference between surveyed levels from GNSS-R and pressure gauge measurements. Deviations from the solid vertical line at 0 cm error suggest a bias.

in the RMSE and the bias). However, the closest weather station was from a town over 27 km away called La Pocatière and it may be possible that a co-located weather station could improve the correction. The weather station data was obtained from climate.weather.gc.ca. We discuss the influence of the state of the atmosphere on the tropospheric delay correction in more detail in the Supplementary Material.

4.9 Conclusion and Discussion

We have developed, for the first time, an efficient moving window algorithm for real-time, in-situ GNSS-R water level processing using multiple low-cost antennas that does not rely on external data sets or additional instrumentation. We tested the algorithm by comparing GNSS-R water levels with a co-located pressure gauge at a site with large daily tidal variations for a 16-day period and at another site with a smaller tidal range for approximately one month. We found instabilities

in the moving window algorithm for real-time measurements but these instabilities could be largely avoided by using a post-processing delay of 1 hour. The GNSS-R water levels were more accurate at the site with smaller tides but it appears that this difference can be largely accounted for by the difference in the azimuth angle range as opposed to the tidal amplitude. Finally, we assessed the bias in the GNSS-R water levels and found that a simple tropospheric delay correction can effectively remove bias in the GNSS-R water levels.

Along with the GNSS-R instrument design developed in DP21 (using multiple low-cost GNSS antennas), this new algorithm opens up a wide range of new applications of GNSS-R and provides a practical and portable solution for near real-time water level monitoring. For example, a network of GNSS-R sensors could be easily deployed before or during flooding conditions to measure inundation levels and validate the output from hydrological models. The GNSS-R sensors could also be easily deployed to monitor the development of an ice jam flooding event. However, an accuracy of several cm for water level measurements may not be good enough for some applications, such as input data for hydrological or ocean modelling (or other applications where mm-scale accuracy is required). Furthermore, as described in more detail in the conclusion of DP21, there are geometry considerations for GNSS-R sites that limit use for some applications. For example, it may not be possible to use this technique to monitor rivers or lakes narrower than 50 m and monitoring such narrow rivers or tributaries is often an important component of flood forecasting.

Despite the limitations described above, it is clear that less accurate data is better than no data for most applications. Especially given that there are large persistent gaps in the global distribution of water level sensors (or tide gauges) in developing countries and in remote areas that are vulnerable to the effects of climate-driven changes. We therefore encourage more widespread use of GNSS-R sensors, especially at sites where there is no water level data and other types of sensors are costly or impractical.

4.10 Supplementary Material

4.10.1 Sensitivity of tropospheric delay correction to atmospheric parameters

We performed additional tests to assess the sensitivity of the state of the lower atmosphere to the magnitude of the tropospheric delay correction, as shown in Figure 4.8. To produce these results, we chose control values of the reflector height, mean satellite elevation angle, atmospheric pressure, temperature and partial pressure of water vapor, as shown by pink dots in Figure 4.8. We then assessed the influence of each parameter by incrementally changing it and producing a tropospheric delay correction (using the methodology described in Section 4.4.4) with the other parameters fixed at their control values. These results show that the reflector height and elevation angle have a much greater control on the tropospheric delay correction (up to 1 m range in corrections) in comparison to the atmospheric parameters (up to 5 cm range in corrections).

4.10.2 Elevation angles and satellite orbit data

The method used to obtain precise satellite elevation angles from NMEA data is an important control on the accuracy of water levels. The results shown in Figure 4.4 were obtained by interpolating the elevation angles directly from the NMEA data format by fitting a spline to the elevation angles, as described in Section 4.4.1. We also tried using the CODE MGEX final orbit solutions to obtain more accurate elevation angle data and found that this marginally improved the accuracy of water levels by 10% relative to when using interpolated elevation angles. This improvement of 10 % may be worth implementing for post-processing and research purposes, but the practical complexity of incorporating this data set into a real-time data processing framework outweighs the minimal improvement.

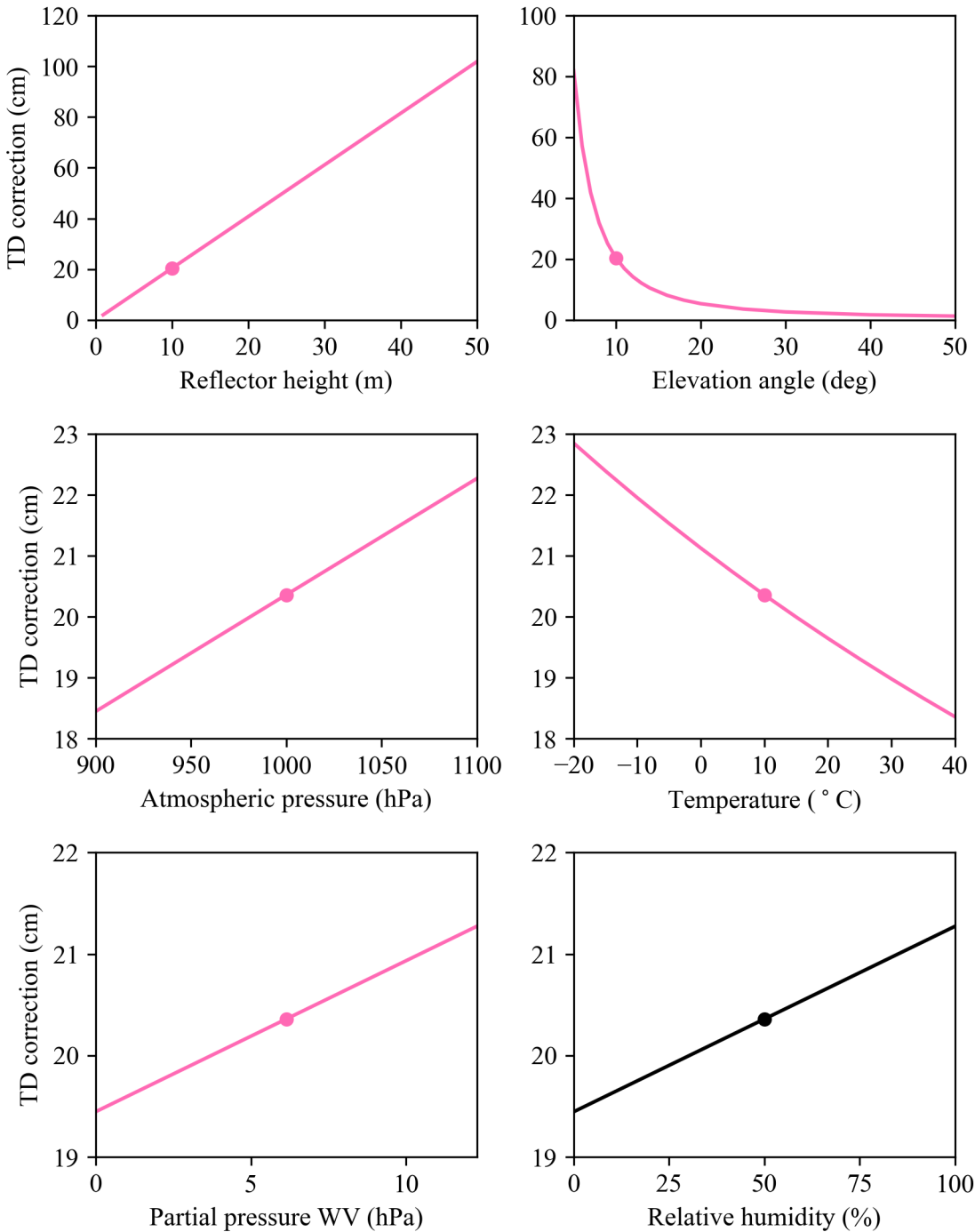


Figure 4.8: Tropospheric delay corrections produced for different geometrical and environmental parameters using the methodology of Nikolaidou et al. (2021). The pink dots refer to control values for each parameter that are fixed whilst the others are varied. The relative humidity is given for reference as it is a standard parameter recorded by weather stations, but it is not independent from temperature and partial pressure of water vapor, hence it is shown in black.

Chapter 5

Discussion

The overarching motivation that links the studies presented in Chapters 2 – 4, is that there are few coastal water level sensors in remote regions. In the face of the predicted rapid changes in remote regions for years and decades to come (Pörtner et al., 2019; IPCC, 2021), observational networks must be urgently expanded. The GNSS-R technique presented in Chapter 3 and then further developed in Chapter 4 is suitable for obtaining water levels in remote regions. For example, A low-cost antenna array could be easily installed on a tripod on rocky coastline or during sub-freezing conditions. It has also been noted throughout this thesis that a limiting factor of the GNSS-R technique is that it is not as precise in comparison to commercially available sensors such as pressure gauges or radar gauges. The technique presented in Chapters 3 and 4 shows significant improvement upon the precision obtained in other GNSS-R literature (including Chapter 2), albeit still less precise than that of pressure gauges or radar gauges.

Further improvements in the precision of the GNSS-R technique are likely possible. However, these improvements may be limited because the nature of GNSS-R measurements is fundamentally different from other commercial water level sensors. Each GNSS-R water level is extracted from a combination of many different SNR measurements from different satellites, averaged over a period of 20 – 60 minutes and over a spatial area extending up to 100 m outward from the antenna (or antennas). On the other hand, a radar gauge takes measurements from a 1-meter wide footprint at a frequency of 1 second (Fiorentino et al., 2019). For a dynamic river or coastline, the point

measurement made by a radar gauge may not be representative of the larger area that a GNSS-R sensor surveys and hence it might not be possible to achieve mm-scale agreement between the two instruments. Integrating GNSS-R sensors into global observational networks will therefore be challenging if they are evaluated solely by their ability to replicate measurements from other commercial water level sensors. I would suggest that it is also productive to evaluate GNSS-R sensors based on their ability to expand observational networks to regions and applications where there is a need for measurements but other devices are less feasible.

Since the publication of Chapters 2 and 3, many new GNSS-R studies have been published, most of which have been focused on developing new techniques and new instrumentation (Li et al., 2021; Altuntas and Tunalioglu, 2021; Wang et al., 2021; Zhang et al., 2021). Examples of GNSS-R techniques being used for research in other fields in Earth science outside of GNSS-R research (i.e., techniques being applied as opposed to solely being developed) remain limited. One interesting exception is in Dahl-Jensen et al. (2021a), where GNSS-R water levels from a geodetic station in Northwest Greenland are studied over a decade from 2008 – 2019 and find a negative trend that is likely associated with local glacier mass loss. There have also been interesting applications of GNSS-R water levels for monitoring a storm surge during Hurricane Harvey (Kim and Park, 2021) (or more generally for monitoring coastal hazards in Kim et al. (2021a)) and for monitoring high-amplitude asymmetric tides (Zeiger et al., 2021). As discussed in Chapter 4, there has also been a recent focus on developing open-source software for GNSS-R analysis (Roesler and Larson, 2018; Altuntas and Tunalioglu, 2021; Martín et al., 2020) and it is hoped that the accessibility of this software will encourage more applications of the GNSS-R technique for research in a range of different fields.

The manuscripts presented in Chapter 2 and 3 have been cited several times in other peer-reviewed articles since their publication. Most notably in Liu and Zhang (2021), where an alternative GNSS-R technique is presented and validated against the results from Chapter 2. The technique is based on the inverse modelling technique first developed by Strandberg et al. (2016), however they use a cubic spline formulation, similar to that used in Chapter 4, and they use an algorithm to account for the differential evolution of the model parameters. They compare their

results using the same data sets that are used in Chapter 2 (from sites SC02 and GTGU) and find an improved precision.

Two other citing articles have specifically discussed the dependence of the elevation angles of satellites on GNSS-R water levels (Zhang et al., 2021; Wang et al., 2021). This elevation angle dependence is also discussed in detail in Chapter 2, where it is found that two important sources of uncertainty - random noise and tropospheric delay - are both highly elevation angle dependant. In both Zhang et al. (2021) and Wang et al. (2021), the authors strive to develop a GNSS-R technique that eliminates the elevation angle dependence of GNSS-R water levels. In Wang et al. (2021), they develop a technique to correct elevation angle bias for a dual-antenna GNSS-R approach (using both an upwards and downwards looking, oppositely polarised antenna). Whereas, in Zhang et al. (2021), they focus on the influence of surface roughness on GNSS-R water level retrievals when using a similar approach to that initially proposed by Martin-Neira et al. (1993), in which water levels are inferred by directly estimating the delay between direct and reflected signals. These examples show the broad range of GNSS-R techniques being simultaneously developed and signal that further improvements on the work presented in this thesis could be achieved by combining different approaches.

The electronics manufacturing landscape has dramatically changed during the course of this thesis, such that the key low-cost electronics components used in Chapters 3 and 4 are now significantly less accessible. The COVID-19 pandemic that began during the latter half of the thesis period caused supply chain issues, which lead to a semiconductor shortage and this limited the availability of components of the low-cost antenna array design. For example, the USB GNSS antennas were bought for 10 USD each pre-pandemic, whereas a similar antenna may cost up to 30 USD each at the time of writing. The Raspberry Pi computers that are necessary for recording the GNSS data were easily available from the manufacturer for 5 USD, whereas now they are only available from resellers, for up to 100 USD each. These costs remain small in comparison to the cost of a single geodetic-standard antenna or radar gauge, but they may limit the application of the low-cost antenna array design for citizen science initiatives in the near future. Without taking into account any potential future global crises that could place additional strain on the global supply

chain, GNSS technology is expected to continue to become more ubiquitous (more accessible), more compact and more powerful in the longer term.

Chapter 6

Summary and Conclusions

This thesis has sought to explore a technique for obtaining coastal water level measurements that is more practical to install and maintain in comparison to the commercial alternatives. This non-intrusive solution for water level monitoring relies on repurposing mass-market GNSS technology. The studies presented drew on work from several previous key GNSS-R studies (Anderson, 2000; Larson et al., 2013a; Strandberg et al., 2016) that focused on using geodetic-standard GNSS instruments to obtain water levels. However, the results from experiments discussed in the previous chapters strongly support the use of low-cost GNSS antennas. Other studies have also shown the benefits of using low-cost GNSS antennas (Fagundes et al., 2021; Williams et al., 2020; Karegar et al., 2021), but the technique developed here is unique in its use of multiple co-located antennas to obtain more precise water levels.

In Chapter 2, a broad study of the uncertainty in ground-based GNSS-R water levels was presented. Prior to this study, there was no focused analysis of the sources of uncertainty in GNSS-R water levels. The proposed method involved modelling the effect of the sources of uncertainty on SNR data and comparing the modelled data with observations. The key discovery in this study, that shaped Chapters 3 and 4, is that random noise is a dominant source of uncertainty. This study also provided a technique for estimating the uncertainty at a stand-alone GNSS-R site (with no co-located water level sensor for validation), which paves the way for GNSS-R water levels to be used for future sea level and hydrology research.

The results from Chapter 2 led to the hypothesis that multiple co-located GNSS antennas could be used to improve the precision of GNSS-R measurements. This hypothesis was tested in both Chapters 3 and 4 by using an array of multiple low-cost GNSS antennas to monitor water levels. The results from these chapters validated the key result from Chapter 2, that random noise is a dominant source of uncertainty and additionally that using co-located low-cost antennas is a practical way to reduce this source of uncertainty. Chapter 3 is a proof of concept for the low-cost antenna array design, in which an algorithm for data processing is adapted from Strandberg et al. (2016) and results from three sites are presented. The algorithm presented in Chapter 3 is not suitable for operational or real-time water level monitoring, hence Chapter 4 focused on developing a more efficient data processing algorithm. Promising results were subsequently presented in Chapter 4 for near real-time water level monitoring at a new site with high-amplitude tides and when using data from one of the sites studied in Chapter 3.

Significant progress towards an operational GNSS-R water level sensor was made through Chapters 2 – 4. However, the following areas require further study or more field work:

- The GNSS-R antenna array should undergo a longer period of field testing in a range of different environments
- The method for uncertainty estimation developed in Chapter 2 should be adapted for the GNSS-R antenna array technique
- The real-time processing technique developed in Chapter 4 should be implemented for in-situ GNSS-R water level processing
- A more thorough investigation of the spacing apart of co-located antennas (and possible interference between them) should be conducted.

Additionally, future studies should investigate the use of this technique for monitoring other environmental variables that have been obtained in previous GNSS-R studies, such as snow depth, permafrost thaw, soil moisture and significant wave height (Larson et al., 2008, 2009; Liu and Larson, 2018; Kim et al., 2021b).

Further study will always be possible (as is the nature of science), but the GNSS-R water level sensor developed in this thesis is already useful for a range of different applications. At this stage in the development of the sensor, feedback from end users of the data is equally if not more valuable than further academic research. My personal motivation for conducting the research presented in this thesis was not to showcase a theoretical or abstract technique for water level monitoring. Rather, I am motivated to build something that is useful for people who are not necessarily GNSS-R experts.

Bibliography

- Adrian, R., O'Reilly, C. M., Zagarese, H., Baines, S. B., Hessen, D. O., Keller, W., Livingstone, D. M., Sommaruga, R., Straile, D., Van Donk, E., Weyhenmeyer, G. A., and Winder, M.: Lakes as sentinels of climate change, *Limnology and Oceanography*, 54, 2283–2297, https://doi.org/10.4319/lo.2009.54.6_part.2.2283, 2009.
- Altuntas, C. and Tunalioglu, N.: GIRAS: an open-source MATLAB-based software for GNSS-IR analysis, *GPS Solutions*, 26, 16, <https://doi.org/10.1007/s10291-021-01201-3>, 2021.
- Anderson, K. D.: Determination of Water Level and Tides Using Interferometric Observations of GPS Signals, *Journal of Atmospheric and Oceanic Technology*, 17, 1118 – 1127, [https://doi.org/10.1175/1520-0426\(2000\)017<1118:DOWLAT>2.0.CO;2](https://doi.org/10.1175/1520-0426(2000)017<1118:DOWLAT>2.0.CO;2), 2000.
- Apel, H., Vorogushyn, S., and Merz, B.: Brief communication – Impact Forecasting Could Substantially Improve the Emergency Management of Deadly Floods: Case Study July 2021 floods in Germany, *Natural Hazards and Earth System Sciences Discussions*, 2022, 1–10, <https://doi.org/10.5194/nhess-2022-33>, 2022.
- Asante, K. O., Macuacua, R. D., Artan, G. A., Lietzow, R. W., and Verdin, J. P.: Developing a Flood Monitoring System From Remotely Sensed Data for the Limpopo Basin, *IEEE Transactions on Geoscience and Remote Sensing*, 45, 1709–1714, <https://doi.org/10.1109/TGRS.2006.883147>, 2007.

- Baumann, T. M., Polyakov, I. V., Padman, L., Danielson, S., Fer, I., Janout, M., Williams, W., and Pnyushkov, A. V.: Arctic tidal current atlas, *Scientific Data*, 7, 275, <https://doi.org/10.1038/s41597-020-00578-z>, 2020.
- Beckmann, P. and Spizzichino, A.: The scattering of electromagnetic waves from rough surfaces, Artech House, 1987.
- Bennett, G. G.: The Calculation of Astronomical Refraction in Marine Navigation, *Journal of Navigation*, 35, 255–259, <https://doi.org/10.1017/S0373463300022037>, 1982.
- Bilich, A. and Larson, K. M.: Mapping the GPS multipath environment using the signal-to-noise ratio (SNR), *Radio Science*, 42, <https://doi.org/https://doi.org/10.1029/2007RS003652>, 2007.
- Boehm, J., Werl, B., and Schuh, H.: Troposphere mapping functions for GPS and very long baseline interferometry from European Centre for Medium-Range Weather Forecasts operational analysis data, *Journal of Geophysical Research: Solid Earth*, 111, <https://doi.org/10.1029/2005JB003629>, 2006.
- Böhm, J., Möller, G., Schindelegger, M., Pain, G., and Weber, R.: Development of an improved empirical model for slant delays in the troposphere (GPT2w), *GPS Solutions*, 19, 433–441, <https://doi.org/10.1007/s10291-014-0403-7>, 2015.
- Braasch, M. S.: Isolation of GPS multipath and receiver tracking errors, *NAVIGATION, Journal of the Institute of Navigation*, 41, 415–434, 1994.
- Caparrini, M., Ruffini, L., and Ruffini, G.: Parfait: GNSS-R coastal altimetry, *arXiv preprint physics/0311052*, 2003.
- Cartwright, D. E.: On the origins of knowledge of the sea tides from antiquity to the thirteenth century, *Earth Sciences History*, 20, 105–126, full publication date: 2001, 2001.
- Cazenave, A., Palanisamy, H., and Ablain, M.: Contemporary sea level changes from satellite altimetry: What have we learned? What are the new challenges?, *Advances in Space Research*, 62, 1639–1653, 2018.

- Church, J. A. and White, N. J.: Sea-Level Rise from the Late 19th to the Early 21st Century, *Surveys in Geophysics*, 32, 585–602, <https://doi.org/10.1007/s10712-011-9119-1>, 2011.
- Cools, J., Innocenti, D., and O’Brien, S.: Lessons from flood early warning systems, *Environmental Science & Policy*, 58, 117–122, <https://doi.org/https://doi.org/10.1016/j.envsci.2016.01.006>, 2016.
- Dahl-Jensen, T. S., Andersen, O. B., Williams, S. D., Helm, V., and Khan, S. A.: GNSS-IR Measurements of Inter Annual Sea Level Variations in Thule, Greenland from 2008–2019, *Remote Sensing*, 13, 5077, 2021a.
- Dahl-Jensen, T. S., Andersen, O. B., Williams, S. D. P., Helm, V., and Khan, S. A.: GNSS-IR Measurements of Inter Annual Sea Level Variations in Thule, Greenland from 2008–2019, *Remote Sensing*, 13, <https://doi.org/10.3390/rs13245077>, 2021b.
- DeConto, R. M., Pollard, D., Alley, R. B., Velicogna, I., Gasson, E., Gomez, N., Sadai, S., Condron, A., Gilford, D. M., Ashe, E. L., et al.: The Paris Climate Agreement and future sea-level rise from Antarctica, *Nature*, 593, 83–89, 2021.
- Devlin, A. T., Jay, D. A., Talke, S. A., Zaron, E. D., Pan, J., and Lin, H.: Coupling of sea level and tidal range changes, with implications for future water levels, *Scientific Reports*, 7, 17021, <https://doi.org/10.1038/s41598-017-17056-z>, 2017.
- Dottori, F., Szewczyk, W., Ciscar, J.-C., Zhao, F., Alfieri, L., Hirabayashi, Y., Bianchi, A., Mongelli, I., Frieler, K., Betts, R. A., and Feyen, L.: Increased human and economic losses from river flooding with anthropogenic warming, *Nature Climate Change*, 8, 781–786, <https://doi.org/10.1038/s41558-018-0257-z>, 2018.
- Dullaart, J. C. M., Muis, S., Bloemendaal, N., and Aerts, J. C. J. H.: Advancing global storm surge modelling using the new ERA5 climate reanalysis, *Climate Dynamics*, 54, 1007–1021, <https://doi.org/10.1007/s00382-019-05044-0>, 2020.

- Durand, M., Fu, L.-L., Lettenmaier, D. P., Alsdorf, D. E., Rodriguez, E., and Esteban-Fernandez, D.: The surface water and ocean topography mission: Observing terrestrial surface water and oceanic submesoscale eddies, *Proceedings of the IEEE*, 98, 766–779, 2010.
- Dutton, A., Webster, J. M., Zwartz, D., Lambeck, K., and Wohlfarth, B.: Tropical tales of polar ice: evidence of Last Interglacial polar ice sheet retreat recorded by fossil reefs of the granitic Seychelles islands, *Quaternary Science Reviews*, 107, 182–196, 2015.
- Egbert, G. D. and Erofeeva, S. Y.: Efficient Inverse Modeling of Barotropic Ocean Tides, *Journal of Atmospheric and Oceanic Technology*, 19, 183–204, [https://doi.org/10.1175/1520-0426\(2002\)019<0183:EIMOBO>2.0.CO;2](https://doi.org/10.1175/1520-0426(2002)019<0183:EIMOBO>2.0.CO;2), 2002.
- Egbert, G. D. and Ray, R. D.: Tidal prediction, *Journal of Marine Research*, 75, 189–237, 2017.
- Elgered, G., Wahlbom, J., Wennerback, L., Pettersson, L., and Haas, R.: The Onsala Tide Gauge Station: Experiences From the First Four Years of Operation, *Proceedings of the 24th European VLBI Group for Geodesy and Astrometry Working Meeting*, pp. 75–79, <https://doi.org/http://dx.doi.org/10.7419/162.08.2019>, 2019.
- Fagundes, M. A. R., Mendonça-Tinti, I., Iescheck, A. L., Akos, D. M., and Geremia-Nievinski, F.: An open-source low-cost sensor for SNR-based GNSS reflectometry: design and long-term validation towards sea-level altimetry, *GPS Solutions*, 25, 73, <https://doi.org/10.1007/s10291-021-01087-1>, 2021.
- Fiorentino, L. A., Heitsenrether, R., and Krug, W.: Wave Measurements From Radar Tide Gauges, *Frontiers in Marine Science*, p. 586, 2019.
- Georgiadou, Y. and Kleusberg, A.: On carrier signal multipath effects in relative GPS positioning, *Manuscripta geodaetica*, 13, 172–179, 1988.
- Geremia-Nievinski, F., Hobiger, T., Haas, R., Liu, W., Strandberg, J., Tabibi, S., Vey, S., Wickert, J., and Williams, S.: SNR-based GNSS reflectometry for coastal sea-level altimetry

- try: results from the first IAG inter-comparison campaign, *Journal of Geodesy*, 94, 70, <https://doi.org/10.1007/s00190-020-01387-3>, 2020.
- GLOSS: Global Sea-Level Observing System (GLOSS) Implementation Plan, IOC Technical Series No. 100 (English), UNESCO/IOC, 2012.
- Goelzer, H., Nowicki, S., Payne, A., Larour, E., Seroussi, H., Lipscomb, W. H., Gregory, J., Abe-Ouchi, A., Shepherd, A., Simon, E., et al.: The future sea-level contribution of the Greenland ice sheet: a multi-model ensemble study of ISMIP6, *The Cryosphere*, 14, 3071–3096, 2020.
- Golledge, N. R., Keller, E. D., Gomez, N., Naughten, K. A., Bernales, J., Trusel, L. D., and Edwards, T. L.: Global environmental consequences of twenty-first-century ice-sheet melt, *Nature*, 566, 65–72, 2019.
- Gomez, N., Mitrovica, J. X., Huybers, P., and Clark, P. U.: Sea level as a stabilizing factor for marine-ice-sheet grounding lines, *Nature Geoscience*, 3, 850–853, 2010.
- Gomez, N., Pollard, D., and Holland, D.: Sea-level feedback lowers projections of future Antarctic Ice-Sheet mass loss, *Nature communications*, 6, 1–8, 2015.
- Goudie, A. S.: Global warming and fluvial geomorphology, *Geomorphology*, 79, 384 – 394, <https://doi.org/https://doi.org/10.1016/j.geomorph.2006.06.023>, 37th Binghamton Geomorphology Symposium, 2006.
- Gómez-Enri, J., Vignudelli, S., Cipollini, P., Coca, J., and González, C.: Validation of CryoSat-2 SIRAL sea level data in the eastern continental shelf of the Gulf of Cadiz (Spain), *Advances in Space Research*, 62, 1405 – 1420, <https://doi.org/https://doi.org/10.1016/j.asr.2017.10.042>, 2018.
- Hay, C. C., Morrow, E., Kopp, R. E., and Mitrovica, J. X.: Probabilistic reanalysis of twentieth-century sea-level rise, *Nature*, 517, 481–484, <https://doi.org/10.1038/nature14093>, 2015.
- Hayden, A.-M., Wilmes, S.-B., Gomez, N., Green, J. A. M., Pan, L., Han, H., and Golledge, N. R.: Multi-Century Impacts of Ice Sheet Retreat on Sea Level

and Ocean Tides in Hudson Bay, *Journal of Geophysical Research: Oceans*, 125, <https://doi.org/https://doi.org/10.1029/2019JC015104>, 2020.

Herschy, R. W.: *Streamflow measurement*, CRC press, 2008.

Hobiger, T., Ichikawa, R., Koyama, Y., and Kondo, T.: Fast and accurate ray-tracing algorithms for real-time space geodetic applications using numerical weather models, *Journal of Geophysical Research: Atmospheres*, 113, <https://doi.org/https://doi.org/10.1029/2008JD010503>, 2008.

Hunter, J. R.: On the Temperature Correction of the Aquatrak Acoustic Tide Gauge, *Journal of Atmospheric and Oceanic Technology*, 20, 1230–1235, [https://doi.org/10.1175/1520-0426\(2003\)020<1230:OTTCOT>2.0.CO;2](https://doi.org/10.1175/1520-0426(2003)020<1230:OTTCOT>2.0.CO;2), 2003.

IOC: *Manual on sea level measurement and interpretation. Volume IV-An update to 2006.*, UNESCO, 2006.

IPCC: IPCC, 2021: *Climate Change 2021: The Physical Science Basis. Contribution of Working Group I to the Sixth Assessment Report of the Intergovernmental Panel on Climate Change*, Cambridge University Press, 2021.

Jain, S. K., Mani, P., Jain, S. K., Prakash, P., Singh, V. P., Tullos, D., Kumar, S., Agarwal, S. P., and Dimri, A. P.: A Brief review of flood forecasting techniques and their applications, *International Journal of River Basin Management*, 16, 329–344, <https://doi.org/10.1080/15715124.2017.1411920>, 2018.

Jin, S., Cardellach, E., and Xie, F.: *GNSS remote sensing*, vol. 16, Springer, 2014.

Jongman, B., Ward, P. J., and Aerts, J. C.: Global exposure to river and coastal flooding: Long term trends and changes, *Global Environmental Change*, 22, 823–835, <https://doi.org/https://doi.org/10.1016/j.gloenvcha.2012.07.004>, 2012.

Karegar, M. A., Kusche, J., Geremia-Nievinski, F., and Larson, K. M.: Raspberry Pi Reflector (RPR): a Low-cost Water-level Monitoring System based on GNSS Interferometric Reflectom-

- etry, Earth and Space Science Open Archive, p. 26, <https://doi.org/10.1002/essoar.10509304.1>, 2021.
- Khan, S. A., Sasgen, I., Bevis, M., van Dam, T., Bamber, J. L., Wahr, J., Willis, M., Kjør, K. H., Wouters, B., Helm, V., et al.: Geodetic measurements reveal similarities between post–Last Glacial Maximum and present-day mass loss from the Greenland ice sheet, *Science advances*, 2, e1600931, 2016.
- Khan, S. A., Bjørk, A. A., Bamber, J. L., Morlighem, M., Bevis, M., Kjør, K. H., Mouginot, J., Løkkegaard, A., Holland, D. M., Aschwanden, A., Zhang, B., Helm, V., Korsgaard, N. J., Colgan, W., Larsen, N. K., Liu, L., Hansen, K., Barletta, V., Dahl-Jensen, T. S., Søndergaard, A. S., Csatho, B. M., Sasgen, I., Box, J., and Schenk, T.: Centennial response of Greenland’s three largest outlet glaciers, *Nature Communications*, 11, 5718, <https://doi.org/10.1038/s41467-020-19580-5>, 2020.
- Kim, S.-K. and Park, J.: Monitoring a storm surge during hurricane Harvey using multi-constellation GNSS-reflectometry, *GPS Solutions*, 25, 1–13, 2021.
- Kim, S.-K., Lee, E., Park, J., and Shin, S.: Feasibility Analysis of GNSS-Reflectometry for Monitoring Coastal Hazards, *Remote Sensing*, 13, 976, 2021a.
- Kim, S.-K., Park, J., Wengrove, M. E., and Dickey, J. E.: Feasibility Study of GNSS Interferometric Reflectometry (GNSS-IR) For Retrieving Significant Wave Height, in: 2021 IEEE Specialist Meeting on Reflectometry using GNSS and other Signals of Opportunity (GNSS+ R), pp. 69–72, IEEE, 2021b.
- Kim, Y., Park, H., Lee, C., Kim, D., and Seo, M.: Development of a cloud-based image water level gauge, *IT Converg. Pract.(INPRA)*, 2, 22–29, 2014.
- Kirezci, E., Young, I. R., Ranasinghe, R., Muis, S., Nicholls, R. J., Lincke, D., and Hinkel, J.: Projections of global-scale extreme sea levels and resulting episodic coastal flooding over the 21st Century, *Scientific Reports*, 10, 11 629, <https://doi.org/10.1038/s41598-020-67736-6>, 2020.

- Kopp, R. E., Hay, C. C., Little, C. M., and Mitrovica, J. X.: Geographic Variability of Sea-Level Change, *Current Climate Change Reports*, 1, 192–204, <https://doi.org/10.1007/s40641-015-0015-5>, 2015.
- Larson, K. M., Small, E. E., Gutmann, E. D., Bilich, A. L., Braun, J. J., and Zavorotny, V. U.: Use of GPS receivers as a soil moisture network for water cycle studies, *Geophysical Research Letters*, 35, 2008.
- Larson, K. M., Gutmann, E. D., Zavorotny, V. U., Braun, J. J., Williams, M. W., and Nievinski, F. G.: Can we measure snow depth with GPS receivers?, *Geophysical Research Letters*, 36, 2009.
- Larson, K. M., Löfgren, J. S., and Haas, R.: Coastal sea level measurements using a single geodetic GPS receiver, *Advances in Space Research*, 51, 1301–1310, 2013a.
- Larson, K. M., Ray, R. D., Nievinski, F. G., and Freymueller, J. T.: The Accidental Tide Gauge: A GPS Reflection Case Study From Kachemak Bay, Alaska, *IEEE Geoscience and Remote Sensing Letters*, 10, 1200–1204, <https://doi.org/10.1109/LGRS.2012.2236075>, 2013b.
- Larson, K. M., Ray, R. D., and Williams, S. D. P.: A 10-Year Comparison of Water Levels Measured with a Geodetic GPS Receiver versus a Conventional Tide Gauge, *Journal of Atmospheric and Oceanic Technology*, 34, 295–307, <https://doi.org/10.1175/JTECH-D-16-0101.1>, 2017.
- Lee, C.-M., Kuo, C.-Y., Sun, J., Tseng, T.-P., Chen, K.-H., Lan, W.-H., Shum, C., Ali, T., Ching, K.-E., Chu, P., et al.: Evaluation and improvement of coastal GNSS reflectometry sea level variations from existing GNSS stations in Taiwan, *Advances in space research*, 63, 1280–1288, 2019.
- Lehner, B., Liermann, C. R., Revenga, C., Vörösmarty, C., Fekete, B., Crouzet, P., Döll, P., Endean, M., Frenken, K., Magome, J., et al.: High-resolution mapping of the world's reservoirs and dams for sustainable river-flow management, *Frontiers in Ecology and the Environment*, 9, 494–502, 2011.

- Leuliette, E. W., Nerem, R. S., and Mitchum, G. T.: Calibration of TOPEX/Poseidon and Jason altimeter data to construct a continuous record of mean sea level change, *Marine Geodesy*, 27, 79–94, 2004.
- Li, Y., Yu, K., Jin, T., Chang, X., Wang, Q., and Li, J.: Development of a GNSS-IR instrument based on low-cost positioning chips and its performance evaluation for estimating the reflector height, *GPS Solutions*, 25, 1–12, 2021.
- Liu, L. and Larson, K. M.: Decadal changes of surface elevation over permafrost area estimated using reflected GPS signals, *The Cryosphere*, 12, 477–489, 2018.
- Liu, Q. and Zhang, S.: An improved sea level retrieval method using the differential evolution of GNSS SNR data, *Advances in Space Research*, 67, 975–984, <https://doi.org/https://doi.org/10.1016/j.asr.2020.10.050>, 2021.
- Löfgren, J. S., Haas, R., and Johansson, J. M.: Monitoring coastal sea level using reflected GNSS signals, *Advances in Space Research*, 47, 213–220, 2011.
- Löfgren, J. S., Haas, R., and Scherneck, H.-G.: Sea level time series and ocean tide analysis from multipath signals at five GPS sites in different parts of the world, *Journal of Geodynamics*, 80, 66 – 80, <https://doi.org/https://doi.org/10.1016/j.jog.2014.02.012>, 2014.
- Marcos, M., Puyol, B., Amores, A., Pérez Gómez, B., Fraile, M. Á., and Talke, S. A.: Historical tide gauge sea-level observations in Alicante and Santander (Spain) since the 19th century, *Geoscience Data Journal*, 8, 144–153, <https://doi.org/10.1002/gdj3.112>, 2021.
- Martín, A., Luján, R., and Anquela, A. B.: Python software tools for GNSS interferometric reflectometry (GNSS-IR), *GPS Solutions*, 24, 94, <https://doi.org/10.1007/s10291-020-01010-0>, 2020.
- Martin-Neira, M. et al.: A passive reflectometry and interferometry system (PARIS): Application to ocean altimetry, *ESA journal*, 17, 331–355, 1993.
- Masters, D., Duly, T., Esterhuizen, S., Irisov, V., Jales, P., Nguyen, V., Nogués-Correig, O., Tan, L., Yuasa, T., and Angling, M.: Status and accomplishments of the Spire Earth observing nanosatel-

- lite constellation, in: *Sensors, Systems, and Next-Generation Satellites XXIV*, vol. 11530, p. 115300V, SPIE, 2020.
- McLeman, R.: Migration and displacement risks due to mean sea-level rise, *Bulletin of the Atomic Scientists*, 74, 148–154, 2018.
- Mekonnen, M. M. and Hoekstra, A. Y.: Four billion people facing severe water scarcity, *Science advances*, 2, e1500323, 2016.
- Merkuryeva, G., Merkuryev, Y., Sokolov, B. V., Potryasaev, S., Zelentsov, V. A., and Lektauers, A.: Advanced river flood monitoring, modelling and forecasting, *Journal of Computational Science*, 10, 77–85, <https://doi.org/10.1016/j.jocs.2014.10.004>, 2015.
- Meysignac, B., Slangen, A. B. A., Melet, A., Church, J. A., Fettweis, X., Marzeion, B., Agosta, C., Ligtenberg, S. R. M., Spada, G., Richter, K., Palmer, M. D., Roberts, C. D., and Champollion, N.: Evaluating Model Simulations of Twentieth-Century Sea-Level Rise. Part II: Regional Sea-Level Changes, *Journal of Climate*, 30, 8565 – 8593, <https://doi.org/10.1175/JCLI-D-17-0112.1>, 2017.
- Mitrovica, J. X., Gomez, N., and Clark, P. U.: The Sea-Level Fingerprint of West Antarctic Collapse, *Science*, 323, 753–753, <https://doi.org/10.1126/science.1166510>, 2009.
- Mitrovica, J. X., Gomez, N., Morrow, E., Hay, C., Latychev, K., and Tamisiea, M. E.: On the robustness of predictions of sea level fingerprints, *Geophysical Journal International*, 187, 729–742, <https://doi.org/10.1111/j.1365-246X.2011.05090.x>, 2011.
- Míguez, B. M., Gómez, B. P., and Fanjul, E. A.: The ESEAS-RI Sea Level Test Station: Reliability and Accuracy of Different Tide Gauges, *The International Hydrographic Review*, 6, 2005.
- Nerem, R. S., Beckley, B. D., Fasullo, J. T., Hamlington, B. D., Masters, D., and Mitchum, G. T.: Climate-change-driven accelerated sea-level rise detected in the altimeter era, *Proceedings of the national academy of sciences*, 115, 2022–2025, 2018.

- Neumann, B., Vafeidis, A. T., Zimmermann, J., and Nicholls, R. J.: Future Coastal Population Growth and Exposure to Sea-Level Rise and Coastal Flooding - A Global Assessment, *PLOS ONE*, 10, 1–34, <https://doi.org/10.1371/journal.pone.0118571>, 2015.
- Nicholls, R. J., Marinova, N., Lowe, J. A., Brown, S., Vellinga, P., De Gusmao, D., Hinkel, J., and Tol, R. S.: Sea-level rise and its possible impacts given a ‘beyond 4 C world’ in the twenty-first century, *Philosophical transactions of the Royal Society A: mathematical, physical and engineering sciences*, 369, 161–181, 2011.
- Nievinski, F. and Larson, K.: Forward modeling of GPS multipath for near-surface reflectometry and positioning applications, *GPS Solutions*, <https://doi.org/10.1007/s10291-013-0331-y>, 2013.
- Nievinski, F. G. and Larson, K. M.: An open source GPS multipath simulator in Matlab/Octave, *GPS Solutions*, 18, 473–481, <https://doi.org/10.1007/s10291-014-0370-z>, 2014.
- Nievinski, F. G. and Larson, K. M.: Inverse Modeling of GPS Multipath for Snow Depth Estimation—Part I: Formulation and Simulations, *IEEE Transactions on Geoscience and Remote Sensing*, 52, 6555–6563, <https://doi.org/10.1109/TGRS.2013.2297681>, 2014a.
- Nievinski, F. G. and Larson, K. M.: Inverse Modeling of GPS Multipath for Snow Depth Estimation—Part II: Application and Validation, *IEEE Transactions on Geoscience and Remote Sensing*, 52, 6564–6573, <https://doi.org/10.1109/TGRS.2013.2297688>, 2014b.
- Nikolaidou, T., Santos, M. C., Williams, S. D. P., and Geremia-Nievinski, F.: Raytracing atmospheric delays in ground-based GNSS reflectometry, *Journal of Geodesy*, 94, 68, <https://doi.org/10.1007/s00190-020-01390-8>, 2020.
- Nikolaidou, T., Santos, M., Williams, S., and Geremia-Nievinski, F.: Development and validation of comprehensive closed formulas for atmospheric delay and altimetry correction in ground-based GNSS-R, <https://doi.org/10.36227/techrxiv.14345153.v2>, 2021.
- Padman, L. and Erofeeva, S.: A barotropic inverse tidal model for the Arctic Ocean, *Geophysical Research Letters*, 31, 2004.

- Panikkar, N. and Srinivasan, T.: The concept of tides in Ancient India, *Indian Journal of History of Science*, 6, 36–50, 1971.
- Pascual, D., Camps, A., Martin, F., Park, H., Arroyo, A. A., and Onrubia, R.: Precision bounds in GNSS-R ocean altimetry, *IEEE Journal of Selected Topics in Applied Earth Observations and Remote Sensing*, 7, 1416–1423, 2014.
- Pattyn, F. and Morlighem, M.: The uncertain future of the Antarctic Ice Sheet, *Science*, 367, 1331–1335, <https://doi.org/10.1126/science.aaz5487>, 2020.
- Peng, D., Hill, E. M., Li, L., Switzer, A. D., and Larson, K. M.: Application of GNSS interferometric reflectometry for detecting storm surges, *GPS Solutions*, 23, 47, <https://doi.org/10.1007/s10291-019-0838-y>, 2019.
- Peng, F. and Deng, X.: Validation of Sentinel-3A SAR mode sea level anomalies around the Australian coastal region, *Remote Sensing of Environment*, 237, 111548, <https://doi.org/https://doi.org/10.1016/j.rse.2019.111548>, 2020.
- Pérez, B., Payo, A., López, D., Woodworth, P., and Alvarez Fanjul, E.: Overlapping sea level time series measured using different technologies: an example from the REDMAR Spanish network, *Natural Hazards and Earth System Sciences*, 14, 589–610, 2014.
- Pollard, D., DeConto, R. M., and Alley, R. B.: Potential Antarctic Ice Sheet retreat driven by hydrofracturing and ice cliff failure, *Earth and Planetary Science Letters*, 412, 112–121, 2015.
- Pomeroy, J. W., Stewart, R. E., and Whitfield, P. H.: The 2013 flood event in the South Saskatchewan and Elk River basins: Causes, assessment and damages, *Canadian Water Resources Journal / Revue canadienne des ressources hydriques*, 41, 105–117, <https://doi.org/10.1080/07011784.2015.1089190>, 2016.
- Pörtner, H.-O., Roberts, D., Masson-Delmotte, V., Zhai, P., Tignor, M., Poloczanska, E., Mintenbeck, K., Alegría, A., Nicolai, M., Okem, A., et al.: Summary for policymakers, IPCC special report on the ocean and cryosphere in a changing climate, 7, 2019.

- Prange, L., Dach, R., Lutz, S., Schaer, S., and Jäggi, A.: The CODE MGEX Orbit and Clock Solution, in: IAG 150 Years, edited by Rizos, C. and Willis, P., pp. 767–773, Springer International Publishing, Cham, 2016.
- Purnell, D., Gomez, N., Chan, N. H., Strandberg, J., Holland, D. M., and Hobiger, T.: Quantifying the Uncertainty in Ground-Based GNSS-Reflectometry Sea Level Measurements, *IEEE Journal of Selected Topics in Applied Earth Observations and Remote Sensing*, 13, 4419–4428, <https://doi.org/10.1109/JSTARS.2020.3010413>, 2020.
- Purnell, D. J., Gomez, N., Minarik, W., Porter, D., and Langston, G.: Precise water level measurements using low-cost GNSS antenna arrays, *Earth Surface Dynamics*, 9, 673–685, <https://doi.org/10.5194/esurf-9-673-2021>, 2021.
- Pytharouli, S., Chaikalis, S., and Stiros, S. C.: Uncertainty and bias in electronic tide-gauge records: Evidence from collocated sensors, *Measurement*, 125, 496 – 508, <https://doi.org/https://doi.org/10.1016/j.measurement.2018.05.012>, 2018.
- Reinking, J.: GNSS-SNR water level estimation using global optimization based on interval analysis, *Journal of Geodetic Science*, 6, <https://doi.org/10.1515/jogs-2016-0006>, 2016.
- Richter, O., Gwyther, D. E., King, M. A., and Galton-Fenzi, B. K.: The impact of tides on Antarctic ice shelf melting, *The Cryosphere*, 16, 1409–1429, <https://doi.org/10.5194/tc-16-1409-2022>, 2022.
- Rius, A., Cardellach, E., and Martin-Neira, M.: Altimetric analysis of the sea-surface GPS-reflected signals, *IEEE Transactions on Geoscience and Remote Sensing*, 48, 2119–2127, 2010.
- Rivas, M. B. and Martin-Neira, M.: Coherent GPS reflections from the sea surface, *IEEE geoscience and remote sensing letters*, 3, 28–31, 2006.
- Roesler, C. and Larson, K. M.: Software tools for GNSS interferometric reflectometry (GNSS-IR), *GPS Solutions*, 22, 80, <https://doi.org/10.1007/s10291-018-0744-8>, 2018.

- Ruf, C. S., Gleason, S., Jelenak, Z., Katzberg, S., Ridley, A., Rose, R., Scherrer, J., and Zavorotny, V.: The CYGNSS nanosatellite constellation hurricane mission, in: 2012 IEEE International Geoscience and Remote Sensing Symposium, pp. 214–216, IEEE, 2012.
- Ruffini, n. G., Soulat, F., Caparrini, M., Germain, O., and Martín-Neira, M.: The Eddy Experiment: Accurate GNSS-R ocean altimetry from low altitude aircraft, *Geophysical research letters*, 31, 2004.
- Santamaría-Gómez, A. and Watson, C.: Remote leveling of tide gauges using GNSS reflectometry: case study at Spring Bay, Australia, *GPS Solutions*, 21, 451–459, <https://doi.org/10.1007/s10291-016-0537-x>, 2017.
- Santamaría-Gómez, A., Watson, C., Gravelle, M., King, M., and Wöppelmann, G.: Levelling co-located GNSS and tide gauge stations using GNSS reflectometry, *Journal of Geodesy*, 89, 241–258, 2015.
- Santamaría-Gómez, A., Gravelle, M., Collilieux, X., Guichard, M., Míguez, B. M., Tiphaneau, P., and Wöppelmann, G.: Mitigating the effects of vertical land motion in tide gauge records using a state-of-the-art GPS velocity field, *Global and Planetary Change*, 98-99, 6 – 17, <https://doi.org/https://doi.org/10.1016/j.gloplacha.2012.07.007>, 2012.
- Seifi, F., Deng, X., and Andersen, O. B.: Assessment of the Accuracy of Recent Empirical and Assimilated Tidal Models for the Great Barrier Reef, Australia, Using Satellite and Coastal Data, *Remote Sensing*, 11, 1211, 2019.
- Sermet, Y., Villanueva, P., Sit, M. A., and Demir, I.: Crowdsourced approaches for stage measurements at ungauged locations using smartphones, *Hydrological Sciences Journal*, 65, 813–822, <https://doi.org/10.1080/02626667.2019.1659508>, 2020.
- Seroussi, H., Nowicki, S., Payne, A. J., Goelzer, H., Lipscomb, W. H., Abe-Ouchi, A., Agosta, C., Albrecht, T., Asay-Davis, X., Barthel, A., et al.: ISMIP6 Antarctica: a multi-model ensemble of the Antarctic ice sheet evolution over the 21st century, *The Cryosphere*, 14, 3033–3070, 2020.

- Slangen, A. B. A., Church, J. A., Agosta, C., Fettweis, X., Marzeion, B., and Richter, K.: Anthropogenic forcing dominates global mean sea-level rise since 1970, *Nature Climate Change*, 6, 701–705, <https://doi.org/10.1038/nclimate2991>, 2016.
- Song, M., He, X., Wang, X., Zhou, Y., and Xu, X.: Study on the quality control for periodogram in the determination of water level using the GNSS-IR technique, *Sensors*, 19, 4524, 2019.
- Strandberg, J., Hobiger, T., and Haas, R.: Improving GNSS-R sea level determination through inverse modeling of SNR data, *Radio Science*, 51, 1286–1296, <https://doi.org/10.1002/2016RS006057>, 2016.
- Strandberg, J., Hobiger, T., and Haas, R.: Real-time sea-level monitoring using Kalman filtering of GNSS-R data, *GPS Solutions*, 23, 61, <https://doi.org/10.1007/s10291-019-0851-1>, 2019a.
- Strandberg, J., Hobiger, T., and Haas, R.: Real-time sea-level monitoring using Kalman filtering of GNSS-R data, *GPS Solutions*, 23, 61, <https://doi.org/10.1007/s10291-019-0851-1>, 2019b.
- Sun, J.: Ground-Based GNSS-Reflectometry Sea Level and Lake Ice Thickness Measurements, Ph.D. thesis, The Ohio State University, Columbus, Ohio, 2017.
- Tabibi, S., Nievinski, F. G., van Dam, T., and Monico, J. F.: Assessment of modernized GPS L5 SNR for ground-based multipath reflectometry applications, *Advances in Space Research*, 55, 1104 – 1116, <https://doi.org/https://doi.org/10.1016/j.asr.2014.11.019>, 2015.
- Tabibi, S., Nievinski, F., and Van Dam, T.: Statistical Comparison and Combination of GPS, GLONASS, and Multi-GNSS Multipath Reflectometry Applied to Snow Depth Retrieval, *IEEE Transactions on Geoscience and Remote Sensing*, PP, 1–13, <https://doi.org/10.1109/TGRS.2017.2679899>, 2017.
- Tabibi, S., Geremia-Nievinski, F., Francis, O., and van Dam, T.: Tidal analysis of GNSS reflectometry applied for coastal sea level sensing in Antarctica and Greenland, *Remote Sensing of Environment*, 248, 111 959, <https://doi.org/https://doi.org/10.1016/j.rse.2020.111959>, 2020.

- Taherkhani, M., Vitousek, S., Barnard, P. L., Frazer, N., Anderson, T. R., and Fletcher, C. H.: Sea-level rise exponentially increases coastal flood frequency, *Scientific Reports*, 10, 6466, <https://doi.org/10.1038/s41598-020-62188-4>, 2020.
- Talke, S. A. and Jay, D. A.: Changing Tides: The Role of Natural and Anthropogenic Factors, *Annual Review of Marine Science*, 12, 121–151, <https://doi.org/10.1146/annurev-marine-010419-010727>, PMID: 31479622, 2020.
- Talke, S. A., Kemp, A. C., and Woodruff, J.: Relative Sea Level, Tides, and Extreme Water Levels in Boston Harbor From 1825 to 2018, *Journal of Geophysical Research: Oceans*, 123, 3895–3914, <https://doi.org/10.1029/2017JC013645>, 2018.
- Tamisiea, M. E., Hughes, C. W., Williams, S. D. P., and Bingley, R. M.: Sea level: measuring the bounding surfaces of the ocean, *Philosophical Transactions of the Royal Society A: Mathematical, Physical and Engineering Sciences*, 372, 20130336, <https://doi.org/10.1098/rsta.2013.0336>, 2014.
- Treuhaft, R. N., Lowe, S. T., Zuffada, C., and Chao, Y.: 2-cm GPS altimetry over Crater Lake, *Geophysical Research Letters*, 28, 4343–4346, 2001.
- UNISDR: Making Development Sustainable: The Future of Disaster Risk Management. Global Assessment Report on Disaster Risk Reduction, Geneva, Switzerland: United Nations Office for Disaster Risk Reduction (UNISDR), 2015.
- van Veen, J.: Bestaat er een geologische bodemdaling te Amsterdam sedert 1700, *Tijdschr K Ned Aardr Gen*, 62, 2–36, 1945.
- Wang, F., Xu, Z., Yang, D., Zhang, G., Xing, J., Shi, Z., Zhang, B., and Yang, L.: An Unbiased Multiparameter Algorithm of Retrieving Sea Surface Height Using Coastal GNSS Reflectometry, *IEEE Journal of Selected Topics in Applied Earth Observations and Remote Sensing*, 14, 12199–12211, 2021.

- Wang, Q., Zhang, P.-Z., Freymueller, J. T., Bilham, R., Larson, K. M., Lai, X., You, X., Niu, Z., Wu, J., Li, Y., et al.: Present-day crustal deformation in China constrained by global positioning system measurements, *Science*, 294, 574–577, 2001.
- Wang, X., He, X., and Zhang, Q.: Evaluation and combination of quad-constellation multi-GNSS multipath reflectometry applied to sea level retrieval, *Remote Sensing of Environment*, 231, 111 229, <https://doi.org/10.1016/j.rse.2019.111229>, 2019.
- Water Resources Branch, Department of Environment, Government of Yukon: Yukon Snow Survey Bulletin and Water Supply Forecast, https://yukon.ca/sites/yukon.ca/files/env/snow_bulletin_may_2022_en.pdf, 2022.
- Watson, C. S., White, N. J., Church, J. A., King, M. A., Burgette, R. J., and Legresy, B.: Unabated global mean sea-level rise over the satellite altimeter era, *Nature Climate Change*, 5, 565–568, <https://doi.org/10.1038/nclimate2635>, 2015.
- Williams, S. D. P. and Nievinski, F. G.: Tropospheric delays in ground-based GNSS multipath reflectometry—Experimental evidence from coastal sites, *Journal of Geophysical Research: Solid Earth*, 122, 2310–2327, <https://doi.org/10.1002/2016JB013612>, 2017.
- Williams, S. D. P., Bell, P. S., McCann, D. L., Cooke, R., and Sams, C.: Demonstrating the Potential of Low-Cost GPS Units for the Remote Measurement of Tides and Water Levels Using Interferometric Reflectometry, *Journal of Atmospheric and Oceanic Technology*, 37, 1925 – 1935, <https://doi.org/10.1175/JTECH-D-20-0063.1>, 2020.
- Woodworth, P. L.: High waters at Liverpool since 1768: the UK’s longest sea level record, *Geophysical Research Letters*, 26, 1589–1592, <https://doi.org/10.1029/1999GL900323>, 1999.
- Woodworth, P. L. and Smith, D. E.: A One Year Comparison of Radar and Bubbler Tide Gauges at Liverpool, *The International Hydrographic Review*, 4, 2003.

- Yamawaki, M. K., Geremia-Nievinski, F., and Monico, J. F.: High-rate altimetry in SNR-based GNSS-R: Proof-of-concept of a synthetic vertical array, *IEEE Geoscience and Remote Sensing Letters* (accepted), <https://doi.org/10.36227/techrxiv.14186930.v1>, 2021.
- Zeiger, P., Frappart, F., Darrozes, J., Roussel, N., Bonneton, P., Bonneton, N., and Detandt, G.: SNR-Based Water Height Retrieval in Rivers: Application to High Amplitude Asymmetric Tides in the Garonne River, *Remote Sensing*, 13, 1856, 2021.
- Zhang, G., Xu, Z., Wang, F., Yang, D., and Xing, J.: Evaluation and correction of elevation angle influence for coastal GNSS-R ocean altimetry, *Remote Sensing*, 13, 2978, 2021.
- Zhang, Z., Zhou, Y., Liu, H., and Gao, H.: In-situ water level measurement using NIR-imaging video camera, *Flow Measurement and Instrumentation*, 67, 95–106, 2019.
- Zuosheng, Y., Emery, K., and Yuix, X.: Historical development and use of thousand-year-old tide-prediction tables, *Limnology and Oceanography*, 34, 953–957, 1989.